Verification of clear-air turbulence forecasts

A. Overeem
June 2002, KNMI
Technisch rapport

KNMI

PREFACE

This report is part of my study Soil, Water and Atmosphere, specialisation meteorology at Wageningen University, the Netherlands. In this report numerical weather predictions of clear-air turbulence are verified. The research has been performed at KNMI (Royal Netherlands Meteorological Institute) during a period of about 35 weeks from August 2001 to May 2002.

I thank my tutors, Mr. H.J. Hemink (senior aviation meteorologist and instructor at training center De Bilt, KNMI) and Dr. L.J.M. Kroon (Meteorology and Air Quality Group, Wageningen University), for their support and reviewing of my report.

I would like to thank the following persons (all KNMI):
Drs. S. Kruizinga and Drs. D.H.P. Vogelezang for providing the ECMWF data, Dr. B. Wichers-Schreur for providing an interpolation program, Mr. M.I.M. van Zijl, Mr. J.C. Hozee, and Mr. J.C. van Vuure for answering technical questions regarding data and solving software problems, Drs. A.R. Moene for his answers to my questions, Drs. E.I.F. de Bruijn and R.M. van Westrhenen for the provision of the code of a clear-air turbulence index and their help by changing this index, Mr. L. Snijders for storing the AMDAR data, Mr. U. Bergman for answering questions concerning the quality of AMDARs, Mrs. A. den Uijl for giving information about the PIREPs received at KNMI, and further all people at KNMI who did make a contribution to my research.

Others I would like to thank are Mr. D.W. McCann (NOAA/AWC) and Mr. G.P. Ellrod (NOAA/NESDIS) for answering questions regarding clear-air turbulence indices, Dr. J.A. Knox (University of Georgia) for providing me a pre-print paper, Mr. D. Lockett (Bureau of Meteorology, Australia) for answering questions about the Australian AMDARs, and Dr. A.C.M. Beljaars (ECMWF) for giving information about the ECMWF high cloud cover.

I especially would like to thank the members of the WMO AMDAR panel who gave me a lot of information about AMDARs and put much effort in answering my questions about AMDARs. The members are Ir. A. Grooters (KNMI), Mr. J. Stickland (Met Office), Mr. B. Truscott (Met Office), and Mr. S. Taylor (Met Office). I particularly thank Ir. A. Grooters for his comments.

I am also very grateful to KLM (Royal Dutch Airlines) for letting me perform a pilot survey to obtain turbulence observations. I especially thank Ir. B.A. Visser (KLM) who organized the survey and of course the many pilots of the unit B737 who filled in the forms and returned over 80% of the surveys we handed out.

I would like to thank KNMI for giving me the opportunity to do my research, which I found to be interesting and a real challenge. In particular I thank Drs. K. Floor, head meteorology training division KNMI, and all other staff members for their hospitality and support.

SUMMARY

Clear-air turbulence (CAT) is non-convective turbulence outside the planetary boundary layer, often in the upper-air. CAT areas have a patchy structure and horizontal dimensions of 80 – 500 km along the wind direction and 20 – 100 km across the wind flow. Vertical dimensions are 500 – 1000 m, and the lifespan of CAT is between half an hour and a day.

Generally two mechanisms can cause CAT: the Kelvin-Helmholtz instability and mountain-waves. The first is the most important mechanism. In case of large vertical wind shear Kelvin-Helmholtz waves can develop and their breaking causes turbulence.

Often CAT is only a nuisance, but CAT can cause structural damage to aircraft, passenger injury, and even fatalities. Therefore a CAT forecast is necessary to avoid CAT areas. Problem is current CAT forecasts, including numerical model forecasts, are not very reliable in forecasting CAT. For that reason often a CAT warning is given after it has been reported by pilots. Currently, most CAT forecasts are based on macro-scale phenomena, while CAT is a micro-scale phenomenon.

In this report seven clear-air turbulence indices, which are numerical model forecasts of CAT, are verified: frontogenesis, TI1, TI2, Brown index, vertical wind shear (VWS), horizontal wind speed, and Dutton index. These indices are calculated with ECMWF model fields from two pressure levels for each layer over which an index is calculated.

Pilot reports of turbulence are subjective and instrumented aircraft reports, such as AMDARs, are preferred. In co-operation with KLM a pilot survey has been held during 8 days in January 2002 to obtain observations over Europe, because few instrumented aircraft reports which report turbulence correctly are available over Europe. Only the TI1 is verified with a pilot survey.

To verify numerical clear-air turbulence forecasts with high quality observations, AMDARs (Aircraft Meteorological DAta Relay) which report DEVG (Derived Equivalent Vertical Gust velocity) are used reported by Australian aircraft flying in the area 30ºE-150ºW and 0ºS-50ºS in the period from 13 November 2001 to 17 February 2002. DEVG takes into account mass, air speed, and characteristics of the aircraft. Seven clear-air turbulence indices have been verified. To exclude convection forecasted high cloud fractions are used.

CAT cannot be detected by current on-board technology like LIDAR and X-band radar. Improvements are possible, but competition for funding and other resources with other aviation hazards limit the implementation of on-board measurement devices.

There is absolutely no correlation between the magnitude of the tested clear-air turbulence indices and the intensity of observed turbulence as reported by DEVG. Main conclusion of this report is that the chance of encountering CAT along a 100 km flight segment in which a CAT index forecasts CAT is very low (5-20%) for different thresholds. These are the values based on the best results, often indices will have a much lower chance. Often a CAT forecast is given, while no CAT is encountered. This large overestimation makes the tested CAT indices not reliable in forecasting CAT. They can only be used as an aid in forecasting CAT and have to be used with precaution.

Recommended is these and other indices are tested for a longer time period with higher-resolution model data. To verify indices over Europe the number of AMDARs which correctly report turbulence according to DEVG should be increased considerably. Most promising option is maybe to test the performance of the CAT indices for different weather situations. Another option is AMDAR data which contain turbulence observations (DEVG) become available in real-time to the aviation meteorologist.

Contents

1 INTRODUCTION

1.1 Background

Definitions of clear-air turbulence (CAT) differ, but most authors agree that CAT is non-convective turbulence outside the planetary boundary layer. Mountain-waves are also included in the definition of CAT.
CAT is of importance for the safe operation of aircraft. Often CAT is only a nuisance, but CAT can cause structural damage to aircraft, passenger injury, and even fatalities. This leads to the conclusion that a CAT forecast is necessary to avoid CAT areas. Problem is that current CAT forecasts are not very reliable. Objective CAT indices based on numerical model output can possibly give better CAT predictions, but until now these indices are also not very convincing (see for example Turner and Bysouth, 1999). Besides at KNMI (Royal Netherlands Meteorological Institute) the aviation meteorologist can use such a CAT index, which is a numerical model prediction of CAT, but the performance of this index is unknown. Often only a CAT warning is given after it has been reported by pilots. Currently, most CAT forecasts are based on macro-scale phenomena, while CAT is a micro-scale phenomenon. This is the main reason why current CAT forecasts are not very reliable.
A pilot survey in Europe held on 8 days in January 2002 and instrumented aircraft reports (AMDARs) over the Southern Hemisphere in the period 13 November 2001 to 17 February 2002 are used to determine the ability of objective CAT indices in forecasting CAT. From the large number of existing CAT indices, seven are verified: frontogenesis, TI1, TI2, Brown index, vertical wind shear, horizontal wind speed, and Dutton index.

1.2 Objective and research questions

In this report we try to give an answer to the following questions:

1. Can the TI1 be used as a predictor of clear-air turbulence over Europe based on the comparison with a pilot survey?
2. Which correlation exists between the magnitude of the tested clear-air turbulence indices and the intensity of observed turbulence by AMDARs?
3. Which of the seven clear-air turbulence indices gives the best prediction of clear-air turbulence over the Southern Hemisphere when compared to AMDAR observations? And for which threshold values?
4. Can a clear-air turbulence index be used in forecasting clear-air turbulence?

1.3 Structure of this report

Chapter 2 contains theory of clear-air turbulence. Chapter 3 gives information about the problems in forecasting CAT and the way CAT influences an aircraft and its occupants. Chapter 4 deals with the theory of the seven clear-air turbulence indices of this report. In Chapter 5 a choice is made between the different types of observations of turbulence which are available. Chapter 6 gives the results of the performance of the TI1 over Europe in January 2002 when compared to a pilot survey, and two case-studies in which the TI1 is compared to the weather situation. In Chapter 7 seven clear-air turbulence indices are compared to instrumented aircraft reports (AMDARs) in an area over the Southern Hemisphere. Chapter 8 deals with the question if a clear-air turbulence forecast can be used to forecast CAT over Europe, and also future improvements in detecting CAT are discussed. Finally, Chapter 9 gives conclusions and recommendations for further research.

2 THEORY OF CLEAR-AIR TURBULENCE

2.1 Introduction

First a general description of turbulence is given and some atmospheric processes are mentioned which contribute to the generation of turbulence. After this an overview is given of the different definitions of clear-air turbulence and is decided which definition is chosen for this report. Further, attention is paid to the mechanisms which presumably produce clear-air turbulence: the Kelvin-Helmholtz instability and mountain-waves. Finally the relation between CAT and macro-scale phenomena, such as jet streams, is discussed.

2.2 Description of turbulence

Most natural flows, which can be of liquids or gases, have the property that they contain turbulence. In this Chapter we will consider the definition of classical turbulence as defined in fluid mechanics and not the definition of aviation turbulence, which is "bumpiness in flight". The latter cannot only be caused by disorganized atmospheric motions, belonging to the definition of classical turbulence, but also by certain organized atmospheric motions (Lester, 1994).
The detailed evolution of a turbulent flow cannot be predicted. Turbulence can be described as a type of fluid flow that is strongly rotational and evidently chaotic. By separating parcels of air, turbulence mixes fluid properties. However, a generally accepted definition of turbulence does not exist, usually a description of turbulence is given (Panofsky and Dutton, 1984). According to Vinnichencko *et al.* (1980) the primary property of turbulent motion is the random nature of the velocity field in time and space.
Stull (1988) divides wind into mean wind, turbulence and waves (see Figure 2.1). Each category can occur alone, but also two or three at the same time. Turbulence or waves can be studied by splitting wind into a mean part and a perturbation part:

$$u = \bar{u} + u' \tag{2.1}$$

The mean part ($\bar{u}$) representing the mean wind, the perturbation part (u') being the wave effect or the turbulence effect superimposed on the mean wind (see Figure 2.2). In this way turbulence is defined as the gustiness superimposed on the mean wind. Turbulence can be envisaged as irregular swirls of motion (eddies) (Stull, 1988). Due to friction the eddies dissipate finally. Larger scale atmospheric motions can create turbulence but also be influenced by the turbulence (Lester, 1994).

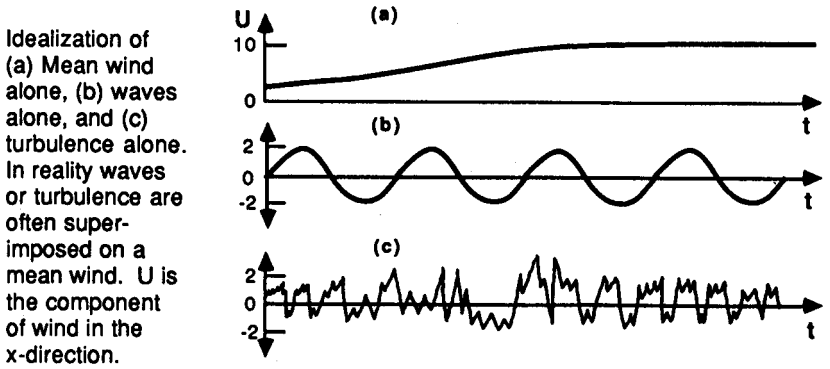

Figure 2.1: Illustration of the three categories in which wind can be classified (Stull, 1988).

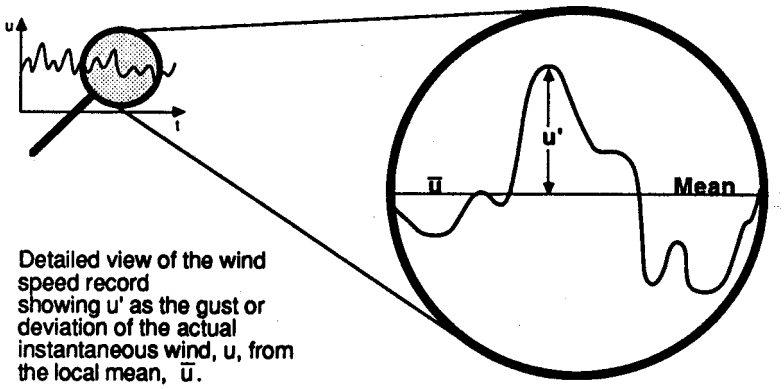

Figure 2.2: Illustration of the mean part and the perturbation part of the wind speed (Stull, 1988).

Especially large gradients in temperature and wind-velocity fields are responsible for turbulence in the atmosphere. The following atmospheric processes, which can strengthen or weaken one another, cause these large gradients:

1. The friction of the airflow at the earth's surface which causes a wind-velocity profile in the planetary boundary layer.
2. Unequal heating of the earth's surface which causes differences in thermal convection.
3. Release of heat due to condensation and crystallization in cloud-forming processes. This leads to differences in temperature.
4. Convergence and interaction of different air masses near fronts, which can also be in the upper-air. This results in large horizontal differences in temperature and wind velocity.
5. Loss of stability of waves which have developed in inversion layers, for example the tropopause, creates turbulent eddies.
6. Modification of air when flowing over mountain barriers. Wavelike disturbances and rotor motions are produced on the lee side.

We consider the amount of turbulent energy at a fixed point of an airflow. Various processes can change this amount:

1. Conversion of energy of the mean motion to turbulent energy.
2. Fluctuations of external forces.
3. Diffusion of turbulent energy.
4. Dissipation of turbulent energy by viscosity.

Process 1 is the energy source for large-scale eddies. The kinetic energy of these large-scale eddies is given continuously to smaller-scale eddies. Finally the smallest-scale eddies dissipate the energy as heat due to viscosity (process 4) (Vinnichenko *et al.*, 1980).

2.3 Definition of clear-air turbulence

2.3.1 Definitions

In literature a number of rather different definitions of clear-air turbulence (CAT) can be found and the most important ones will be given here.
The turbulence of importance for aviation can be divided in low-level turbulence, turbulence in and near thunderstorms, clear-air turbulence and mountain-wave turbulence (Lester, 1994). So clear-air turbulence is just one of four possible types of turbulence. Clear-air turbulence can be defined by "a variety of irregular fluctuating motions in a clear atmosphere at high altitude". Some of these fluctuating motions are undulant rather than truly turbulent (Pao and Goldburg, 1969a).
According to Lester (1994) CAT is "Turbulence which occurs in the free atmosphere away from visible convective activity". According to Bass (1999a) CAT can be associated with mountain-wave activity, tropopause surfaces, troughs, and upper fronts. LMG (1995) uses as definition: turbulence experienced outside clouds. Beckwith (1971) states that "CAT is generally applied to all turbulence not of convective origin and separated from mechanical turbulence in the friction layers near the surface". According to Keller (1986) "CAT should actually be considered a generic term in that it represents turbulence occuring in statically stable shear layers which need not be cloud-free, but may

contain non-convective clouds. However, it does rule out the turbulence associated with convectively unstable planetary boundary layers (whether clear or not) and deep convection, such as thunderstorms, as well as mechanical turbulence due to wind flowing over the earth's surface". According to de Villiers and van Heerden (2001) and Bakker (1993) CAT can be generated by mountain-waves. Clear (2001) describes CAT as "the bumpiness experienced by aircraft at high altitudes (above 18,000 feet) in either cloud-free conditions or in stratiform clouds"

2.3.2 Definition of CAT in this report

Despite these varying definitions of clear-air turbulence most authors agree that clear-air turbulence is non-convective turbulence and outside the planetary boundary layer. Mountain-waves are often not specifically excluded from the CAT definition.
A clear-air turbulence index is a weather forecast of clear-air turbulence calculated on the basis of a numerical weather model, but is better expressed in terms of probabilities of encountering CAT (Dutton, 1980). CAT indices do not take into account turbulence induced by mountains or convection and are calculated for layers between 400 (7200 m) and 150 hPa (13600 m) in our research.
Based on the above considerations the following CAT definition is chosen for the verification of the CAT indices: "Turbulence in clear-air or in non-convective clouds between 400-150 hPa (7200-13600 m above the earth's surface according to the ICAO standard atmosphere) not caused by mountain-waves". Nevertheless, in the theory of this report also the generation of mountain-waves will be explained, since mountain-waves are often included in the CAT definition.

2.4 Properties and causes of clear-air turbulence

2.4.1 Properties

According to Meteorological Office College (1997) the dimensions of CAT areas are horizontally 80 – 500 km along the wind direction and 20 – 100 km across the wind flow. The vertical dimensions are 500 – 1000 m, though vertical dimensions may be even 25 m or 4500 m. The lifespan of CAT is between half an hour and a day (Bakker, 1993). Reports of transport aircraft prove the time span of encountering CAT is limited to about ten minutes. CAT is reported twice as much over land than over sea. This is especially due to mountain-waves (LMG, 1995.). According to Pao and Goldburg (1969b) the clear-air turbulence at high altitude is often sporadic and patchy and does often occur in a strongly stable region. So CAT will not be encountered in each part of a CAT area.
Large-scale phenomena, such as the jet stream, produce shear layers with a length of typically hundreds of kilometers and have a lifetime of a day or more. Because of these vertically sheared stable layers a CAT area can develop with a length of tens of kilometers or more and CAT can last longer than half an hour while it is a micro-scale phenomenon.
CAT is more present in the upper troposphere and lower stratosphere than elsewhere in the free atmosphere and reaches a maximum frequency of occurrence between 10 km (30,000 ft) to 15 km (45,000 ft) (Lester, 1994). On the basis of a large pilot survey over northwestern Europe and the North Atlantic held by Dutton in March and April 1976 (1980), approximately 11% of the distance flown CAT is present in cruise flights, and according to Lester (1994) the probability of a random encounter with CAT of any intensity along a 100 nautical mile (180 km) segment of flight path somewhere in the upper troposphere or lower stratosphere is about 15%. Note that these results are probably entirely based on subjective pilot reports.

2.4.2 Mechanisms of CAT formation

1. Mechanisms

Hopkins (1977) mentions two generally accepted mechanisms which cause turbulence in clear-air: standing waves in the lee of a mountain barrier (mountain-waves) and the Kelvin-Helmholtz instability, which occurs in thin stable layers with strong vertical wind shear. These mechanisms are strongest in the winter months when wind speed and horizontal temperature gradients are largest (Hopkins, 1977; Clear, 2001).
It is thought that the Kelvin-Helmholtz instability is the primary cause of CAT. Theoretical studies and empirical evidence link CAT with Kelvin-Helmholtz instabilities, but some atmospheric scientists

think the majority of CAT occurrences are not explained by the Kelvin-Helmholtz instability. Maybe this instability is only the triggering mechanism (Hopkins, 1977; Keller, 1990; Lester, 1994).
CAT can also be the result of strong shear waves, which are caused by strong winds coming across the tops of thunderstorm clouds (Clear, 2001). Internal gravity waves generated by boundary layer convection, mountains, thunderstorms, and jet streaks may also contribute to CAT production by increasing vertical wind shear, or by breaking of waves (Lester, 1994).
Conclusion is that in general the Kelvin-Helmholtz instability is seen as the main mechanism in the formation of CAT, but also mountain-waves are mentioned. Little proof exists for the importance of other mechanisms in the production of CAT.

2. CAT formation in a layer

It appears that nearly all CAT is reported in areas of small vertical size with large vertical shear and thermally stable layers. The name of such an area is an internal front or a baroclinic zone. Figure 2.3 illustrates the effect of CAT on a layer. Before the onset of CAT a stable lapse rate exists. After the onset of CAT an adiabatic layer bounded by two inversions, an uniform wind speed and a constant water vapour mixing ratio within this layer have formed. This is due to the vertical mixing by eddies which transport heat and momentum. In this way shear and instability should be found near the bottom and the top of the adiabatic layer, thus increasing the turbulence conditions.
A turbulent layer should obtain a larger thickness once it has formed, unless the increased stability near top and bottom of the layer nullifies the increase in shear (Panofsky and Dutton, 1984; Reiter, 1969).

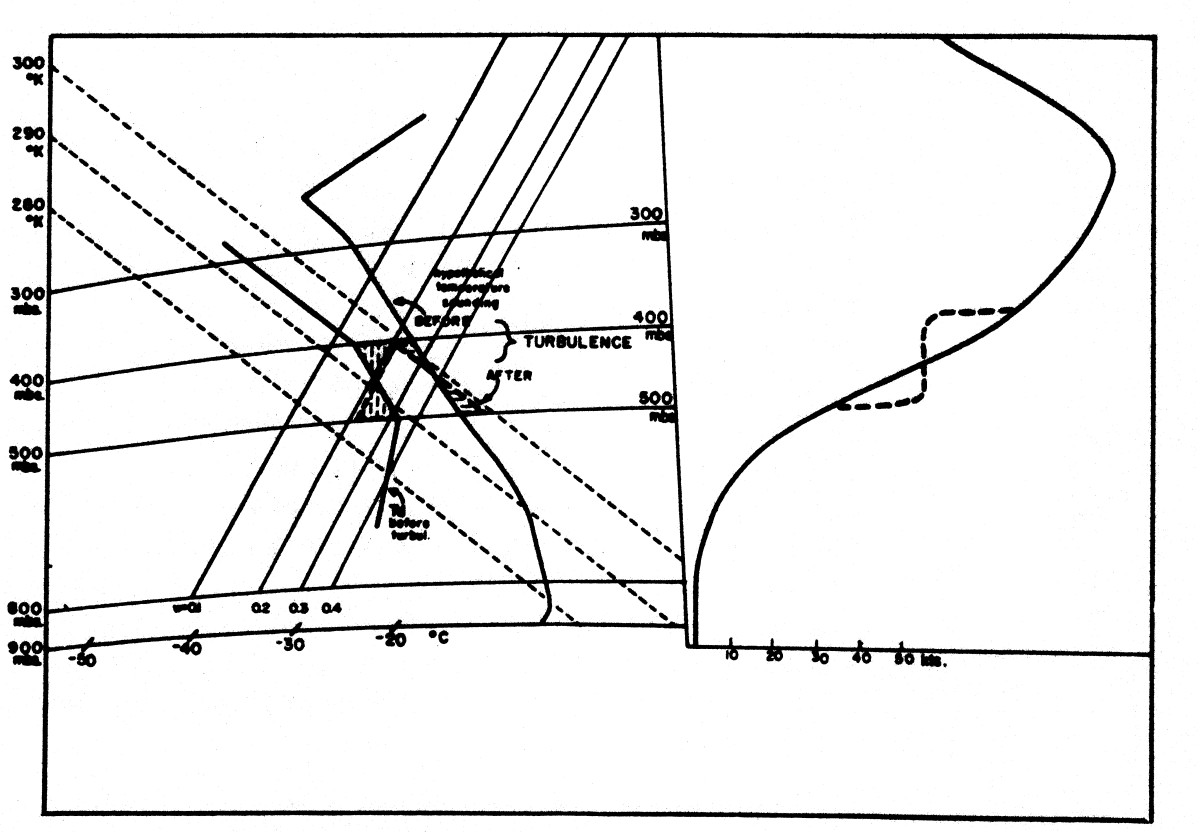

Figure 2.3: Effects of clear-air turbulence on vertical wind, temperature and humidity profiles. Solid lines indicate the situation before the onset of turbulence, striped lines indicate the situation after the turbulent layer has formed (Reiter, 1969).

2.4.3 Kelvin-helmholtz instability

The mechanical energy produced by the vertical wind shear is the energy source of Kelvin-Helmholtz (KH) instability. If turbulence lacks, an initiating process is needed to produce the motions that will get their energy from the velocity shears to produce turbulence. The onset of the KH instability can be hindered by a large static stability unless the vertical wind shear is large enough.

CAT can persist and grow if the energy production is increased by primarly strong vertical wind shears and if the stratification is not so stable that most kinetic energy is used immediately to increase potential energy. Under these conditions turbulence will increase in intensity until the dissipation rate equals the net production rate. Sinks of energy of KH instability are smaller-scale turbulent motion, negative buoyancy of the stable layer, and heat. Presumably large or meso-scale motions create the conditions needed for CAT formation. These motions have to be ageostrophic. Geostrophic motions cannot change the potential temperature gradient. If large-scale motions have produced conditions favourable for CAT, this not always results in CAT (Badgley, 1969; Brown, 1973; Hopkins, 1977).
If the wind velocity changes sharply in the free atmosphere, often a density discontinuity is observed. This is the case for atmospheric fronts, the tropopause layer, inversions above clouds, et cetera. The waves formed in these zones are shearing-gravity waves, also known as KH waves. These waves are caused by the KH instability (Vinnichencko *et al.*, 1980).
In case of CAT these waves have wave heights of 30 to 500 m and wavelengths from about a hundred m to a few km, and create up- and downdrafts, particularly if they break. These up- and downdrafts are experienced as turbulence by aircraft. The waves break in case of a strong vertical wind shear. In the extreme case the more dense air in the wave crest moves over the less dense air in the wave trough. In normally 5 to 30 minutes this unstable situation, caused by the vertical wind shear, is created and ended by the breaking of the wave. Billow clouds (banded clouds) are sometimes formed by thickening of the clouds in the updrafts and dissipation of the clouds in the downdrafts of shearing-gravity waves, and may thus form evidence of a KH instability (Lester, 1994).
Figure 2.4 illustrates a laboratory experiment of a KH wave. Two fluids, water and dyed brine, with a different density move in the opposite direction, thus causing a velocity shear between the layers. This begins in the first picture when the flow is still laminar. If the shear is large enough it causes the flow to become dynamically unstable noticeable by the small waves in the second picture. This is the case if:

$$k\rho_1\rho_2(U_1 - U_2)^2 > g(\rho_1^2 - \rho_2^2) \qquad (2.2)$$

U_1 and U_2 are the velocities of the fluids, ρ_1 and ρ_2 the densities of the fluids, g the acceleration of gravity and k the wavenumber, which is $2\cdot\pi$ divided by the wavelength. Subscript 1 refers to the underlying fluid, subscript 2 refers to the overlying fluid.
After this the waves grow in amplitude and eventually break, thus forming a KH wave (third picture). Then within each wave some lighter fluid is being rolled under denser fluid (fourth picture). This results in static instability. If the waves become larger it costs more work to exchange the lower density fluid with the higher density fluid. So, the more stable the layer, the more work it costs to overcome the gravity. The waves can only become larger if they obtain more kinetic energy from the flow than the energy which is consumed for overcoming the gravity.
The wave in picture four causes on a small scale a large vertical wind shear and an increase in the density gradient, and this brings about a further growth of the unstable layer resulting in a wave that breaks down into small-scale eddies. Now the stage of picture five is reached: the waves have become turbulent due to the static instability and the continued dynamic instability. Finally, in picture six the turbulence is present in a large area and the different fluids are mixed, so some momentum can be exchanged between the fluids thus reducing the shear between the fluids. The sharp interface between the fluids changes into a wider shear layer with smaller shear and static stability. Due to the mixing the shear decreases and the dynamic instability can vanish. In this case the turbulence in the interface region will decay if there are no continued forcings to restore the shear.
Not only in the laboratory by means of fluids but also in the atmosphere these KH waves can sometimes be observed, because in the rising portions of the waves parallel cloud bands (billow clouds) can form. Figure 2.5 gives an example of a KH instability in the atmosphere. The instability can be seen in the tops of cirrus clouds (Glickman, 2000; LMG, 1995; Stull, 1988; Woods, 1969).

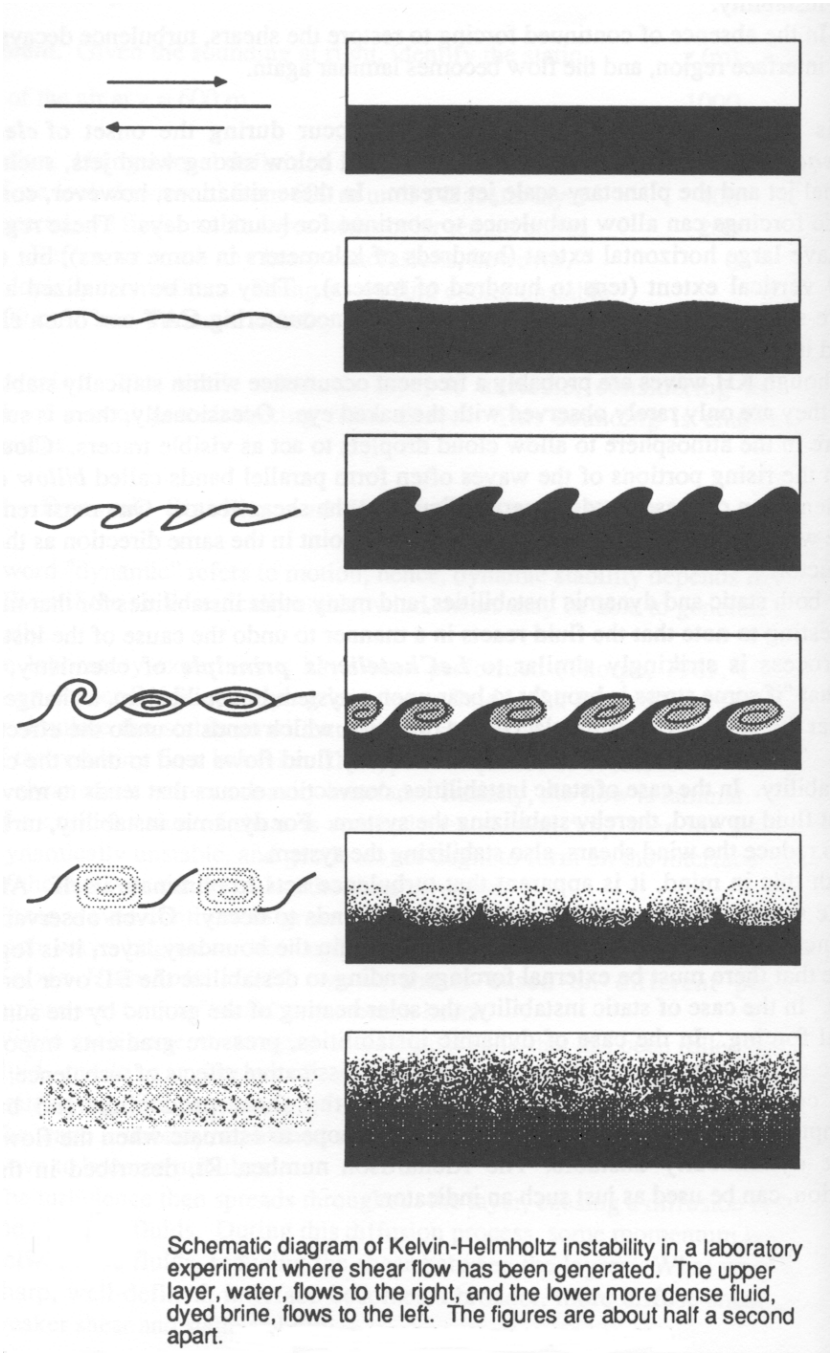

Figure 2.4: Laboratory experiment of a Kelvin-Helmholtz instability (Thorpe and Woods according to Stull, 1988).


Figure 2.5: Kelvin-Helmholtz instability in the tops of cirrus clouds (Clear, 2001).

2.4.4 Mountain-waves

According to Lester (1994) mountain-wave turbulence is: "Turbulence produced in connection with mountain lee waves. It includes high amplitude mountain waves, rotors, turbulence in highly sheared

layers near the tropopause and near the surface, three dimensional wakes behind isolated mountain peaks, and downslope windstorms".
Airflow is changed over mountains by the rising motions of the air on the windward side and the descent of air on the lee side of the mountains. Mountain-waves are usually build up on the lee side. Their wavelength is usually about 10 km, but varies from 2-3 to 40-45 km. Sometimes mountain-waves can be perceived by lenticular (Sc and Ac lenticularis) and billow (Sc and Ac undulatus) clouds. Mountain-waves cause vertical motions of the air and great horizontal wind-velocity fluctuations (Vinnichenko *et al.*, 1980). See Figure 2.6 for an example of an encounter of an aircraft with a severe mountain-wave. In the direction of the wind flow the mountain-wave turbulence zone is generally smaller than is found for CAT caused by the Kelvin-Helmholtz instability. Depending on the length of the mountain ridge, mountain-wave CAT may extend laterally over a larger distance (Houghton, 1985).
Turbulence generated by mountain-waves is generally observed in case of a sufficiently strong wind component normal to a ridge line at the mountain-top level. The shape of the ridge top and the presence of mountain passes seem to affect the mountain-wave production capacity (Hopkins, 1977). A large mountain-wave can create turbulence by two processes:

1. If a mountain-wave becomes sufficiently large, this wave can create vertical shears in itself. In case of a large enough shear, local disturbances can get unstable and develop into turbulence.
2. Overturning instability, which is probably the main process. The mountain-wave amplitude increases to a certain value large enough to reverse the local density variation with height. The result is potentially heavy air over lighter air.

(Long, 1969).

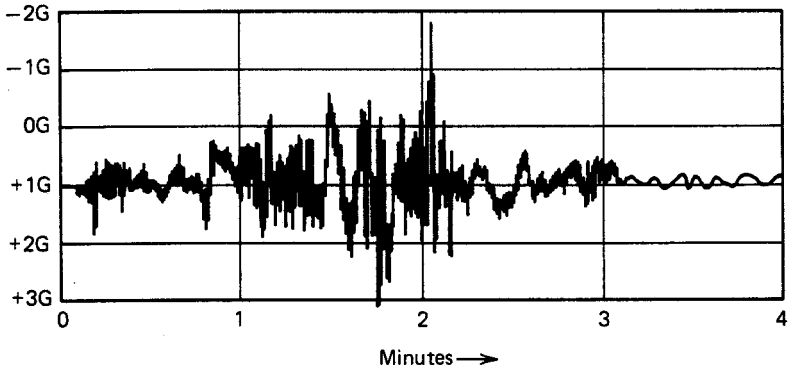

Flight recorder trace of vertical accelerations experienced during a severe turbulence encountered in clear-air turbulence (CAT) by a four-engine turbojet (B-747). This turbulence was generated by a severe mountain wave off the Rocky Mountains east of Helena, Montana. Note that nine excursions to zero gravity (weightlessness) occurred in a period of 1 minute.

Figure 2.6: An encounter of a Boeing 747 with a severe mountain-wave (Houghton, 1985).

The behaviour of airflow over an obstacle depends mainly on:

1. The vertical wind profile
2. The stability structure
3. The shape of the obstacle

Air flowing over a barrier is vertically displaced. On the lee side this displacement is opposed by the restoring force of gravity. Often the air comes above the equilibrium position and vertical oscillations can develop.
If we choose a stable stability structure and a long ridge perpendicular to the airflow, three basic types of flow can be distinguished because of the vertical wind speed profile. Necessary conditions for laminar streaming (picture a in Figure 2.7) are light winds approximately constant with height. Only shallow waves and weak vertical currents develop. In case of somewhat stronger winds and a moderate increase of wind speed with height, standing eddies will form due to the overturning of air on the lee side of the barrier (picture b). If the vertical increase of wind speed becomes even larger, a train of lee waves and wave clouds for 25 km or more downwind will form. These waves are known as stationary gravity waves (picture c, wave streaming). Conditions for lee waves are generally a deep

airflow within 30º of the perpendicular line to the ridge, at most small changes in wind direction with height, and a minimum horizontal wind speed of approximately 7 m s^{-1} at the summit for low ridges (1 km) and 15 m s^{-1} for high ridges (4 km). When the airflow separates from the surface, as is the case for picture b, c, and d, rotor motions develop below the wave crests. Rotors are very turbulent and hazardous to aircraft. Picture d (rotor streaming) gives the most pronounced example of rotor clouds. Convective conditions on the lee slope increase the chance of a separation of the airflow from the surface and so the forming of rotors will be enhanced (Barry, 1992).

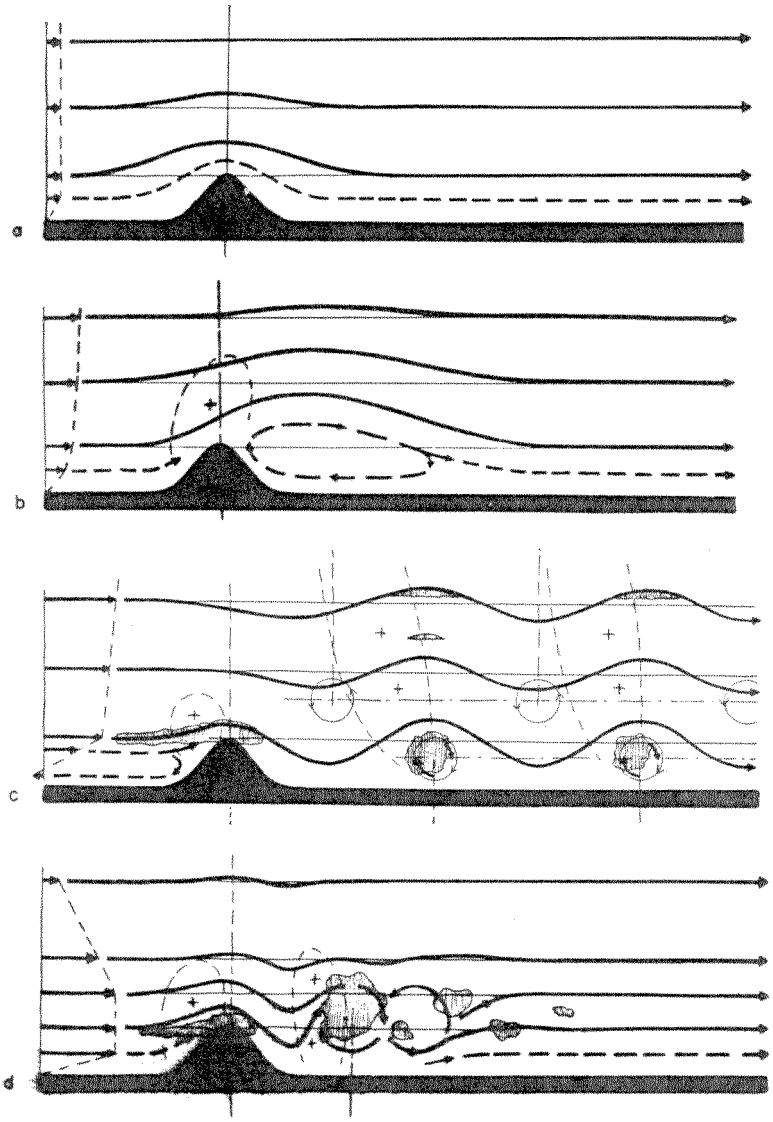

Figure 2.7: Possible types of airflow over a mountain barrier in case of a stable stability structure and a long ridge perpendicular to the flow (Corby according to Barry, 1992).

2.5 Link between CAT and the jet stream and other weather phenomena

One of the places where CAT exist is on the warm side just above an upper-level front, there the atmosphere is stable. When the temperature gradient increases (frontogenesis), the vertical wind shear will also increase according to the thermal wind equation, thus creating the necessary condition for the genesis of the Kelvin-Helmholtz instability. Deformation may increase this temperature gradient (Bakker, 1993).

Many cases of CAT occur in areas with strong horizontal and/or vertical wind shear. On the side of the jet stream with the lowest temperatures, the underside of the jet stream and the area between the jet stream and the tropopause wind shear is large. About 60% of CAT reports is near jet streams. So clear-air turbulence is often related to the jet stream, but not all jet streams contain CAT.

See Figure 2.8 for an overview of the most important turbulence-prone areas between 500 and 200 hPa. Often moderate or severe CAT is coupled with certain cirrus (Ci) boundaries and cloud patterns which visualize jet streams accompanied by large temperature gradients, shears, deformation, atmospheric waves and instability. Usually turbulence is within 3º latitude of the cloud or moisture edge. Transverse Ci bands, Ci "scallops" and billows at jet aircraft cruising level possibly indicate the presence of CAT (LMG, 1995; Meteorological Office, 1971; Meteorological Office College, 1997). According to Ellrod and Knapp (1992) the confluence zone of the polar and subtropical jet-stream branches is a favourable place for CAT. And according to Roach and Bysouth (2002) CAT usually occurs in layers of strong wind shear below and above the cores of temperate-latitude and subtropical jet streams.

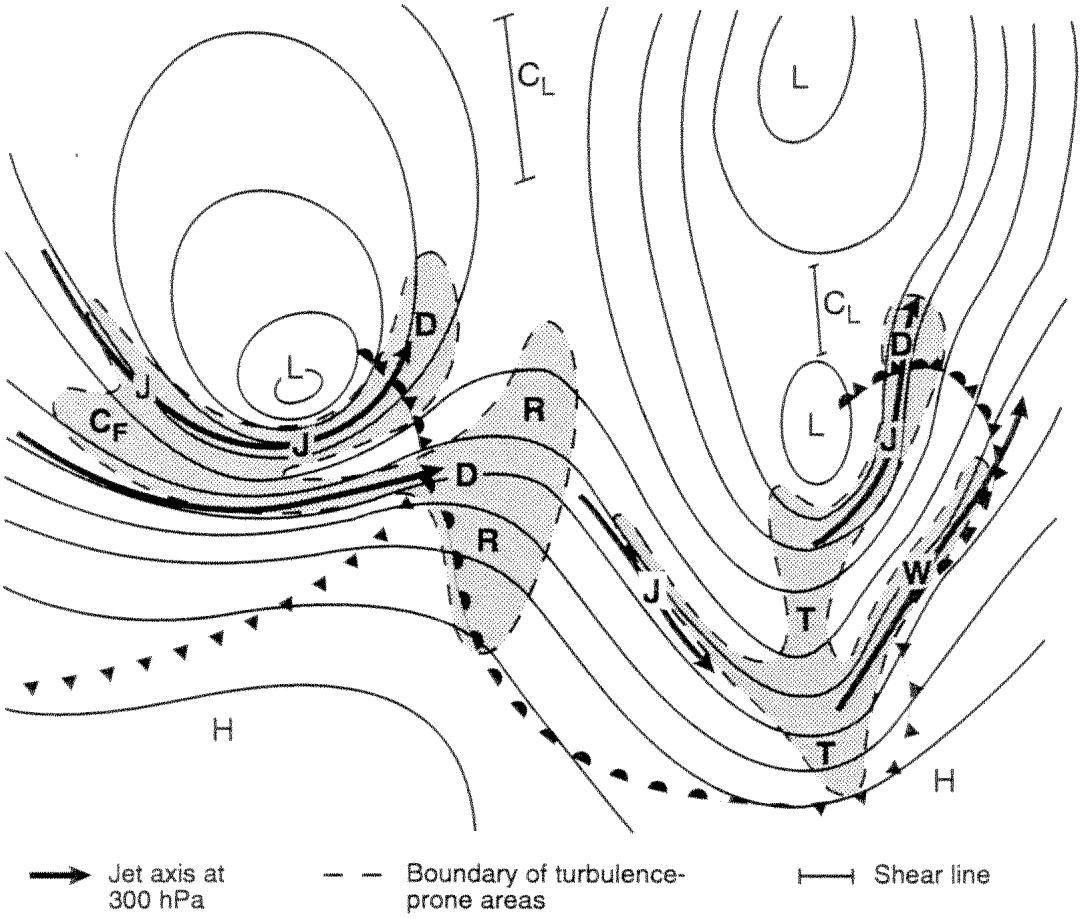

Main turbulence-prone areas between 500 and 200 hPa as related to features of the 300 hPa chart.

—	300 hPa contours. Fronts marked are at surface.
C_F	Region of confluence between two jet streams.
C_L	Upper-air col. Turbulence occurs in narrow bands along marked shear line.
D	Diffluent region of jet stream.
J	Jet-stream turbulence on low-pressure side.
R	Developing upper ridge.
T	Sharp upper trough.
W	Developing wave depression.

Figure 2.8: Main CAT-prone areas between 500 and 200 hPa (Meteorological Office College, 1997).

In midlatitudes the tropopause height often has a discontinuity, with a low northern tropopause and a high southern tropopause which do not connect. This discontinuity is called a tropopause break. The jet stream is often found in the vicinity of a tropopause break, see Figure 2.9.

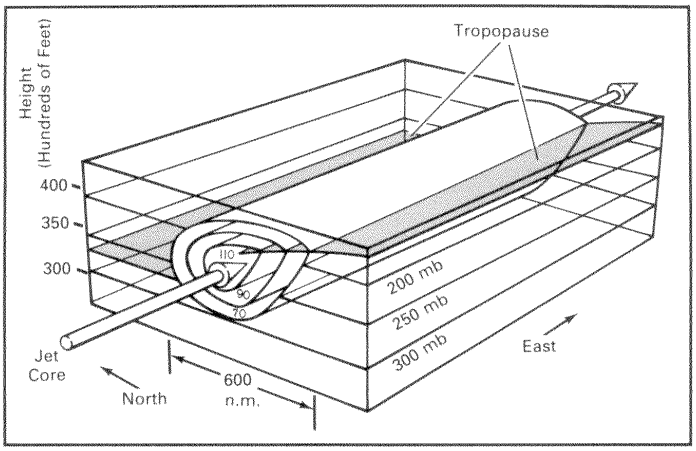

Figure 2.9: Jet stream in relation to tropopause break (Lester, 1994).

In the upper troposphere and lower stratosphere macro-scale waves, the tropopause, jet streams, and jet stream fronts are important in the production of CAT. Macro-scale waves can often be seen on upper-air charts (Lester, 1994).

3 PROBLEMS IN FORECASTING CAT AND THE INFLUENCE OF CAT ON AVIATION

3.1 Introduction

Severe turbulence encountered by aircraft in clear-air at cruising level was acknowledged as a new airline problem in 1946 (Beckwith, 1971). According to the Joint Action Group for Aviation Weather (1999) non-convective turbulence is a major aviation hazard and is possible at any altitude and under quite different weather conditions. It often occurs in relatively clear skies and is then referred to as clear-air turbulence. Regions of convective turbulence in the free atmosphere are nearly always visible by cumulus-type clouds. Severe convective turbulence is generally in regions with liquid drops or ice crystals that can be identified by radar and therefore aircraft can largely avoid it. Since CAT usually occurs without the appearance of clouds, except in mountain-waves, it cannot be avoided by visual observation. Pilots are hardly or not warned in advance until the aircraft comes into the edge of the CAT zone. This unexpected and sudden occurrence of CAT is particularly problematic. Although, sometimes a few minutes of undulation are present before the sudden start of CAT (Bass, 1999a; Houghton, 1985; Panofsky and Dutton, 1984).
The average continuous time an aircraft flies in a patch of light or greater CAT is approximately 16 minutes and the average continuous flight time in severe or greater CAT is just a few minutes (Lester, 1994). Often CAT is only a nuisance, but sometimes CAT causes structural damage to aircraft, injures passengers, and can even cause fatalities (Hopkins, 1977).
The quality of the current CAT forecasts will be examined in 3.2. In 3.3 the influence of CAT on aviation will be discussed with emphasis on the influence on the aircraft and the influence on the humans in the aircraft.

3.2 Problems in forecasting CAT

3.2.1 Recognition of CAT on satellite images

Satellite images may sometimes give useful clues to the presence of CAT. Signatures in infrared, visible and water vapour imagery are present for most large CAT outbreaks. The signatures which are considerable common in infrared and visible imagery are transverse cirrus cloud banding, oriented perpendicular to the wind direction. These transverse clouds can often be found on the equatorward side of the subtropical jet stream (Ellrod, 2000). Other wave clouds which can reveal the presence of CAT are billows, which are regularly spaced and narrow patterns in cirrus or middle level clouds. Like transverse cloud bands, they are also oriented perpendicular to the wind direction. Transverse bands distinguish themselves from billows by being more irregular, their larger spacing and their larger width. Transverse bands usually belong to the low latitude subtropical jet stream, and they indicate large vertical and maybe horizontal wind shears. Billows in cirrus clouds may indicate a Kelvin-Helmholtz instability is present (Ellrod, 1989).
Deformation can produce CAT. Cloud or moisture edges along the stretching axis of the deformation zones can reveal the presence of such a zone and therefore of CAT. Also darkening of water vapour images in time often indicates moderate or greater turbulence (Ellrod, 2000). See Figure 3.1 for an example of cloud features which may indicate the presence of CAT.
The information above regards CAT which is not related to mountain-wave activity. According to Ellrod (1989) turbulence in mountainous regions may occur without any noticeable image features. Although CAT can sometimes be derived from satellite images, according to Knox (2001) the detection of CAT with remote sensing is very difficult and not performed operationally. So satellite images seem to be of limited use in predicting CAT.

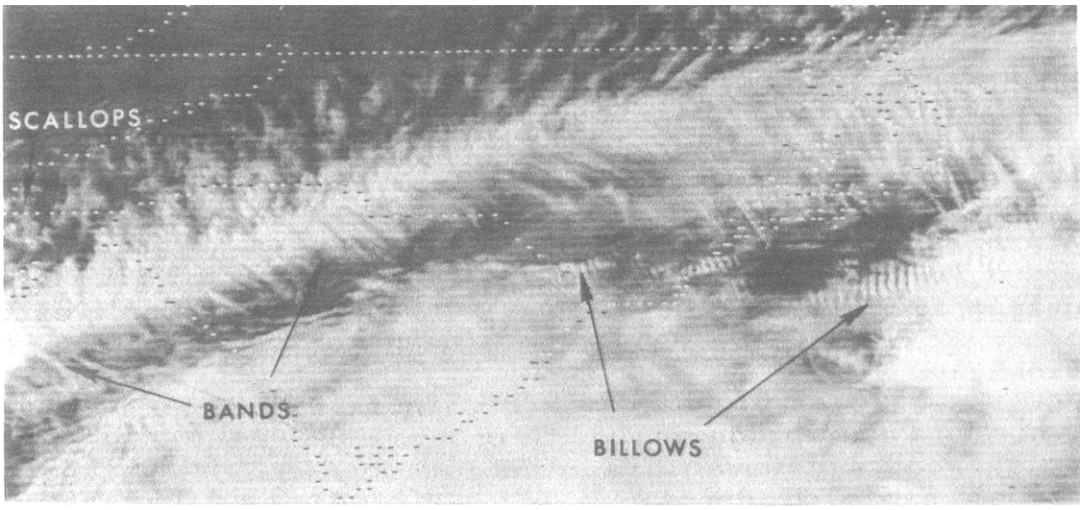

Figure 3.1: GOES visible image of transverse bands and billows, not to be confused with billow clouds which cannot be seen on a satellite image (Ellrod, 1989).

3.2.2 Forecasting methods of CAT

CAT is generally a micro-scale phenomenon. CAT has small temporal and spatial dimensions. To predict CAT macro- or synoptic scale meteorological features are used, because micro-scale features are harder or impossible to predict (Hopkins, 1977). Turbulence associated with mountain-wave activity can be predicted rather well, but other CAT is more difficult to forecast, for instance associated with tropopause surfaces, troughs, and upper fronts (Bass, 1999a). Vinnichenko *et al.* (1980) state that no reliable methods of predicting clear-air turbulence in the atmosphere exist, this being mainly caused by the absence of a well-developed theory of clear-air turbulence. According to Ellrod (1989) CAT changes quickly in character with time and often is not detected by the upper-air observing network.

The occurrence of CAT in time and space is rather changeable, which hinders forecasting. In general only Significant Weather Charts (SWC) contain a CAT forecast. A SWC gives areas and levels in which CAT theoretically may occur. Often hardly any or no CAT is encountered in these areas, so these forecasts are likely to be taken less serious (LMG, 1995). According to Lester (1994) probabilities of encountering significant turbulence in a forecasted CAT area will be small, even when the forecaster is aware that large-scale conditions are favourable.

In this report numerical model predictions of CAT are verified, the Turbulence Index (TI) as developed by Ellrod and Knapp (1992), is one of the indices to be verified. Ellrod and Knapp (1992) state that the TI cannot successfully predict every case of CAT, but it often alerts forecasters to areas that normally would not be considered high-turbulence threat regions. Other research (McCann, 1993; Turner and Bysouth, 1999) also indicates the limitations of CAT indices based on respectively rawinsonde data and numerical model output.

CAT is not visible and not detectable by contemporary technology in aircraft. Systems such as LIDAR and X-band radar have to be improved to increase their range and ability to detect CAT (Matthews, 2001).

The conclusion is that no reliable CAT prediction or detection seems to exist at present.

3.3 Influence of CAT on aviation

3.3.1 Influence on the aircraft

The influence of atmospheric turbulence on an aircraft is noticeable by vibrations, jolts and severe vertical and horizontal accelerations. If and in which way turbulence is experienced depends on size, construction and velocity of the aircraft, but also on the size of the eddies and the velocity of the turbulent movement. Though, it is difficult to determine if a sudden force on the aircraft is caused by unordered air movements or by (nonturbulent) flow changes over a short distance (LMG, 1995).

Lester (1994) distinguishes two models to explain why an aircraft encounters turbulence: the eddy model and the wave motions model.

1. The eddy model

It is assumed the eddy maintains its shape and circulation as the average wind transports this eddy (see Figure 3.2). When there is a change of wind with height with the presence of such an eddy, the eddy will transport faster horizontal winds downward ahead of the eddy and slower horizontal winds upward behind the eddy. This eddy also creates gustiness in the vertical winds. Figure 3.3 shows three different patterns of vertical motions. The aircraft's speed is much higher than the speed of the eddies moving downwind. Figure 3.3 shows that the character of the turbulence as experienced by the aircraft depends on the size of the eddies and the speed of the aircraft. Further, turbulence can also manifest itself by wave motions.

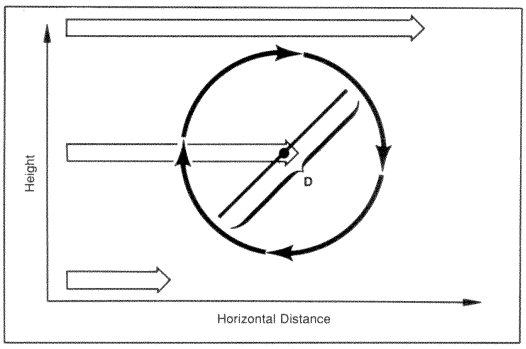

Figure 3.2: Simplified eddy structure (Lester, 1994).

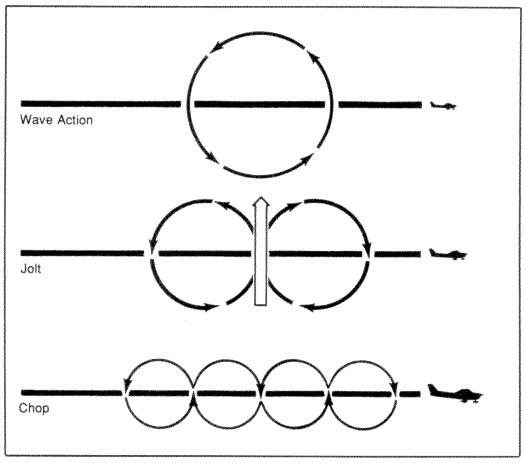

Figure 3.3: Effect of eddies with varying sizes (Lester, 1994).

2. The wave motions model

Wave-like disturbances are common in the atmosphere. Figure 3.4 shows three motions of varying wavelength. The magnitude of vertical motions increases as the wind relative to the wave increases or as the ratio of wave amplitude and wavelength increases. The eddy model and the wave model are only crude approximations of actual turbulence structures (Lester, 1994).

An aircraft responds only to a relatively narrow portion of the turbulence spectrum. In the case of long-period disturbances an aircraft adjusts itself to the air motion. And high-frequency disturbances are practically unnoticed. Intense clear-air turbulence generally causes a very rapid loss of height. Pilots cannot always stop the dive. Figure 3.5 gives an example. A Boeing 720B experienced clear-air turbulence over the western U.S. during approximately 4 minutes, of which some 30 seconds in very severe turbulence with deviations from the acceleration of gravity (g) of +2.0-2.8g. In these 4 minutes the air speed varied between 505 to 575 km/h and the aircraft descended around 2 km (Vinnichenko *et al.*, 1980).

Aircraft can be influenced by atmospheric motions on all scales, but in general micro-scale motions cause the turbulence noticed in aircraft. Within this micro-scale a small range of sizes of circulations, known as the critical range, constitute important turbulence. Eddies smaller than the critical range do not have enough time to influence the lift of the aircraft, while for eddies larger than the critical range the influence of a gust is more spread out in time. Within the critical range, sensitivity to turbulence diminishes with wing loading and rises with altitude and air speed. This implies that turbulent eddies of the same size and strength may have different impacts on different aircraft (Lester, 1994).

According to Schairer and Hollingsworth (1969) the characteristics of clear-air turbulence can be of importance in the design for structural strength and for stability and control characteristics of aircrafts and aerospace vehicles.

Clear-air turbulence has a large impact on the efficiency of flight operations because of rerouting and delays. Diversions en route lead to additional fuel and other costs for all types of aircraft (Joint Action Group for Aviation Weather, 1999). Encountering and avoiding incidents can cost money (Bysouth, 2000).

The breaking of shearing-gravity waves is an important cause of CAT. In very stable conditions these waves may cause a large temperature variation in a short distance which can influence the engine performance at high altitudes (Lester, 1994).

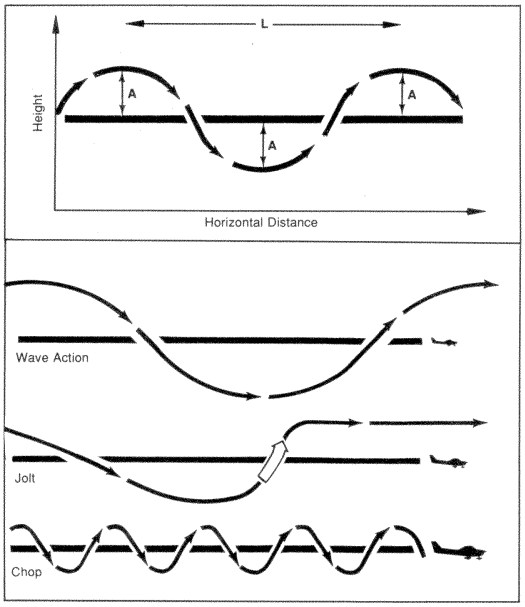

Figure 3.4: Effect of different wave motions (Lester, 1994).

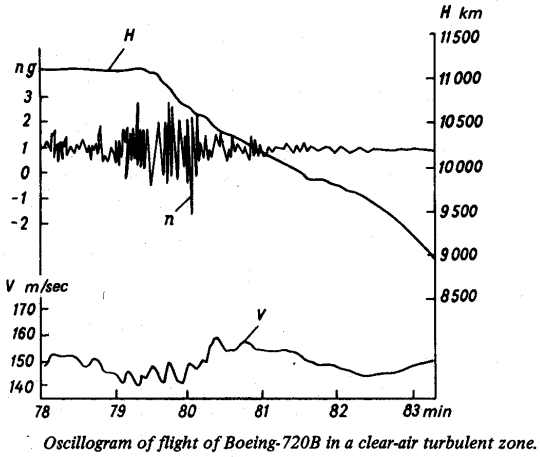

Figure 3.5: An aircraft encountering clear-air turbulence. *V* is the air speed, *H* the height, and *n* the vertical acceleration of the aircraft plus the acceleration of gravity (Vinnichenko *et al.*, 1980).

3.3.2 Influence on humans

Pilot performance is negatively influenced by turbulence, depending on the intensity of the turbulence, the rapidity of onset of the turbulence, and the frequency of the turbulence. Light turbulence causes passenger and crew discomfort (Lester, 1994). In commercial passenger aircraft non-convective turbulence seldom causes passenger fatalities. The number of turbulence-related injuries is not clear, since airlines do not have to report such incidents unless in case of flight attendant injury, severe passenger injuries or death (Joint Action Group for Aviation Weather, 1999). Often CAT is only a nuisance, but CAT can cause structural damage to aircraft, passenger injury, and even fatalities (Hopkins, 1977). From 1981 through 2000 there were 156 turbulence accidents (wake turbulence excluded) with U.S. air carriers, of which just 3 caused substantial damage to aircraft. In this period just 3 fatalities of the total 2,944 fatalities in airline operations are attributed to turbulence, but turbulence caused 218 of the 802 serious injuries, and approximately 1600 minor injuries. Since 1995 the number of turbulence accidents has increased sharply. Turbulence accidents would almost not occur if occupants were seated and properly secured. These statistics regard all types of turbulence, while CAT only accounts for up to 20 percent of the 156 turbulence accidents (Matthews, 2001). But the main cause of injuries in non-fatal airline incidents is CAT. In 1999 131 U.S. commercial airline passengers and crew members were injured by CAT (Morrison according to Knox, 2001).
Avoidance of moderate to severe turbulence is both a safety and an economic issue. The costs of passenger and cabin crew injuries are significant (Lindsey, 1998). Insurance claims can be much higher in the United States than in Europe, as a result of which the flight safety and so the avoidance of dangerous weather has large priority (Hemink and Verbeek, 1997).
Bass (1999a) states encounters with CAT continue to influence significantly the safety and efficiency of commercial aviation.

4 TURBULENCE INDICES

4.1 Introduction

Many clear-air turbulence indices exist, and seven of them are used in this report. First we will explain why the forecasts these indices give have to be verified again and why these indices have been chosen. The chosen indices are frontogenesis, TI1, TI2, Brown index, vertical wind shear (VWS), horizontal wind speed, and Dutton index.
Deformation and convergence are important components of some of the chosen indices, so these terms will be explained in 4.3. Also the derivations and/or equations of the different chosen clear-air turbulence indices are given, and finally some attention is paid to the calculation of these indices from numerical model data.

4.2 Choice of the clear-air turbulence indices and why their forecasts are verified

Although many other CAT indices exist, versions of the Turbulence Index (TI) developed by Ellrod and Knapp (1992) are tested most extensively in this report. Reason to test the TI is that one version, the TI1, is already in use at KNMI for several years. At KNMI output of the ECMWF model is used to calculate TI1. The T1I distribution can be visualized by the aviation meteorologist on a meteorological workstation (MWS), so forecasted CAT areas become visible. Also the Aviation Weather Center (AWC) in the U.S. calculates a version of the TI, the TI2 (Aviation, 2002).
Using TI Ellrod and Knapp (1992) found a probability of detection (POD) which varied from 70% - 84%, but a false-alarm ratio (FAR) in the range of 22% - 40% for different versions of the TI. They did not use nonturbulence observations to get an impression of the overestimation of the index. Important is that the TI only accounts for CAT related to the jet stream and upper fronts and does not account for mountain-waves or thunderstorm turbulence (Clear, 2001). The TI has been verified in other studies (Ellrod and Knapp, 1992; de Villiers and van Heerden, 2001). Reasons to verify numerical clear-air turbulence forecasts again:

1. As far as the author knows, until now clear-air turbulence indices have only been tested while they are calculated with output from other models than the ECMWF model. The latter is used at KNMI to calculate the TI1. Another model resolution can imply that the threshold values of moderate and severe turbulence can become different (de Bruijn, pers. com). Bakker (1993) used the threshold values determined for the NMC global aviation model (AVN) for a small test of the TI based on analyses of the ECMWF. Bakker (1993) used the same threshold values since the horizontal resolution of the ECMWF model was about the same as for the AVN model. But the performance of the index based on ECMWF forecasts was never tested. Nowadays the ECMWF data received at KNMI still has a horizontal resolution of 1.5º, though the ECMWF model itself has a resolution of 0.5º and that is much higher than the resolution in 1993.
2. Nowadays more objective observations, instrumented aircraft reports (AMDAR/ASDAR), are available. Many verifications of clear-air turbulence indices have been done by comparison with pilot reports, which are subjective. Only some verifications used instrumented aircraft reports.
3. The TI1 is hardly used at KNMI due to unfamiliarity with the existence and the quality of the index. Often first a PIREP (pilot report) of turbulence has to be received before a clear-air turbulence warning is given. A new verification of the TI1 could take away this unfamiliarity (Hemink, pers. com.).

Because the TI1 is used at KNMI it will be verified. Since leaving out the convergence term is physically incorrect, the TI2 which includes the convergence term will also be calculated. TI1 and TI2 can be derived physically from a frontogenesis equation, but due to the many assumptions they are in fact empirical indices. To test a physically more correct index, the frontogenesis will also be calculated.
Based on aircraft measurements and radiosonde profiles significant CAT is among others more prevalent in regions of vertical wind shear (speed and directional) (Ellrod and Knapp, 1992).

Therefore we decide to calculate the vertical wind shear (speed and directional) alone. The Dutton index and the Brown index sometimes perform reasonably well compared to other indices and are also calculated (Dutton, 1980; Turner and Bysouth, 1999). Since often CAT is related to the jet stream, it may be expected CAT relates well to the horizontal wind speed. So, horizontal wind speed is also calculated.

4.3 Background information: deformation and convergence

4.3.1 Deformation

A description of deformation is: a kinematic property of the flow that tends to transform an original circle of fluid into an elongated elliptical shape.
Deformation is important in producing or destroying horizontal temperature gradients and therefore upper-level frontal zones. Deformation is a property of a flow and can be found in cols, troughs and the exit region of the jet stream.
Deformation consists of the deformation by horizontal stretching (s^{-1}) :

$$D_{st} = \frac{\partial u}{\partial x} - \frac{\partial v}{\partial y} \tag{4.1}$$

and the deformation by horizontal shear (s^{-1}):

$$D_{sh} = \frac{\partial v}{\partial x} + \frac{\partial u}{\partial y} \tag{4.2}$$

u: Easterly component of the wind (m s^{-1})
v: Northerly component of the wind (m s^{-1})

These two forms of deformation can cause an increase in the horizontal temperature gradient.

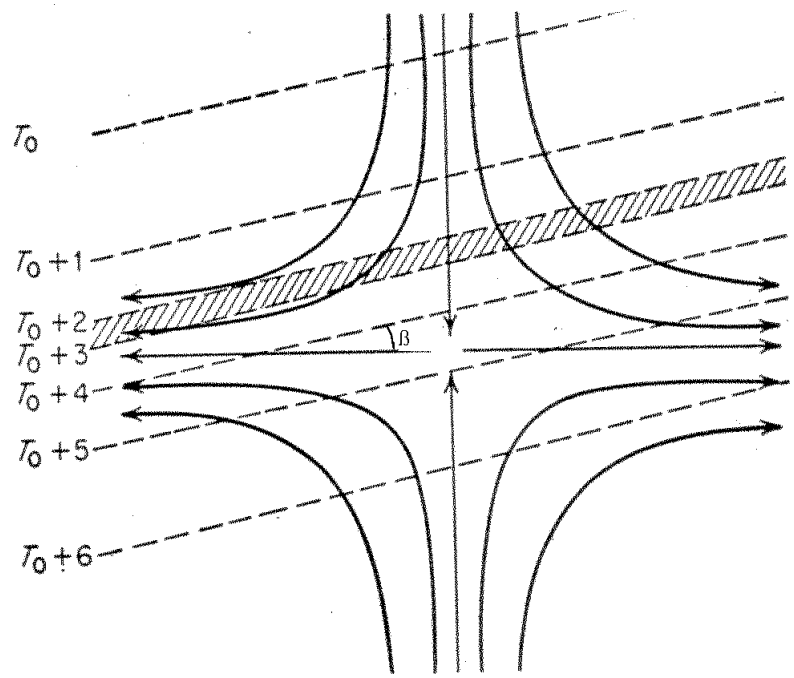

Figure 4.1: Example of a field of deformation and example of frontogenesis. The hatched line is the line of frontogenesis and moves toward the axis of dilation (the horizontal line), while the temperature contrast increases (Petterssen, 1956).

The total deformation is defined by:

$$D = (D_{st}^{\ 2} + D_{sh}^{\ 2})^{1/2} \tag{4.3}$$

By increasing the horizontal temperature gradients, deformation strengthens upper-level frontal zones, thereby increasing the chance of CAT occurrence. Figure 4.1 gives an example of a deformation field (Ellrod and Knapp, 1992; Mancuso and Endlich, 1966; Reap, 1996).

4.3.2 Convergence

Ellrod and Knapp (1992) define convergence as "the compaction of a fluid caused by the confluence of streamlines and/or deceleration of air parcels". If we assume that the atmosphere is an incompressible fluid, air must ascent or descent in regions of convergence. Convergence increases frontogenesis and by disturbing the tropopause inversion gravity waves may be created, which may start the development of a Kelvin-Helmholtz instability. See Figure 4.2 for some examples of convergence (Ellrod and Knapp, 1992).

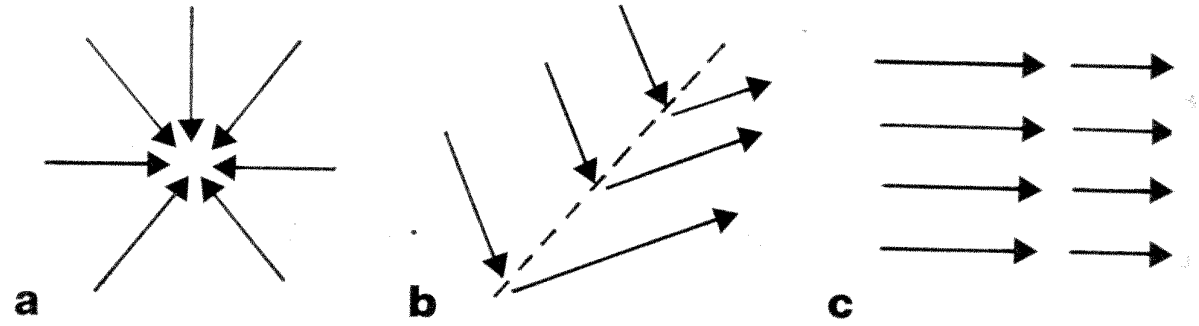

Figure 4.2: (a) Pure convergence at a point, (b) convergence resulting from a sharp change in wind direction at a trough line, (c) "speed" convergence resulting from decelerating flow, as in the exit region of the jet (Ellrod and Knapp, 1992).

4.3.3 Explanation of D_{sh}

Figure 4.3 gives an idealized example how a horizontal wind shear can increase the temperature gradient. See the left picture: a southwesterly wind (upper arrow) gives cold advection and an northeasterly wind (lower arrow) advects warm air. Since these winds are opposite to each other and advect air with a different temperature, the isotherms tilt (see right picture in Figure 4.2) and the perpendicular distance between the isotherms decreases, meaning the temperature gradient increases (Bakker, 1993).

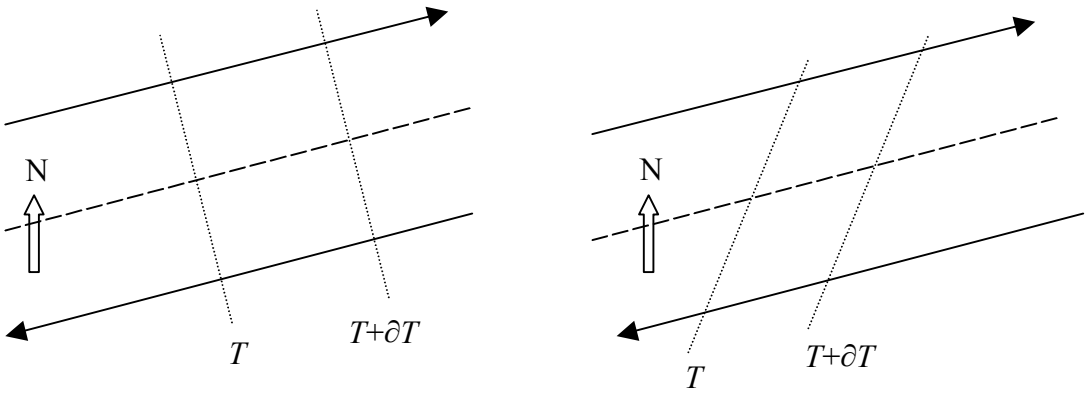

Figure 4.3: Example of deformation by horizontal wind shear. Large arrows indicate the wind direction, dotted lines isotherms and striped lines the axis of shear. Left picture is valid for *t*, right picture is valid for *t*+d*t*.

4.3.4 Explanation of D_{st}

Figure 4.4 gives an example of horizontal stretching increasing the temperature gradient in part of the field. In the left picture we assume a certain horizontal temperature gradient. The arrows indicate the flow of the air in different regions. Because of the flow the isotherms will accumulate in the right undercorner (see right picture) and the temperature gradient will weaken in the right uppercorner because of the large speed of the flow. So in this case deformation leads to an increase in the temperature gradient near the axis of dilatation (Bakker, 1993).

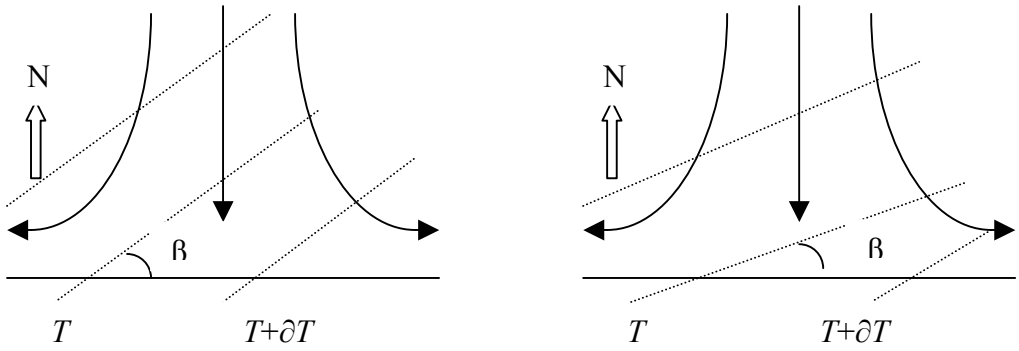

Fig. 4.4: Example of deformation by horizontal stretching. Large arrows indicate the wind direction, dotted lines isotherms and the horizontal line is the axis of dilatation. Left picture is valid for *t*, right picture is valid for *t*+d*t*. β is the angle between isotherms and axis of dilatation.

4.4 Derivation of frontogenesis

In this section we derive the frontogenesis equation as given by Petterssen (1956). This is of importance since we want to use the frontogenesis as a clear-air turbulence index.

A front or a frontal surface is a sloping quasi discontinuity in the density field. Frontogenesis is a tendency toward formation of a discontinuity or intensification of an existing zone of transition. In case of frontolysis this tendency is negative. The pressure being continuous, any process that tends to create a discontinuity in density will create one in temperature and potential temperature also. Frontogenesis is primarily a kinematical phenomenon. If air masses from different and distant source regions come together, a front will form. Often physical and dynamical processes (radiation, conduction, mixing et cetera) will counteract this kinematical frontogenesis. These non-conservative processes will be neglected.

We make the assumption that motion is adiabatic implying potential temperature is conserved ($\frac{d\theta}{dt} = 0$). Now, frontogenesis can only result from horizontal and vertical confluence. See Figure 4.5.

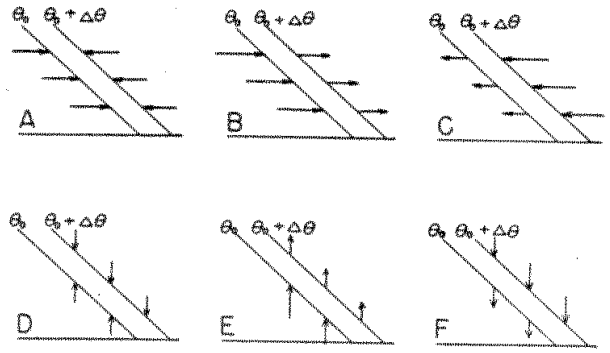

Figure 4.5: Horizontal (A - C) and vertical (D - F) confluence associated with frontogenesis (Petterssen, 1956).

In the derivation we consider a line along which the frontogenesis takes place, namely the line of frontogenesis, which may be stationary or moving, and curved or straight. We define $|\nabla\theta|$ as the magnitude of the gradient of potential temperature (K m^{-1}), and $\frac{\delta}{\delta t}$ is the time differentiation in a

system of co-ordinates which is fixed to a particle of the moving line of frontogenesis. The intensity of frontogenesis (K m^{-1} s^{-1}) is then defined by:

$$F = \frac{\delta|\nabla\theta|}{\delta t} \tag{4.4}$$

So, frontogenesis ($F > 0$) means an increase in the potential temperature gradient. $|\nabla\theta|$ must increase more rapidly on the line of frontogenesis than elsewhere, so F has to be maximum on this line. If we choose a n-axis which crosses the line of frontogenesis perpendicular, F is maximum on the line of frontogenesis for:

$$\frac{\partial F}{\partial n} = 0 \quad \text{and} \quad \frac{\partial^2 F}{\partial^2 n} < 0 \tag{4.5}$$

The adiabatic assumption, the conservative assumption ($\frac{d}{dt} = 0$) and the assumption the vertical motion may be neglected along the earth's surface yields the following equation for the change of potential temperature in time:

$$\frac{\partial\theta}{\partial t} = -\vec{v} \cdot \nabla_h \theta \tag{4.6}$$

$\vec{v}$: Horizontal wind (m s^{-1})
$\nabla_h\theta$: Horizontal temperature gradient (K m^{-1})

At sea level air is forced to move horizontally, so frontogenesis is caused by horizontal movements. In the free atmosphere vertical movements can contribute significantly to frontogenesis. Note we will use the frontogenesis in the free atmosphere, so the assumption that vertical motion is neglected can give a significant error.
The line of frontogenesis must be a substantial line consisting of the same particles, otherwise the frontogenetical effect would steadily act on new air particles, and there would be no frontogenesis.
If all the above mentioned conditions are fulfilled, a front could form depending on the intensity (F) and the duration of the process.

Time differentiation $\frac{\delta}{\delta t}$ in a moving system of co-ordinates is given by the symbolic equation:

$$\frac{\delta}{\delta t} = \frac{\partial}{\partial t} + \vec{V} \cdot \nabla \tag{4.7}$$

$\vec{V}$: velocity of the system of co-ordinates.

If we assume the potential temperature gradient from Eq. 4.4 is only horizontal and combine this with Eq. 4.7 we obtain:

$$F = \frac{\partial|\nabla_h\theta|}{\partial t} + \vec{V} \cdot \nabla|\nabla_h\theta| \tag{4.8}$$

To obtain an expression which is independent of the time variation we assume conservation of θ ($\frac{d\theta}{dt} = 0$), and substitute Eq. 4.6 in Eq. 4.8:

$$F = \frac{-\nabla_h\theta \cdot \nabla\vec{v} \cdot \nabla_h\theta - \nabla_h\theta \cdot \nabla_h\nabla_h\theta \cdot (\vec{v} - \overrightarrow{V})}{\left|\nabla_h\theta\right|} \tag{4.9}$$

Which is the rate at which the magnitude of the ascendant of θ increases per unit time in a moving system of co-ordinates, θ being a conservative property.

Now we interpret $\vec{V}$ as the velocity of a substantial line, for example the line of frontogenesis, and assume the line moves with the wind $\vec{v}$, so assume:

$\vec{v} = \vec{V}$

Substituting this in Eq. 4.9 gives:

$$F = -\frac{\nabla_h\theta \cdot \nabla\vec{v} \cdot \nabla_h\theta}{\left|\nabla_h\theta\right|} \tag{4.10}$$

Then we make the assumption that the field of motion is linear: the distribution of $\vec{v}$ can be represented by a Taylor series. The linear terms of this serie generally predominate in a restricted area. Neglecting second and higher order terms of the Taylor series, a linear field of motion is given by:

$$u = u_0 + \left(\frac{\partial u}{\partial x}\right)_0 x + \left(\frac{\partial u}{\partial y}\right)_0 y \tag{4.11}$$

$$v = v_0 + \left(\frac{\partial v}{\partial x}\right)_0 x + \left(\frac{\partial v}{\partial y}\right)_0 y \tag{4.12}$$

u_0 and v_0 are respectively the wind speed components in the x- and y-direction at a chosen origin and represent the mean wind, which can be related to the displacement of weather systems.

Eq. 4.11 and Eq. 4.12 can also be written as:

$$u = u_0 + 0.5(-C_{vg} + D_{st})x + 0.5(D_{sh} - \zeta)y \tag{4.13}$$

$$v = v_0 + 0.5(D_{sh} + \zeta)x + 0.5(-C_{vg} - D_{st})y \tag{4.14}$$

In which the rotation or vorticity (s^{-1}) is: $\zeta = \frac{\partial v}{\partial x} - \frac{\partial u}{\partial y}$ (4.15)

The terms C_{vg}, D_{st}, D_{sh}, and ζ are the perturbation terms, which determine together with the vertical wind shear the evolution of weather systems.

If the system of co-ordinates is rotated a certain angle ψ such that $D_{sh} = 0$, which means the x-axis has been chosen along the axis of dilatation, Eq. 4.13 and Eq. 4.14 become:

$$u = u_0 + 0.5D_{st}x - 0.5C_{vg}x - 0.5\zeta y \tag{4.16}$$

$$v = v_0 - 0.5D_{st}y - 0.5C_{vg}y + 0.5\zeta x \tag{4.17}$$

Since D is constant for a varying co-ordinate system, and consists of the terms D_{sh} and D_{st}, this rotation may be applied.

Eq. 4.16 and 4.17 can be written in vector notation:

$$\vec{v} = \vec{i}\left(u_0 + 0.5(D_{st} - C_{vg})x - 0.5\zeta y\right) + \vec{j}\left(v_0 + 0.5(-D_{st} - C_{vg})y + 0.5\zeta x\right) \tag{4.18}$$

The vector notation of the horizontal potential temperature gradient may be written as:

$$\nabla_h \theta = \left|\nabla_h \theta\right|(a\vec{i} + b\vec{j}) \tag{4.19}$$

Substituting Eq. 4.18 and Eq. 4.19 in Eq. 4.10 gives:

$$F = -0.5\left|\nabla_h \theta\right|\left(D_{st}(a^2 - b^2) - C_{vg}\right) \tag{4.20}$$

We define α as the angle from the *x*-axis (which is in this case the axis of dilatation) to the vector $\nabla\theta$, and the angle β as the angle from the *x*-axis to the isotherms of potential temperature. Then:

$$a = \cos(\alpha) = -\sin(\beta)$$
$$b = \sin(\alpha) = \cos(\beta)$$

and then:

$$a^2 - b^2 = \sin^2(\beta) - \cos^2(\beta) = -2\cos^2(\beta) + 1 = -\left(\cos(2\beta) + 1\right) + 1) = -\cos(2\beta) \tag{4.21}$$

Substituting Eq. 4.21 in Eq. 4.20 yields the frontogenesis equation we wanted to derive, which calculates the intensity of frontogenesis:

$$F = 0.5\left|\nabla_h \theta\right|(D\cos(2\beta) + C_{vg}) \tag{4.22}$$

F: Intensity of frontogenesis (K m^{-1} s^{-1})
$|\nabla_h \theta|$: Magnitude of the horizontal gradient of potential temperature (K m^{-1})
D: Deformation (s^{-1})
C_{vg}: Convergence (s^{-1}), $-(\frac{\partial u}{\partial x} + \frac{\partial v}{\partial y})$
β: The angle from the axis of dilatation to the isotherms of potential temperature (º)

Since *D* does not change in case of a rotated co-ordinate system, D_{st} is equal to *D*, and has been replaced by *D*. Only the divergent and the deformative components of the field of motion can produce frontogenesis. If β is within 45º, the pre-existing temperature gradient increases (frontogenesis), otherwise it weakens (frontolysis). See Figure 4.1 for an example of frontogenesis. This pattern can seldom be found on weather maps, because in general the mean wind speed changes the pattern. Thus we have obtained the frontogenesis which will be used as a clear-air turbulence index, and will be used in the derivation of the TI1 and TI2 (Petterssen, 1935; Petterssen, 1956; Saraber, 1999).

4.5 Derivation of TI1 and TI2

Approximate thermal wind relationship is given by:

$$\frac{\partial T}{\partial y} = -\frac{f_c T}{g}\frac{\partial U_g}{\partial z} \tag{4.23}$$

$$\frac{\partial T}{\partial x} = + \frac{f_c T}{g} \frac{\partial V_g}{\partial z} \tag{4.24}$$

T: Temperature (K)
f_c: Coriolis parameter (s^{-1})
g: Acceleration of gravity ($m\ s^{-2}$)
U_g: u-component of geostrophic wind ($m\ s^{-1}$)
V_g: v-component of geostrophic wind ($m\ s^{-1}$)
(Stull, 1988)

The magnitude of the horizontal temperature gradient is then given by:

$$\left|\nabla T\right| = \left(\left(\frac{\partial T}{\partial x} \right)^2 + \left(\frac{\partial T}{\partial y} \right)^2 \right)^{0.5} = \left(\frac{f_c^2 T^2}{g^2} \left(\left(\frac{\partial U_g}{\partial z} \right)^2 + \left(\frac{\partial V_g}{\partial z} \right)^2 \right) \right)^{0.5} = \frac{f_c T}{g} \left| \frac{\partial \vec{v}}{\partial z} \right| \tag{4.25}$$

$\left| \frac{\partial \vec{v}}{\partial z} \right|$: vertical wind shear ($s^{-1}$)

So it is assumed the geostrophic wind is equal to the horizontal wind. If frontogenesis takes place on a constant pressure surface, the thermal wind equation (Eq. 4.25) can be substituted in Eq. 4.22. To achieve this the following assumption has to be made (see Ellrod and Knapp, 1992; Mancuso and Endlich, 1966):

$$\left|\nabla \theta\right| = \left|\nabla T\right| \tag{4.26}$$

This assumption is questionable. Further, Ellrod and Knapp (1992) make the assumption that $\cos(2\beta) = 1$, so A_t will be maximized. This assumption will often give an overestimation of clear-air turbulence, so is questionable. This together yields when applied to Eq. 4.22:

$$A_T = 0.5 \frac{f_c T}{g} (D + C_{vg}) \left| \frac{\partial \vec{v}}{\partial z} \right| \tag{4.27}$$

A_T: Intensity of frontogenesis on a constant pressure surface ($K\ s^{-1}$)

According to Mancuso and Endlich (1966), who correlated frequency of moderate or severe turbulence with meteorological parameters, the product of vertical wind shear and deformation gives the highest correlation (0.43-0.48). Therefore, Ellrod and Knapp (1992) simplify Eq. 4.27 by assuming the product of f_c and T is constant. This is doubtful. Further they leave out the constant 0.5 and the C_{vg}. This yields:

$$TI1 = D \left| \frac{\partial \vec{v}}{\partial z} \right| \tag{4.28}$$

The C_{vg} is often much smaller than D, but can sometimes be of importance. The AWC, mentioned earlier in this Chapter, uses the TI2 which includes the C_{vg} (Ellrod and Knapp, 1992):

$$TI2 = \left(D + C_{vg}\right)\left|\frac{\partial \vec{v}}{\partial z}\right| \tag{4.29}$$

Since many assumptions have been made during the derivation of the TI1 and TI2, the physical basis of these indices is poor. Correlations between meteorological parameters and turbulence observations particularly determined the final indices, thus making the TI1 and TI2 empirical. Marroquin (1999) states the TI is developed on the basis of empirical correlations between PIREPs (pilot reports) of turbulence and synoptic-scale flow configurations and thus confirms the index is empirical.

4.6 Equation of the Brown index

Brown (1973) derived the modified index (Φ_m):

$$\Phi_m = (0.3\zeta_a^2 + D_{sh}^2 + D_{st}^2)^{0.5} \tag{4.30}$$

The vertical component of absolute vorticity (s^{-1}) is given by:

$$\zeta_a = \frac{\partial v}{\partial x} - \frac{\partial u}{\partial y} + f \tag{4.31}$$

The shearing deformation (D_{sh}) and the stretching deformation (D_{st}) have been defined earlier in this Chapter (Brown, 1973). According to Marroquin (1999) the Brown index is based on empirical correlations between PIREPs of turbulence and synoptic-scale flow configurations. Brown (1973) derived the Brown index, and made many assumptions, thus indicating the index is more an empirical than a physical index.

4.7 Equation of vertical wind shear

The vertical wind shear (s^{-1}), further referred to as VWS, is given by:

$$\left|\frac{\partial \vec{v}}{\partial z}\right| = \left(\left(\frac{\partial u}{\partial z}\right)^2 + \left(\frac{\partial v}{\partial z}\right)^2\right)^{0.5} \tag{4.32}$$

4.8 Equation of horizontal wind speed

CAT occurs usually in the vicinity of the jet stream, but a strong relation between CAT and wind speed has not been found (Ellrod and Knapp, 1992). The horizontal wind speed is given by:

$$\left|\vec{v}\right| = \left(u^2 + v^2\right)^{0.5} \tag{4.33}$$

4.9 Equation of the Dutton index

Dutton (1980), who used a large pilot survey, derived an empirical index (E) with multiple linear regression analyses to obtain the best combination of indices:

$$E = 1.25S_H + 0.25S_V^2 + 10.5 \tag{4.34}$$

S_H: Horizontal wind shear (m s^{-1} per 100 km)
S_V: Vertical wind shear (m s^{-1} per km)

The horizontal wind shear is given by:

$$S_H = \frac{1}{\left(u^2+v^2\right)^{0.5}}\left(uv\frac{\partial u}{\partial x} - u^2\frac{\partial u}{\partial y} + v^2\frac{\partial v}{\partial x} - uv\frac{\partial v}{\partial y}\right) \tag{4.35}$$

and the vertical wind shear by:

$$S_V = \frac{\partial\left|\vec{v}\right|}{\partial p}\frac{\partial p}{\partial z} \tag{4.36}$$

A good association between CAT and vertical wind shear is to be expected because of the Kelvin-Helmholtz instability. Since layers in the atmosphere with large vertical shear are often tilted with a typical slope of about 1 in 100, a component of wind shear appears in the horizontal, thus explaining the correlation between horizontal wind shear and CAT. The Dutton index is based on pilot reports which are not divided per aircraft type (Dutton, 1980).

4.10 Calculation of clear-air turbulence indices from numerical model data

4.10.1 Calculation of TI1, TI2, and frontogenesis

Calculating of D and C_{vg} on constant pressure surfaces can be achieved by using the u- and -v component of the wind on one pressure level from a numerical weather model. The infinitesimal differences have to be approached by the differences between grid-points. If we for example calculate $\frac{\partial u}{\partial x}$ in point B(x,y) on a pressure level, than this is approximated by using the grid-point values of the u-component of the wind speed in point A(x-1,y) and C(x+1, y) (see Figure 4.6):

$$\frac{\Delta u_B}{\Delta x_B} = \frac{u(x+1,y) - u(x-1,y)}{2n} \tag{4.37}$$

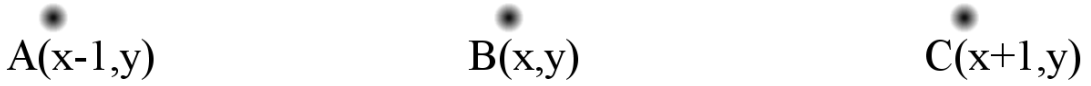

Figure 4.6: Grid-points A, B, and C.

In which n is the distance in the x-direction between two grid-points, and the subscript B refers to point B. In a similar manner other terms in x- and y-direction, necessary to calculate D and C_{vg}, are calculated.
The vertical wind shear, speed and directional, over a layer for a grid-point is approximated by:

$$\left(\left(\frac{u_{top}(x,y) - u_{bottom}(x,y)}{\Delta z}\right)^2 + \left(\frac{v_{top}(x,y) - v_{bottom}(x,y)}{\Delta z}\right)^2\right)^{0.5} \tag{4.38}$$

Δz: Height difference between top and bottom of the layer (m)
u_{top}: u-component of wind speed at top of layer
u_{bottom}: u-component of wind speed at bottom of layer
v_{top}: v-component of wind speed at top of layer
v_{bottom}: v-component of wind speed at bottom of layer

In the calculation of vertical wind shear by Eq. 4.32 we have assumed that the *u*- and *v*- components of the wind are geostrophic, while this is not entirely true. It should be noted that the top and the bottom of the layer are always a constant pressure level. If we for example calculate the TI2 for the layer 300-250 hPa, we use model data from 300 and 250 hPa.
At KNMI the TI1 is already calculated for many years. The deformation is only calculated at the top of the layer, so is assumed to be valid for the whole layer. The TI2 we test calculates the deformation and convergence at the bottom and at the top of the layer and the average of these values is taken as the deformation or convergence in that layer.
For frontogenesis deformation and convergence are also calculated at the top and at the bottom of the layer. For top and bottom of the layer the frontogenesis is calculated and these two values are averaged to give the frontogenesis for a layer.
The angle of local axis of dilatation is given by:

$$\delta = 0.5 \arctan\left(\frac{D_{sh}}{D_{st}}\right) \tag{4.39}$$

The angle from the axis of dilatation to the isotherms β is then given by:

$$\beta = \arcsin\left(\frac{-\cos(\delta)\frac{\partial\theta}{\partial x} - \sin(\delta)\frac{\partial\theta}{\partial y}}{\left|\nabla_h \theta\right|}\right) \tag{4.40}$$

We use temperature fields on constant pressure levels and convert these according to Eq. 4.41 by choosing p_s = 1000 hPa and p the pressure of the level we use in calculating a CAT index.

$$\theta = T\left(\frac{p_s}{p}\right)^{\kappa} = \left(\frac{1000}{p}\right)^{\kappa} \tag{4.41}$$

In which κ is a constant and approximately 0.286.
The derivatives of potential temperature are calculated in the same manner as Eq. 4.37. Frontogenesis is calculated for top and bottom of the layer and the average of these two values yields the frontogenesis for the layer (http, 2002).

4.10.2 Calculation of Brown index, VWS, horizontal wind speed, and Dutton index
The deformation terms and the absolute vorticity are calculated at top and bottom of the layer. The coriolis force (s^{-1}) is calculated according to:

$$f = -2 \cdot 7.292 \cdot 10^{-5} \sin(-1 \cdot rlat) \tag{4.42}$$

In which *rlat* is the latitude in decimal degrees. We only use data from the Southern Hemisphere so a minus sign has been added to Eq. 4.42. The Brown index is calculated at top and bottom of the layer and these values are averaged and yield the Brown index for that layer.
The vertical wind shear is calculated according to Eq. 4.38. Horizontal wind speed calculation is according to Eq. 4.33.
The vertical wind shear in the Dutton index is estimated by Eq. 4.38. The horizontal wind shear is calculated for top and bottom of the layer according to Eq. 4.35. These two values are averaged and yield the horizontal wind shear for a layer.

5 DATA

5.1 Introduction

Two types of data are required to verify a numerical model of clear-air turbulence: data from a meteorological model to calculate a CAT index and turbulence observations in the upper-air.
Two types of turbulence observations are available:

1. PIREP (pilot report or in WMO terminology: AIREP) or a survey for pilots: see Dutton (1980); Ellrod and Knapp (1992); Marroquin (1999); de Villiers and van Heerden (2001).
2. Instrumented aircraft reports (AMDAR/ASDAR): see Bysouth (2000); Turner and Bysouth (1999).

Other types of turbulence observations are difficult to obtain. First an impression of the quality and quantity of the two types of turbulence observations is given. Next is explained why the AMDAR (Aircraft Meteorological DAta Relay) data and a pilot survey have been chosen. Also the choice for the meteorological model data is explained. Finally, some information is given about the AMDAR reporting system of turbulence which has been chosen.

5.2 PIREPs and surveys

With a pilot survey is meant that a pilot fills in a form during the flight and reports several meteorological and geographical elements. This section discusses PIREPs, which are routine pilot reports which are send per latitude and in case of specific events, like significant turbulence (Grooters, pers. com.). The use of PIREPs for research purposes is criticized by Schwartz (1996), who used PIREPs over the continental United States and Alaska from 1993. One problem are reports in which pilots do not mention turbulence. This means no turbulence has been encountered or the pilot did not report anything about turbulence. Another problem is that PIREPs do not indicate for certain the encountered turbulence is CAT. Further, pilots could report lighter turbulence than they were used to do, because they have gained more experience. Not always the aircraft type is mentioned in a PIREP (Schwartz, 1996). See Figure 5.1 for an example of PIREPs over the U.S.

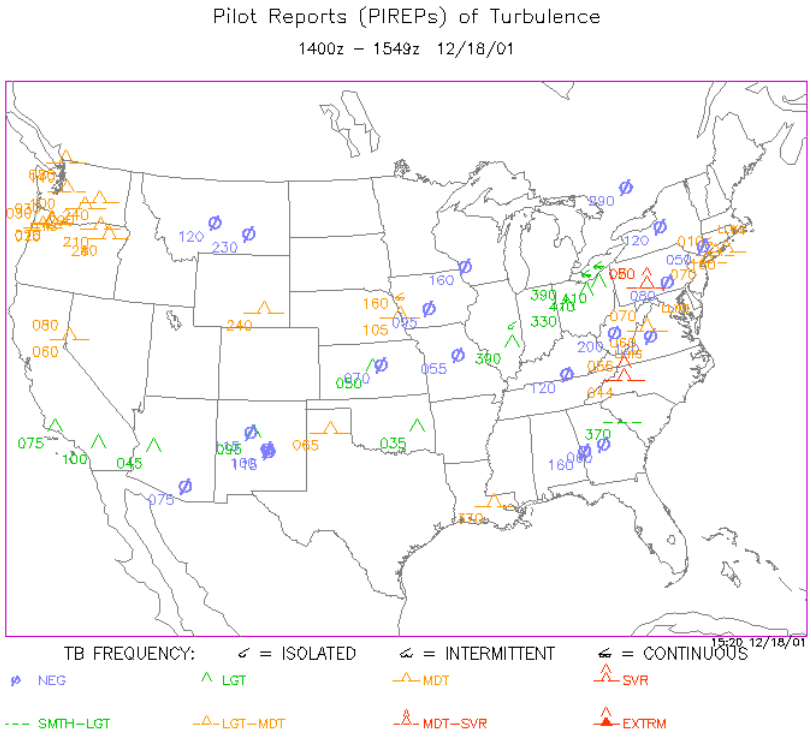

Figure 5.1: Example of PIREPs over the U.S (ADDS, 2001).

The pilot's interpretation of turbulence is very much guided by what the pilot feels and is very subjective. The experience of the pilot influences the reported turbulence. Another problem is that a given turbulence bump will effect different parts of the aircraft in different ways. For example, the back of an aircraft is always more severely affected than the center of gravity or the flight deck. Cases exist where the pilot experienced very little (no coffee spilled) but people at the back of the plane were injured (Stickland, pers. com.).
Definitions for turbulence reporting are imprecise. Another problem is that aircraft react differently to turbulence because of different typical operating air speeds, air density, weight, wing surface area and wing sweep angle (Bass, 1999b).
PIREPs received at KNMI sometimes report aircraft type. Meteorologists put the PIREPs in the computer system (den Uijl, pers. com.). PIREPs are routinely available in the U.S., but at KNMI PIREPs are only available from a few countries, if available it may be possible to obtain them from more countries.
Conclusion is PIREPs are not really suitable to verify numerical clear-air turbulence forecasts. With a pilot survey more data on nonturbulence events could be obtained, thus eliminating an important shortcoming of PIREPs. Though most other disadvantages of PIREPs also hold for a pilot survey.

5.3 Instrumented aircraft reports

5.3.1 Introduction

Instrumented aircraft reports (AMDAR/ASDAR) contain among others geographical position, pressure altitude, wind speed and wind direction, temperature, turbulence, and aircraft identifier. Modern commercial aircraft have aircraft condition monitoring sensors and associated sophisticated data acquisition and processing systems. The obtained real-time data are input to the aircraft flight management, control and navigation systems and other on-board systems. A subset of these data are also sent to the ground automatically by the Aircraft Communication and Reporting System (ACARS) for internal use by the airline or the Aircraft to Satellite Data Relay (ASDAR) to be used by meteorological centers for weather prediction. The first uses the VHF (Very High Frequency) communication system and the latter uses satellite radio links to send the data to the ground. ACARS is most common and preferred, based on ease of implementation and worldwide applicability. ASDAR will not be developed any further. Installing the equipment of ASDAR systems in an aircraft is expensive, but sending information is free. Installing of ACARS systems requires only implementation of software and is therefore cheap, but the costs of sending data are in general high. AMDAR (Aircraft Meteorological DAta Relay) is a software based data acquisition and processing system, using the available aircraft communication system (ACARS) for reporting the meteorological observations to the meteorological services (Grooters, pers. com.; Painting, 2001).
AMDARs are making an increasingly important contribution of upper-air information to the observational database of the World Weather Watch (WWW) of the WMO. The source data for meteorological observations have to be corrected significantly and has to undergo a complex processing. The quality of the wind and temperature observations is superior to radio-sonde systems. If AMDARs are made their resolution and accuracy is high for use in numerical weather prediction (NWP).
The Australian AMDAR system became the first operational system on domestic aircraft in 1986. Later AMDAR systems were implemented in The Netherlands, U.K., France, U.S., Germany and Sweden. On international routes the Australian AMDARS are reported by Boeing aircraft of the Qantas fleet. The costs for the observations are about $1500 per aircraft per year. The AMDARS are send from the aircraft to a Remote Ground Station (RGS) which belongs to a network, such as SITA AIRCOM. Different compatible networks have together a coverage over most of the land areas of the globe through the remote ground stations. These aeronautical data communication systems are used primarily for automation of maintenace, engine monitoring, flight operations and logistic support. Meteorological data can be attached to these messages (Grooters, pers. com.; Painting, 1997).

5.3.2 Turbulence reporting systems

In instrumented aircraft reports four different turbulence reporting systems exist:

1. Delta g

A simple peak value of the deviation from normal vertical acceleration (1g). This is not an aircraft independent measure and results in very big differences in turbulence reports from small to large aircraft flying through the same turbulent airmass.

2. The ICAO categories of turbulence

Also a peak value from normal acceleration, but the turbulence is reported in categories:

0 = None (acceleration less than 0.15g)
1 = Light (acceleration from 0.15g to, but not including 0.5g)
2 = Moderate (acceleration from 0.5g to, but not including 1.0g)
3 = Severe (acceleration > 1.0g)

It responds to whatever the aircraft experiences. It does not take into account the aircraft mass. If a small aircraft flying through a patch of turbulence experiences moderate or severe turbulence, a fully laden Boeing 747-400 would probably report none or light turbulence if it enters the same area of turbulence. The mass of different aircraft types varies considerably, therefore also the acceleration varies accordingly under the same force. It is recommended to research each aircraft type separately. The turbulence measurement according to ICAO categories is a peak value of the period since the previous event. During level flight the period is 7 minutes between two observations, except when the maximum wind is measured.

3. Maximum Derived Equivalent Vertical Gust Velocity (DEVG)

An aircraft independent measure of the vertical gust (equated to ground atmospheric conditions) that gave rise to the deviation in vertical acceleration. Aircraft independent implies that the characteristics (such as mass) of the aircraft are taken into account, so turbulence measurements from different aircraft types are comparable. DEVG is a very sensitive technique and values are reported in tenths of m s^{-1}. The DEVG in general has not been implemented correctly by the airlines, because the DEVG is given as an instantaneous value and not as a peak value. Australian airlines form a positive exception: in level flight in the Southern Hemisphere the DEVG is a peak value over 7 minutes, but in the Northern Hemisphere it is a peak value over 21 minutes. The latter seems not useful for turbulence observations, but the Southern Hemisphere measurements are useful.

4. Eddy Dissipation Rate (EDR)

This algorithm is developed at National Center for Atmospheric Research (NCAR, Boulder, U.S.) and on trial on some U.S. aircraft and recently adopted by ICAO for automated reporting. It is claimed to be aircraft independent. An extensive number of simulations using data from flight data recorders will be needed to be sure that this algorithm indeed provides results independent from velocity and aircraft type. EDR will therefore not be operational in a short time (Grooters, pers. com.; Stickland, pers. com.; Truscott, pers. com.).

All four reporting systems use a deviation from normal vertical acceleration, measured in the center of gravity of the aircraft, and assume turbulence is isotropic, that is the properties of turbulent motion are independent of direction. The assumption that turbulence is isotropic is often probably not too far from the truth but in some particular conditions such as the breaking of mountain-waves or certain convective conditions absolutely not true.

Measuring horizontal acceleration would improve the turbulence measurement a bit, but vertical acceleration is a far more important measure than horizontal acceleration to an airline for safe operations of the aircraft and passenger safety and comfort. Horizontal movements of the aircraft cannot cause a disturbance of the turbulence measurement based on vertical acceleration.

The format in which an AMDAR is sent from an aircraft is by definition without errors, but sending an AMDAR can cause communication errors. Further, a lower air speed of an aircraft increases the chance of encountering turbulence. Thus, air speed but also wind can give an error in measuring turbulence, since in this way circumstances differ between aircraft types. Except probably for DEVG because it includes the air speed. In future turbulence measurements will be divided in more turbulence categories and the EDR could become more used if proven operationally valuable.

Wind speed, wind direction, and temperature are the only reported elements which are quality controlled at KNMI, but these observations have not been used in our research. The reported position in an AMDAR is known with an accuracy of approximately 2 km.
Conclusion is AMDARs are an accurate and objective reporting method of turbulence with a higher quality than PIREPs (Bergman, pers. com.; Grooters, pers. com.; Stickland, pers. com.; Vinnichencko *et al.*, 1980).

5.4 Choice of aircraft data for this report

5.4.1 Choice between PIREPs and AMDARs

For AMDARs the exact position of the turbulence is not known. PIREPs being event driven give a more exact location of the turbulence, but the turbulence intensity they give is rather subjective and they are hardly available over Europe. AMDARs are an accurate and objective reporting method of turbulence with a higher quality than PIREPs (Grooters, pers. com.). A pilot survey has an advantage when compared to PIREPs, because you can also explicitly measure nonturbulence events.
Conclusion: AMDARs are chosen to verify numerical clear-air turbulence forecasts.

5.4.2 Choice of the type of AMDAR data and choice for a pilot survey

KNMI does not store AMDARs, thus only real-time data available from 13 November 2001 to 17 February 2002 (97 days) can be used.
EDR is still in its experimental stage. The DEVG is superior to the other turbulence reporting systems. It is only for certain that Australian aircraft over the Southern Hemisphere correctly report DEVG. For turbulence reported according to the ICAO categories it is only for certain they are correctly reported by ASDAR based aircraft. The latter yields very few turbulence observations above Europe and the Atlantic, which is of most interest for KNMI. Therefore we decide to choose a research area over the Southern Hemisphere where approximately 90% of the Australian DEVG observations have been given: 0ºS-50ºS and 30ºE-150ºW. DEVG is aircraft independent because it takes into account aircraft mass, air speed, and flight characteristics of the aircraft type. It is possible some Australian aircraft do not report turbulence correctly, but it is reasonably certain the data is correctly reported (Lockett, pers.com.; Stickland, pers. com.). We also choose to perform a pilot survey over Europe, since weather situations over the Southern Hemisphere will be quite different from Europe.

5.5 Choice of model data

The original ECMWF data (12 UTC run) has a horizontal resolution of 0.5º. From these data the 1.5º data are derived and used to calculate the clear-air turbulence indices (Kruizinga, pers. com.).
The new HIRLAM model (version 5.06) has not been used. This 0.2º·0.2º model with 31 layers gives model fields over Europe and the Atlantic but does not give the necessary model fields on all pressure levels, so only a very small number of turbulence observations can be used (Moene, pers. com.).
To verify with as many AMDARs as possible four forecasts (+18, +24, +30, and +36 hour) of the ECMWF are chosen. These forecast are most useful for the aviation forecaster at KNMI. The +12 hour forecasts becomes available at the time when it is valid, so the +18 forecast is the first real forecast which can be used. Probably the differences in forecasting skills between the forecasts are small (Kruizinga, pers. com.).

5.6 The DEVG

The DEVG in an AMDAR message (U_{de}) is a number in tenths of meters per second:

$$U_{de} = \frac{10 A m |\Delta n|}{V} \tag{5.1}$$

$|\Delta n|$: Peak modulus value of deviation of aircraft normal acceleration from 1g (in units of g)
m: Total aircraft mass (metric tonnes)
V: Calibrated air speed at the time of occurrence of the acceleration peak (kt)
A: An aircraft specific parameter which varies with flight conditions

A can be approximated:

$$A = \overline{A} + c_4(\overline{A} - c_5)\left(\frac{m}{\overline{m}} - 1\right) \tag{5.2}$$

and $\overline{A}$ is:

$$\overline{A} = c_1 + \frac{c_2}{c_3 + H} \tag{5.3}$$

$\overline{A}$: Value of A when mass of aircraft equals reference mass
$\overline{m}$: Reference mass of aircraft (metric tonnes)
H: Altitude (kft)
c_1, c_2, c_4, c_5: Parameter (-)
c_3: Parameter (kft)

c_1, c_2, c_3, c_4, and c_5 are based on the typical flight profile of the aircraft. For the definition of the DEVG this profile is: take off at speed V_1, accelerate to calibrated air speed V_c by height h_1 and maintain the lesser of V_c or mach M_c to cruise altitude h_c (reverse the procedure during descent). The parameters c_1 .. c_5 differ per aircraft type. The parameters of the flight profile and the parameters c_1 .. c_5 for the aircraft types which report DEVG in our research area are given in Table 5.1. Table 5.2 gives the turbulence intensity categories for DEVG. The measured deviation of aircraft normal acceleration has a sampling frequency of 8 Hz. (Truscott, 2002).

Table 5.1: Parameters of the flight profile and parameters c_1 .. c_5 for different aircraft (after Truscott, 2002).

Aircraft type	V_1 (kt)	V_c (kt)	M_c (Mach)	h_1 (ft)	h_c (ft)	$\overline{m}$ (Tonne)	c_1	c_2	c_3 (kft)	c_4	c_5
B747-400	140	300	0.85	5000	40000	250	-7.78	3260	120	0.62	10.2
B767-300	140	300	0.8	3000	40000	100	13.1	821	42	0.69	19.4
B767-200	140	300	0.8	3000	40000	110	12.8	918	46	0.65	19.8
B737-300	120	300	0.73	3000	35000	40	56.4	328	15	0.56	54.7

Table 5.2: Turbulence intensity categories for DEVG in m s^{-1} (after Truscott, 2002).

Turbulence intensity	DEVG
None	DEVG < 2 m s^{-1}
Light	2 m s^{-1} ≤ DEVG < 4.5 m s^{-1}
Moderate	4.5 m s^{-1} ≤ DEVG ≤ 9 m s^{-1}
Severe	DEVG > 9 m s^{-1}

DEVG is a measure of the vertical gust velocity which would, at sea level, give the same vertical acceleration as the peak acceleration reported by an aircraft due to turbulence. The values of derived equivalent gust velocity reported by two different aircraft with the same gust are comparable, but experimental comparisons are difficult. DEVG is not an actual velocity, but derived from the measured vertical acceleration. The correlation between DEVG and true vertical gust velocity is small. The mass and height of the aircraft are determined once each 7 minute period. V may change significantly during a 7 minute period. The maximum acceleration during each 5 second period is divided by the simultaneous value of the air speed. The maximum value of this ratio during a 7 minute period is used to calculate the DEVG for this 7 minute period.
The real mass of the aircraft varies considerably during flight due to fuel consumption and is known within 3%, and under most conditions within 1%. The error in the calibrated air speed is less than 1 kt at 200 kt, 2 kt at 100 kt, and 4 kt at 60 kt. The primary error in the vertical acceleration measurement is due to longitudinal displacement between the accelerometer and the center of gravity of the aircraft, thus yielding a maximum error of approximately 2%. The total maximum error in the vertical acceleration is 0.2g. The possible error in A is hard to estimate (Bass, 1999b; Grooters, pers. com.; Sherman, 1985).

6 VERIFICATION OF THE TI1 MODEL FORECAST WITH A PILOT SURVEY AND TWO CASE-STUDIES

6.1 Introduction

The aviation meteorologist at KNMI can visualize the TI1, which is calculated with ECMWF model output with a horizontal resolution of 1.5º, on a Meteorological Workstation (MWS) to identify CAT areas. To obtain turbulence observations over Europe a pilot survey has been held, so that the usefulness of the currently available CAT index (TI1) at KNMI in forecasting CAT becomes obvious. Section 4.2 describes in detail why the TI1 has to be verified. In section 6.2 the pilot survey is explained. Further, the results of the verification of the TI1 are presented and discussed and the conclusions are given. Finally some case studies will be performed which describe the synoptic situation of some days in relation to the TI1 and the pilot observations.

6.2 Explanation of the pilot survey

In our research we approached KLM (Royal Dutch Airlines) with the request to perform a survey in which the pilot has to fill in a form during a flight (see Appendix A for an example of such a form). KLM was willing to co-operate and we were allowed to hand out surveys to Boeing 737 pilots during January 2002. Because several days did not have a high value of TI1 and because of time, the survey was limited to 8 days. 97 surveys were returned, meaning a high response of over 80%, this being probably due to handing out the forms personally to the pilots and of course because of the willingness of the pilots to fill in the form. 188 (78%) of all received observations are usable. 62 observations did mention turbulence was encountered and 150 observations did mention no turbulence was encountered.

Most flights were entirely over Europe. Pilots were asked to fill in a few measurements during the flight, also when no turbulence was encountered. We especially asked the pilots to fill in a measurement if turbulence was encountered. Because we want to test the +24 hour forecast of the ECMWF 12 UTC run, we selected flights within the period between 9 UTC and 15 UTC. The elements to be reported were: position (latitude/longitude in degrees and minutes), time, flight level (further referred to as FL), wind speed, temperature, presence of clouds (yes/no), turbulence and remarks like "fasten seatbelts sign on". The turbulence is reported according to the ICAO categories and that is what the pilots are used to. An advantage of the pilot survey is the use of the same aircraft type, the Boeing 737. The KLM operates three different versions of the Boeing 737 (See Table 6.1).

Table 6.1: Technical information of the Boeing 737 (Boeing 737-300, 2001; Boeing 737-400, 2001; Boeing 737-800, 2001).

Aircraft type	Boeing 737-300	Boeing 737-400	Boeing 737-800
Max. number of passengers	109	129	158
Max. take-off weight (kg)	57,100	63,000	74,150
Average cruise speed (km/h)	800	800	850
Wingspan (m)	28.9	28.9	34.3
Length (m)	33.4	36.4	39.5
Height (m)	11.1	11.1	12.5

22% of the observations were not used because they were not reported between FL 240 and 390 or between 9 and 15 UTC and because of inaccuracies in position. The observations have been divided in three layers: FL240-300 (400-300 hPa), FL300-340 (300-250 hPa), FL340-390 (250-200 hPa), and for these layers the TI1 is calculated. The height of the aircraft is reported according to the standard ICAO atmosphere. Most turbulence observations have been reported as light turbulence and only few as

moderate turbulence. Table 6.2 gives an overview of the number of observations which meet the selection criteria.

Table 6.2: Number of observations, turbulence and nonturbulence, which meet the selection criteria. Total number of observations is given and the number of observations for each layer and each day.

Day:	Total number	FL 240-300 (400-300 hPa)	FL 300-340 (300-250 hPa)	FL 340-390 (250-200 hPa)
8 jan	36	19	8	9
9 jan	33	5	15	13
15 jan	33	4	10	19
16 jan	28	9	7	12
18 jan	24	3	13	8
22 jan	34	11	12	11
28 jan	9	2	1	6
31 jan	15	2	9	4
Total	212	55	75	82

6.3 Results

6.3.1 Introduction

The observations were plotted on the TI1 charts and two threshold values were verified: $2 \cdot 10^{-7}$ s^{-2} and $4 \cdot 10^{-7}$ s^{-2}. If the TI1 is above or is equal to the threshold this means CAT is forecasted and the forecast is assigned "Yes". If the TI1 is below the threshold the forecast is assigned "No". If the pilot experienced lighter or greater turbulence the observation was assigned "Yes", and if no turbulence was experienced it was assigned "No". When the forecast is "Yes" and the observation is "Yes", or the forecast is "No" and the observation is "No", the forecast is correct.

6.3.2 Threshold of $2 \cdot 10^{-7}$ s^{-2}

Table 6.3 contains the results for a threshold of $2 \cdot 10^{-7}$ s^{-2}. Almost 44% of the turbulence observations is not predicted for a threshold value of 2. 38% of the nonturbulence observations is not predicted correctly, so the turbulence area is considerably overestimated, especially because nonturbulence situations are far more common than turbulence situations.

Table 6.3: Results for threshold = $2 \cdot 10^{-7}$ s^{-2}.

Forecast	**Observation Yes**	**No**
Yes	35 (56.5%)	57 (38.0%)
No	27 (43.5%)	93 (62.0%)

6.3.3 Threshold of $4 \cdot 10^{-7}$ s^{-2}

66% of the turbulence observations are not predicted for a threshold value of $4 \cdot 10^{-7}$ s^{-2} (see Table 6.4). 21% of the nonturbulence observations are not predicted correctly, so the turbulence area is overestimated, though the percentage of correctly forecasted nonturbulence observations has increased from 62% to 79% compared to a threshold of 2, so the overestimation of the CAT area is smaller when compared to a threshold of 2. If the threshold value would be further increased, the number of well predicted nonturbulence observations would increase, but the number of well predicted turbulence observations will further decrease.

Table 6.4: Results for threshold = $4 \cdot 10^{-7}$ s^{-2}.

Forecast	**Observation Yes**	**No**
Yes	21 (33.9%)	31 (20.7%)
No	41 (66.1%)	119 (79.3%)

6.4 Discussion

6.4.1 Interpretation of turbulence

One reason for errors in the turbulence data is the subjectiveness of reporting. Some pilots did mention "occasionally 1", meaning "occasionally light turbulence", and we found this too little turbulence so assigned it the value "0", meaning "no turbulence encountered". But it is possible another pilot also encountered "occasionally 1", but reported "1". We processed "0/1" as a nil report and "30 seconds during climb light turbulence" was interpreted as "light turbulence". Observations made during descent or ascent have also been included. For a comprehensive review of the subjectiveness of pilot reports see Chapter 5.

6.4.2 Mountain-waves and convection

The TI1 cannot predict turbulence related to thunderstorms and mountain-waves (Ellrod and Knapp, 1992). Mountain-waves and convective turbulence have not been excluded. Large part of the reports are not over mountainous areas. Convective turbulence caused by thunderstorms will play a minor role since the survey has been held in January and then thunderstorm activity will in general be low over Europe. It seems reasonable that convective turbulence has not been excluded.

6.4.3 Period of the survey

The 8 day survey, with 62 turbulence and 150 nonturbulence observations, is rather small to draw definite conclusions. For example the number of different weather situations will be small.

6.5 Conclusion

Comparing the results of threshold values, it can be concluded that the threshold value of $2 \cdot 10^{-7}$ s^{-2} gives a better prediction of clear-air turbulence than a threshold value of $4 \cdot 10^{-7}$ s^{-2}, since 56.5% of the turbulence observations is predicted against 33.9% for the threshold of $4 \cdot 10^{-7}$ s^{-2}. The latter has the advantage that the overestimation of CAT is smaller, but it seems far more important to detect turbulence areas, and therefore the threshold of $2 \cdot 10^{-7}$ s^{-2} is in favour. Though, the threshold of $2 \cdot 10^{-7}$ s^{-2} is not very useful in forecasting CAT, since only 56.5% of the CAT observations has been forecasted and this threshold gives a large overestimation of CAT areas because 38.0% of the nonturbulence observations is not forecasted correctly. Further, nonturbulence conditions are far more common than turbulence conditions, so the chance of encountering CAT in a forecasted CAT area will be low. These conclusions are based on a rather small number of observations. The survey gives an indication of the performance of the TI1 over Europe in winter conditions. The TI1 has to be used with precaution.

6.6 Case studies

6.6.1 Introduction

Two casestudies are presented. One forecast which gives a reasonably good prediction of CAT (22 January 2002) and one forecast which does not forecast a number of pilot reports of turbulence (8 January 2002). Purpose of these case-studies is to give some insight into the weather situations associated with CAT.

Figure 6.1 explains how the symbols of the turbulence observations have to be interpreted. A "0" indicates the pilot reported "no turbulence encountered". The sign in the middle indicates "light turbulence", this is a deviation from the official meaning of this symbol, which is "moderate turbulence". The sign on the right indicates "moderate turbulence", while the official meaning is "severe turbulence". The intersection of the two thin lines indicates the exact position of the observation.

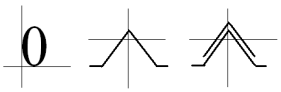

Figure 6.1: Symbols for nonturbulence and turbulence observations.

6.6.2 Case study 22 January 2002

22 January 2002 8 reports of turbulence encounters were received in the layer from 400 to 300 hPa (FL 240-300), see Figure 6.2. Seven of these reports correspond to values of the TI1 of about 6 or higher. One report corresponds with a TI1 below 2. For that reason the turbulence in this layer is predicted well, though two nil reports correspond with a value of about 7.

According to the METEOSAT satellite images (Figure 6.3 and 6.4) no cumulonimbi are present. The VIS image, Figure 6.4, reveals a billow structure which is maybe associated with CAT. It is not clear to which pressure level this structure belongs. The structure is only visible on the 11.30, 12.00, and 12.30 UTC VIS satellite images. The turbulence observation in the vicinity of this billow structure is from 13.46 UTC, so cannot be linked to the billows. Further, the IR images reveal some bands which can be associated with the jet stream.

The model forecast of geopotential height at 300 hPa indicate a through, which is known to be a place for CAT (see Figure 6.5). Also a sharp change in wind direction and a considerable change in wind speed can be seen. Figures 6.6 and 6.7 give the measured wind direction. The change in wind direction is most pronounced at the 300 hPa level. Observed wind speeds of 160 km hour^{-1} indicate the presence of the jet stream. The curvature of the wind can be linked to the presence of CAT, the vertical wind shear between the 400 and 300 hPa level is for most turbulence observations rather small.

The TI1 indicates that a change in height pattern is present which can be related to CAT. On the cold side of the jet stream a trough with a turning wind is present.

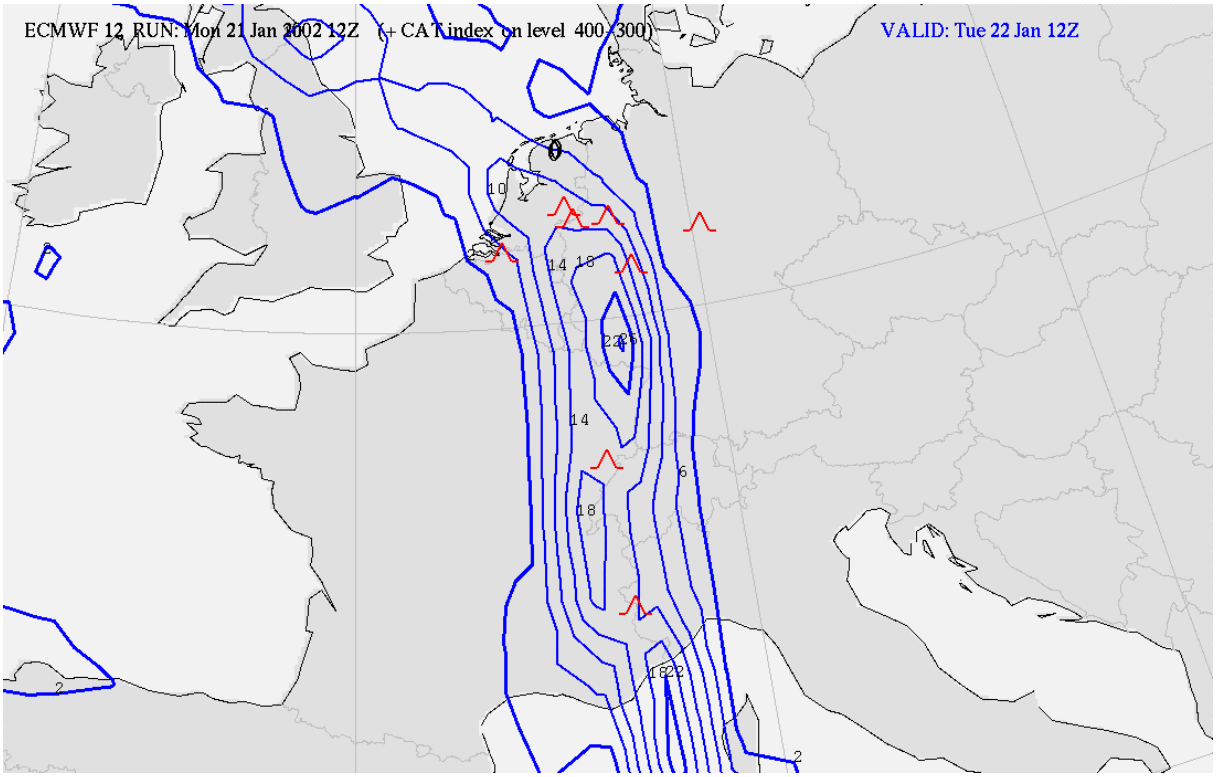

Figure 6.2: +24 hour forecast of the TI1 valid for 22 January 12 UTC together with turbulence observations within 3 hours of the model forecast.

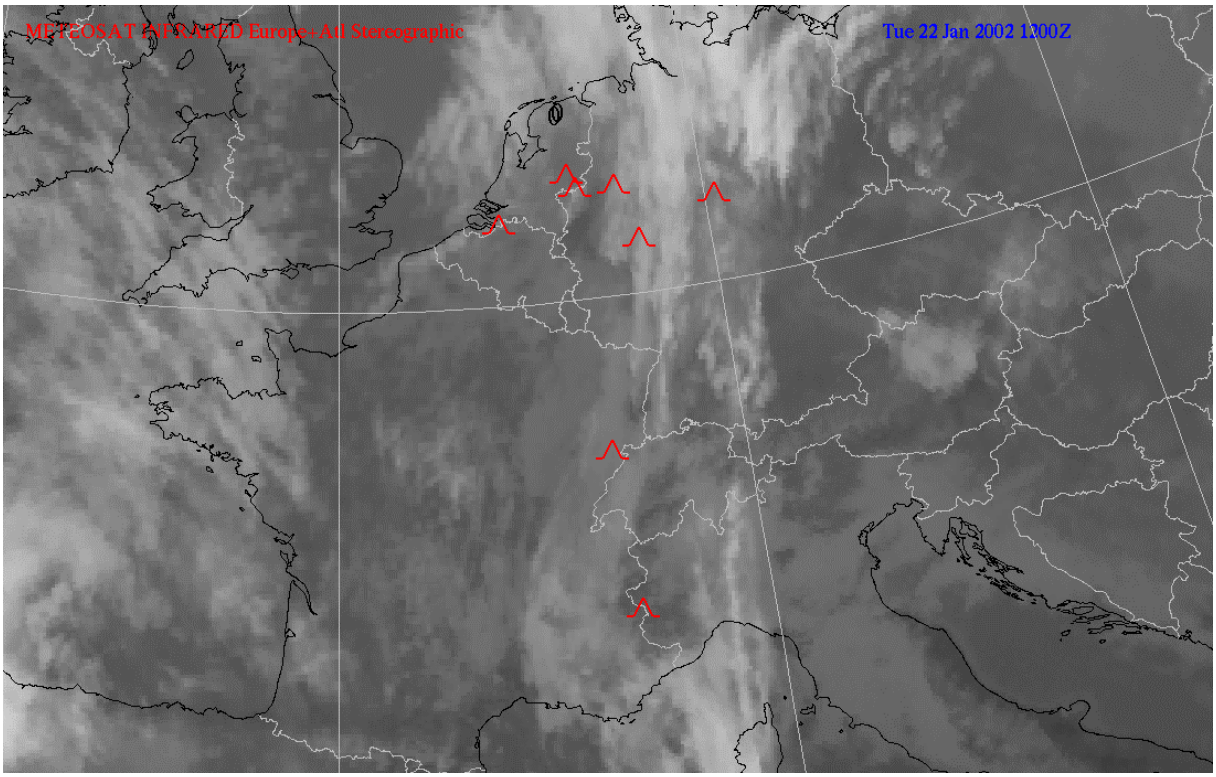

Figure 6.3: METEOSAT IR image valid for 22 January 2002 12 UTC.

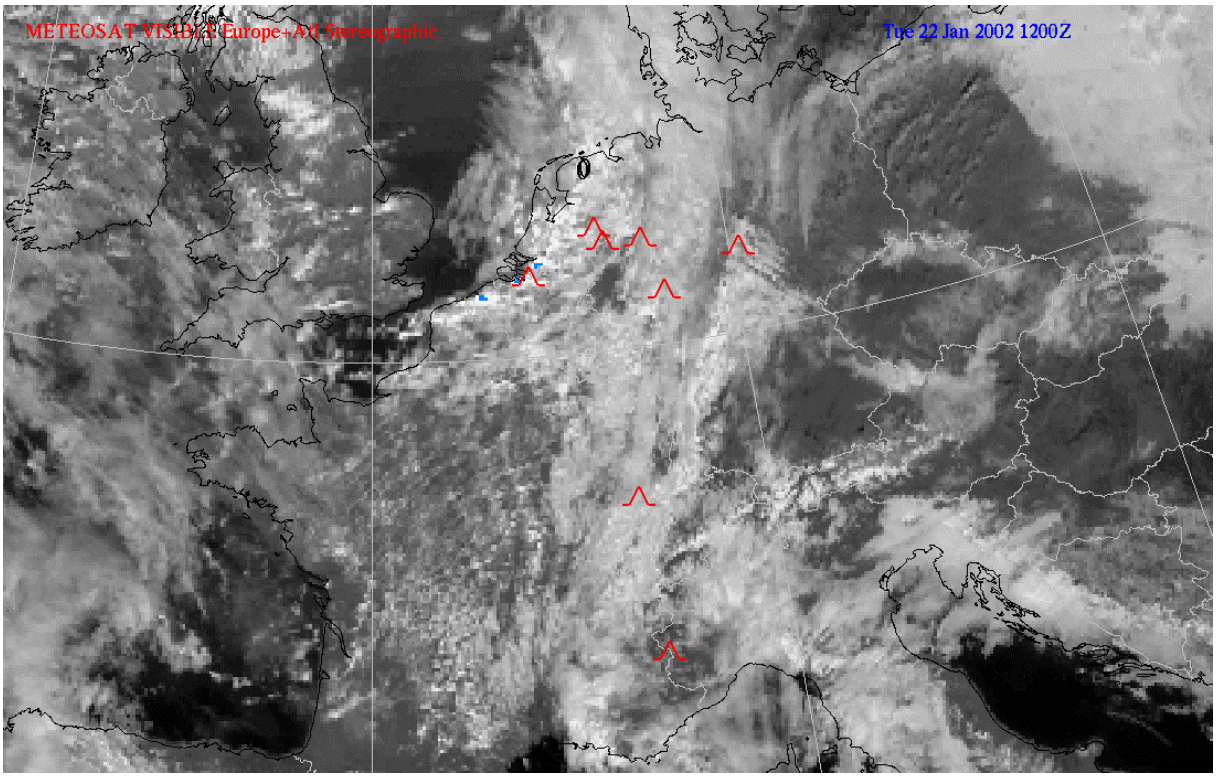

Figure 6.4: METEOSAT VIS image valid for 22 January 2002 12 UTC.

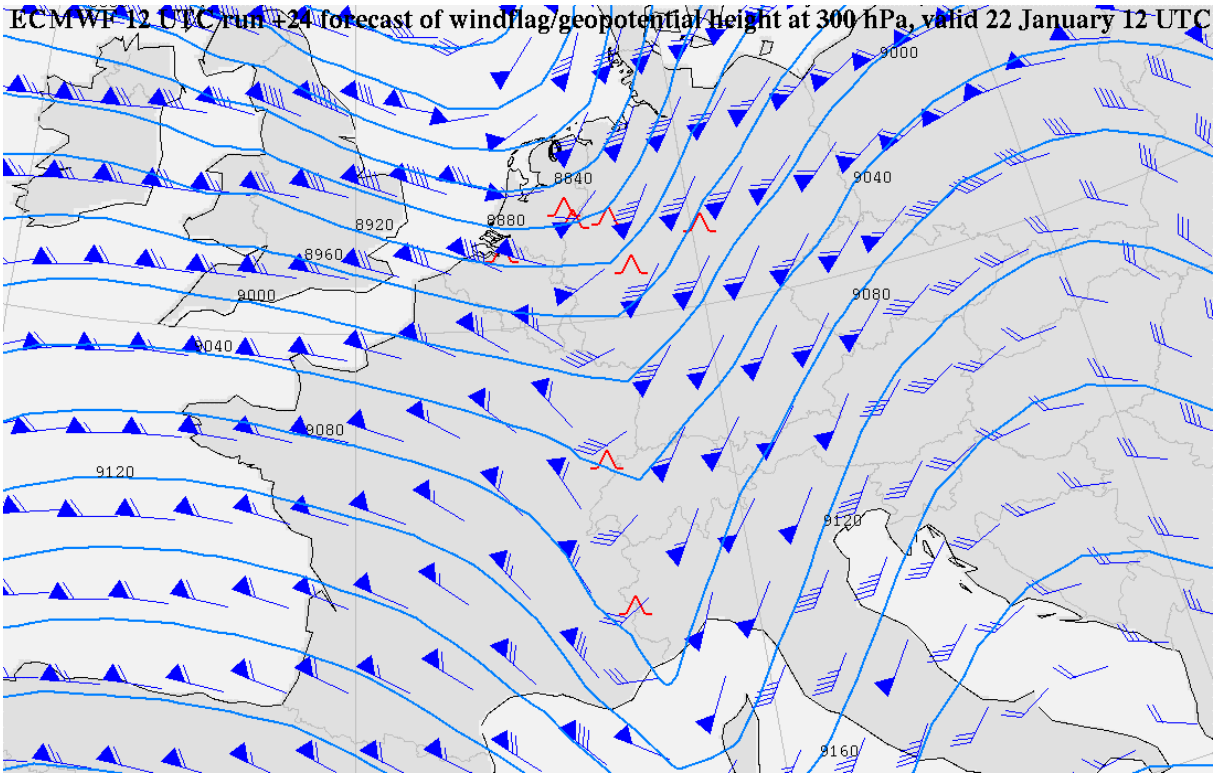

Figure 6.5: Forecasted geopotential height and winds at 300 hPa level for the +24 hour forecast of the ECMWF 12 UTC run valid for 22 January 2002 12 UTC.

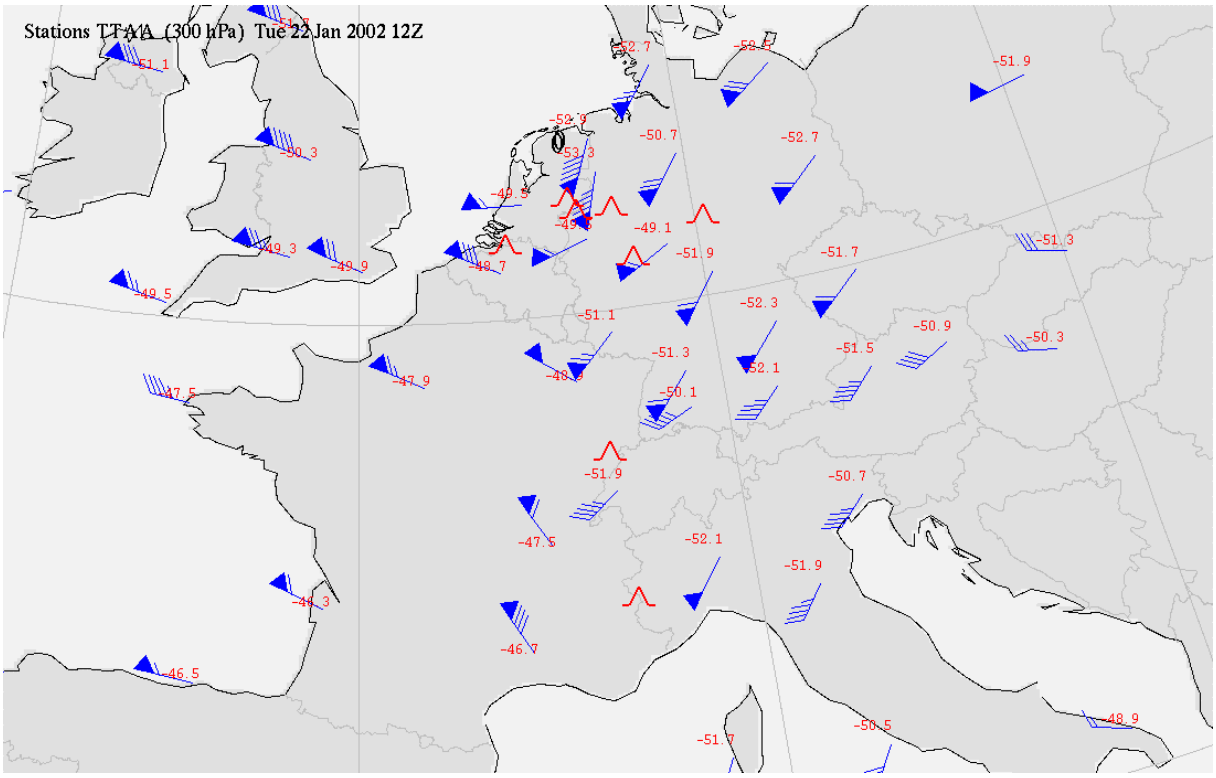

Figure 6.6: Measured radiosonde wind speeds and temperatures at 300 hPa valid for 22 January 2002 12 UTC.

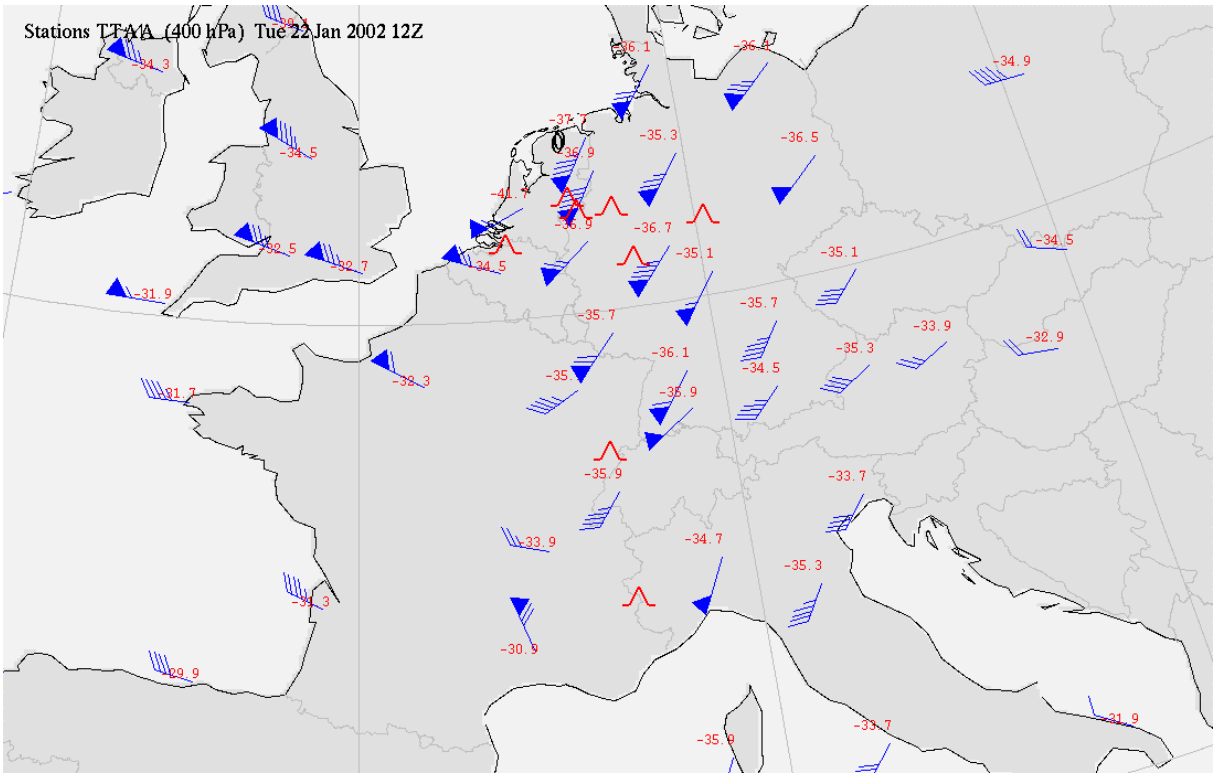

Figure 6.7: Measured radiosonde wind speeds and temperatures at 400 hPa valid for 22 January 2002 12 UTC.

From Figure 6.8 is it clear the tropopause height increases significantly from West to East. This indicates the tropopause break, which extends from the northeast of the Netherlands to southwestern Germany. Part of the measurements falls in this tropopause break. Figure 6.9 gives a tephigram of station ETGM, which is in the vicinity of three turbulence observations which are reported between FL260 and FL270, just below the tropopause. The vertical wind shear in the layer 300-400 hPa (FL240-300) is small, thus giving further evidence that the horizontal wind shear (particularly directional) plays an important role and the vertical wind shear is of minor importance in the forming of CAT in this case. But it has to be said that CAT is a micro-scale phenomenon thus vertical wind shear in layers of small thickness might be large compared to the vertical wind shear in the layer 300-400 hPa.

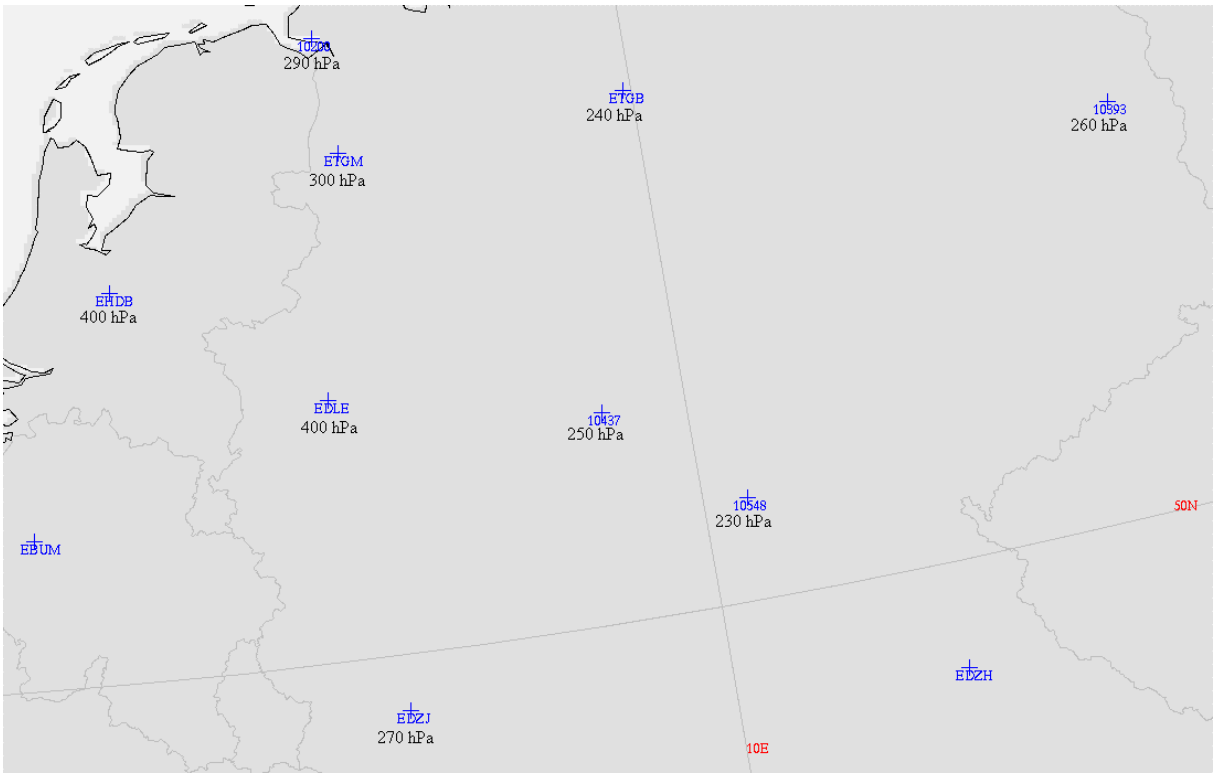

Figure 6.8: Location of temp stations. Below the identification the height of the tropopause is given estimated from observed temps from 22 January 12 UTC.

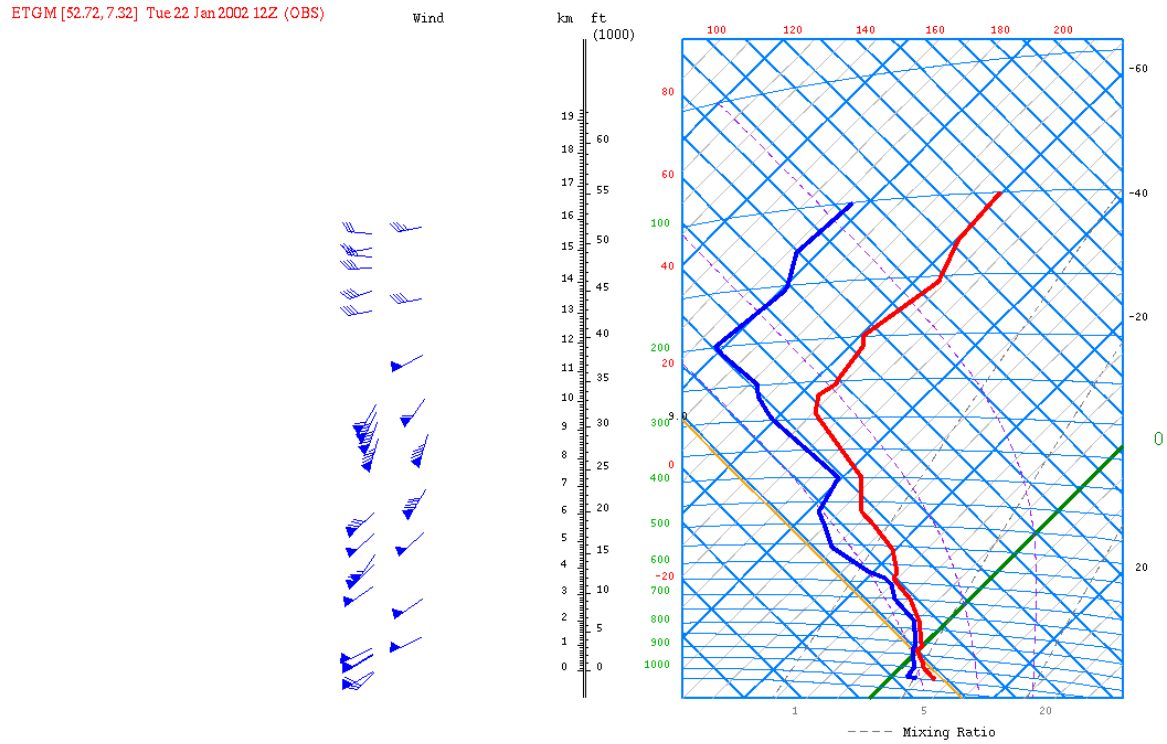

Figure 6.9: Tephigram of station ETGM.

6.6.3 Casestudy 8 January 2002

Again the observations are given for FL 240-300. Four turbulence observations have a TI1 below 2. Most nil reports correspond with a TI1 below 2, but three nil reports correspond with a TI1 above 2 and two of them with a TI1 of 6. See Figure 6.10. Most observations are located in a high pressure area without fronts.

No jet stream is present in the vicinity of most of the observations. The turbulence observations cannot be associated with vertical wind shear. Only some horizontal wind shear (especially directional) could be a cause. See Figures 6.11 and 6.12.
The turbulence observation over Denmark could be associated with a horizontal temperature gradient of 2ºC at 400 hPa. The other two examined turbulence observations cannot be linked with a large horizontal temperature gradient or with cumulonimbi, only some banded cloud features can be seen (see Figures 6.13 and 6.14). Conclusion is the turbulence observations cannot be linked to macro-scale features. The many nil reports close to the turbulence observations indicate the micro-scale character of CAT.

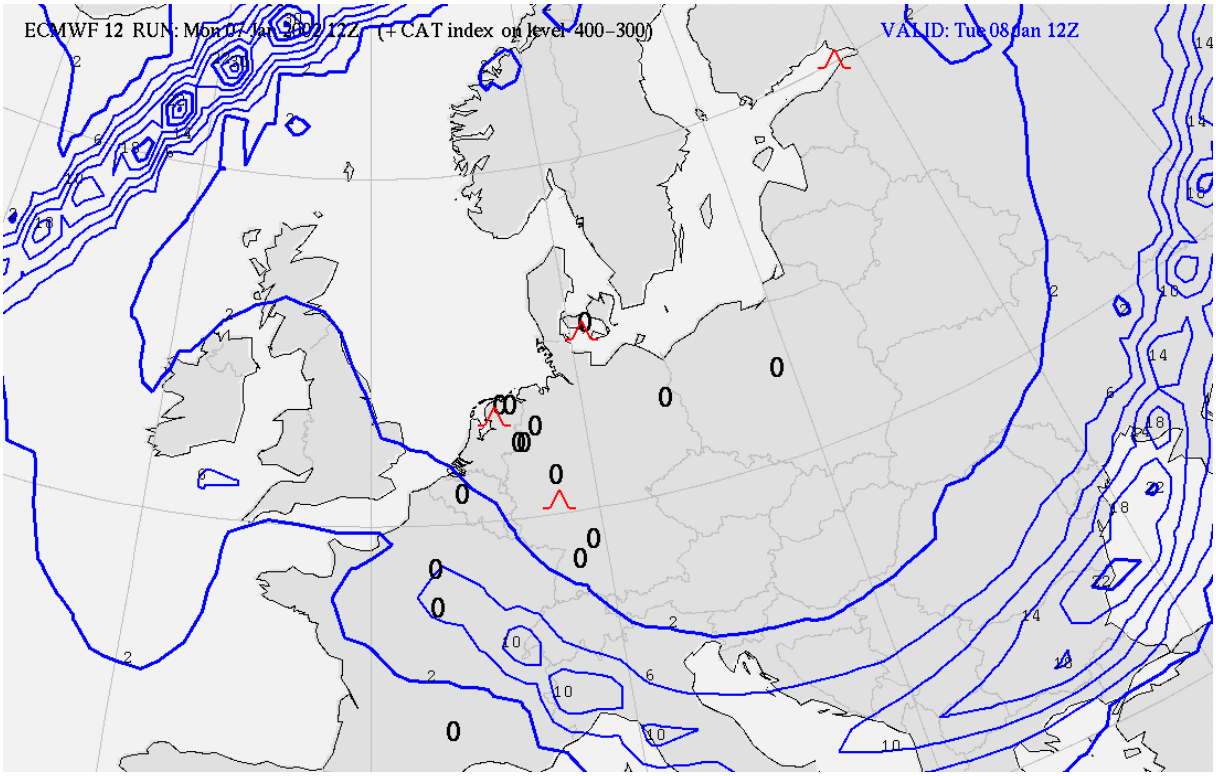

Figure 6.10: +24 hour forecast of the TI1 valid for 8 January 12 UTC together with turbulence observations within 3 hours of the model forecast.

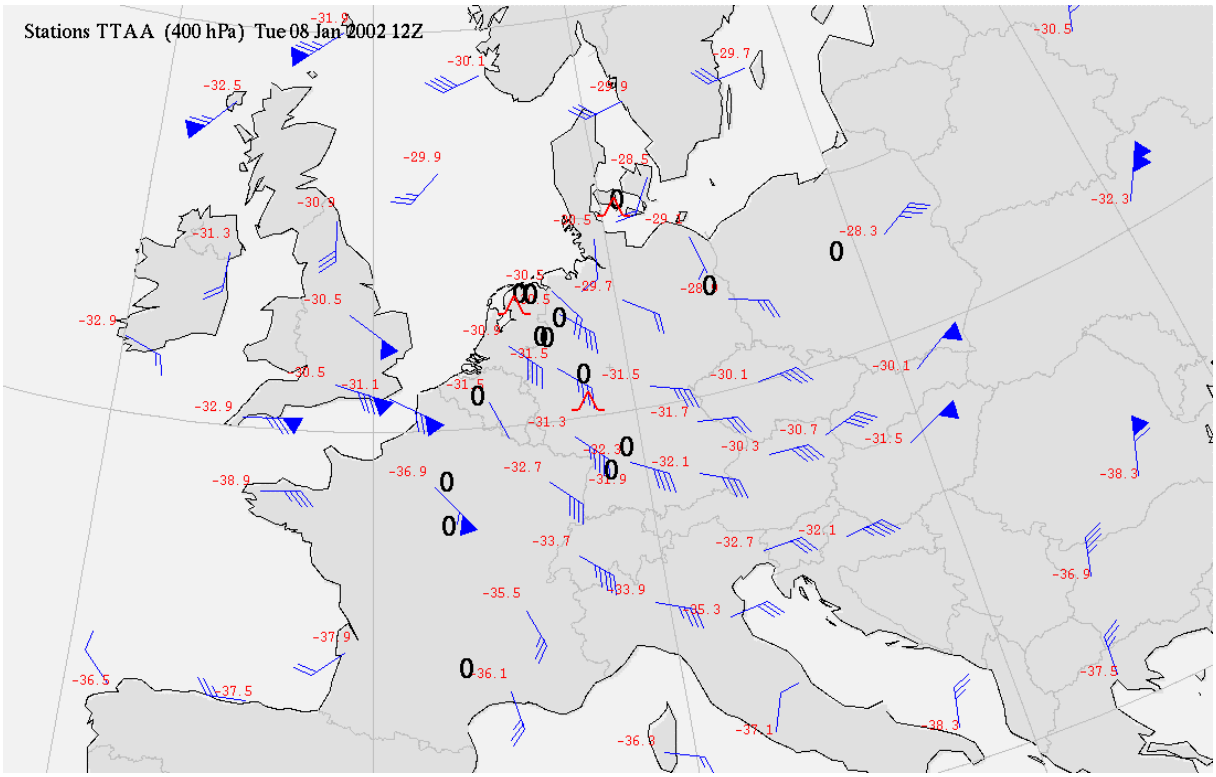

Figure 6.11: Measured radiosonde wind speeds and temperatures at 400 hPa valid for 8 January 2002 12 UTC.

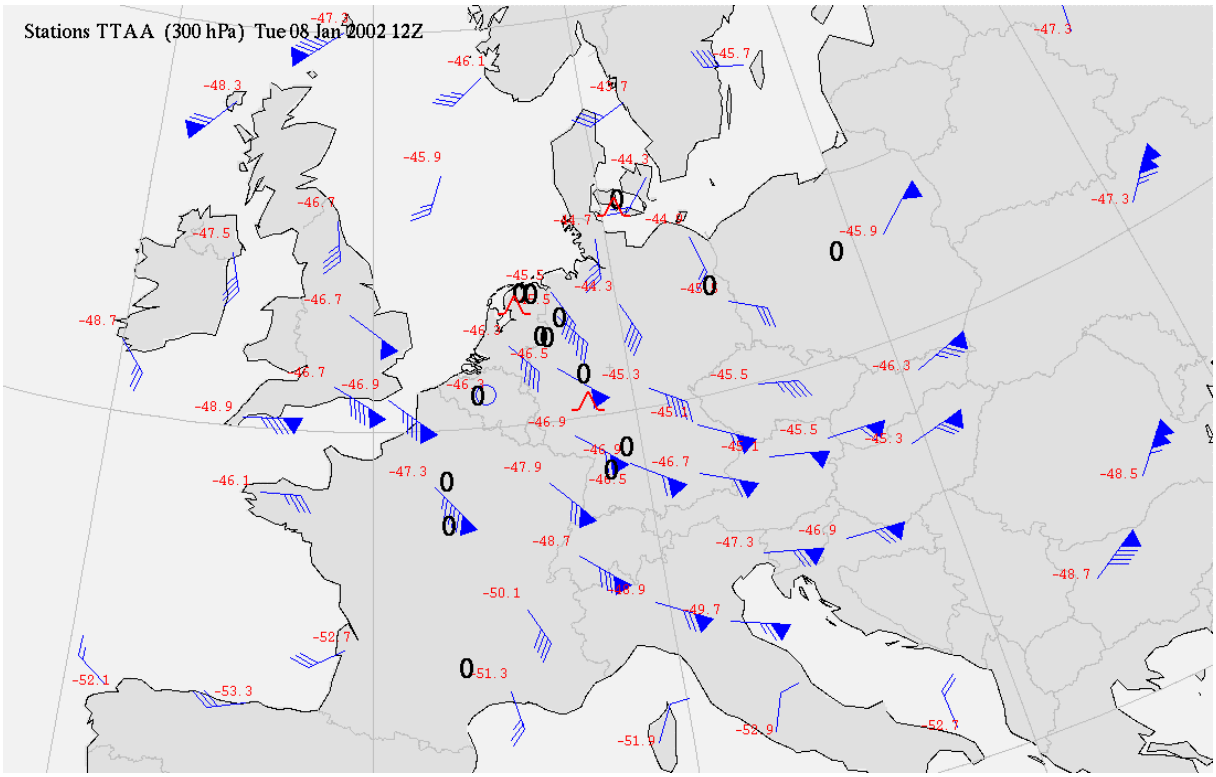

Figure 6.12: Measured radiosonde wind speeds and temperatures at 300 hPa valid for 8 January 2002 12 UTC.

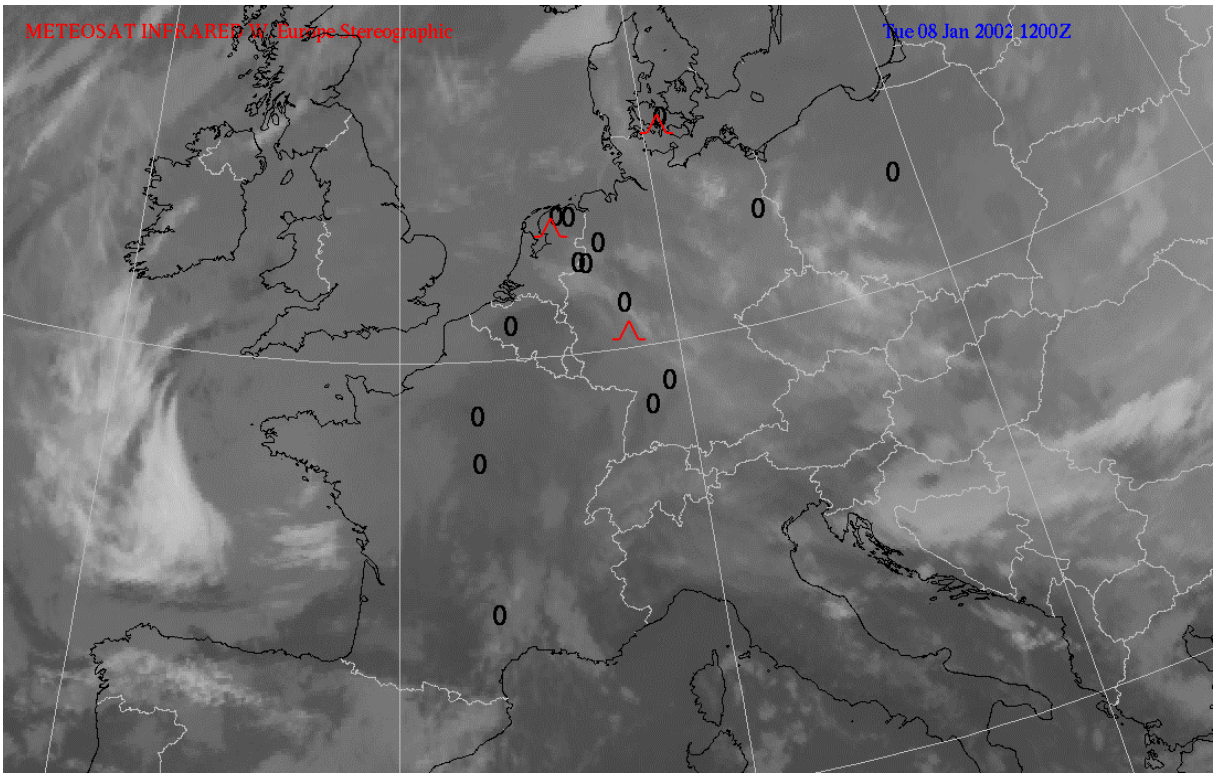

Figure 6.13: METEOSAT IR image valid for 8 January 2002 12 UTC.

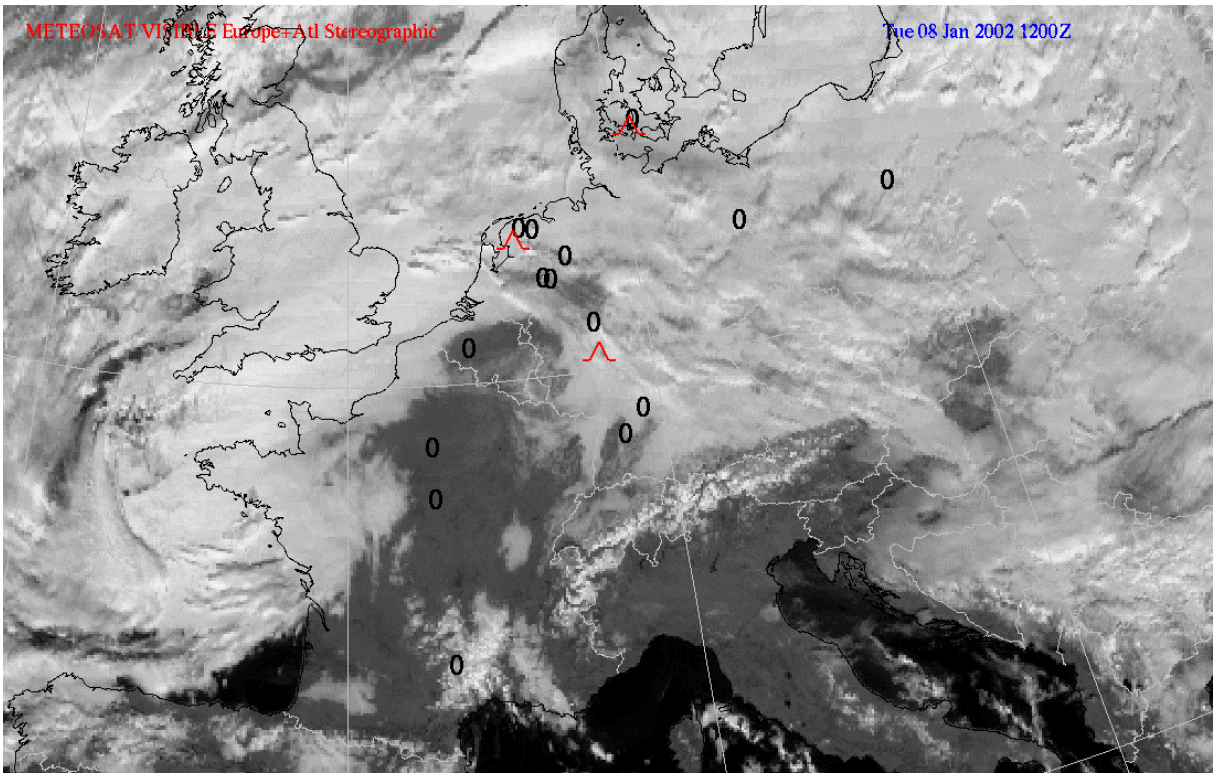

Figure 6.14: METEOSAT VIS image valid for 8 January 2002 12 UTC.

7 VERIFICATION OF NUMERICAL CLEAR-AIR TURBULENCE FORECASTS WITH AMDARS

7.1 Introduction

In this Chapter forecasts of CAT based on seven clear-air turbulence indices are verified with AMDARs. The seven CAT indices are: frontogenesis, TI1, TI2, Brown index, VWS, wind speed, and Dutton index.
From 13 November 2001 to 17 February 2002 AMDARs were received at KNMI and many selections have to be made to obtain AMDARs which are usable to verify numerical clear-air turbulence forecasts. Also the calculation of the clear-air turbulence index for the geographical position of an AMDAR is explained. Next the verification methods are mentioned. To verify numerical clear-air turbulence forecasts a threshold value is varied in the range of the CAT index. The best threshold value found is based on the percentage of correctly forecasted turbulence observations. Also the results of the verification of the CAT indices are given together with the discussion. The correlation between the magnitude of clear-air turbulence indices and reported turbulence intensities is also investigated. Finally the conclusion is given.

7.2 Selection of AMDARs

7.2.1 Introduction

From the 2,609,975 AMDAR messages received in this period only a limited number are suitable for verifying numerical model forecasts of CAT, particularly because only Australian AMDARs which report DEVG are selected. See section 5.4.2 why these data have been chosen.
Many selections have to be made and these are often a compromise between quantity and quality of the data. On the Southern Hemisphere Australian aircraft in level flight send an AMDAR message every 7 minutes. We define the previous AMDAR as the message sent before the present AMDAR. Because of differences in operating speed between aircraft types and flights, and because of considerable differences in wind speed, the distance travelled in these 7 minutes can vary from approximately 50 km to 150 km. On average the distance is around 100 km.
A DEVG of 2.0 m s^{-1} or higher is defined as a turbulence observation and a DEVG below 2.0 m s^{-1} is defined as a nonturbulence observation (see section 5.6).

7.2.2 Selections

The meaning of the remark "under same conditions" in the criteria below is that all selections are obeyed except the selection where the remark is made. For our research an AMDAR has to comply with the following criteria:
1. Previous AMDAR has a different geographical position than present AMDAR.
2. Aircraft identifier starts with "AU", meaning Australian aircraft.
3. Previous AMDAR is from same aircraft (has same aircraft identifier) as present AMDAR.
4. Previous AMDAR and present AMDAR have a geographical position between 1.5ºS-49.5ºS and 31.5ºE-151.5ºW. The ECMWF data are from 0ºS-51ºS and 30ºE-150ºW. The AMDARs within 1.5º of these boundaries are left out to avoid calculation errors on the borders of the model field.
5. Present AMDAR is exactly 7 minutes later than previous AMDAR.
6. Turbulence observations have to be within two hours of each forecast time. Therefore each present AMDAR has to be given between 4.07 and 8.00 UTC, 10.07 and 14.00 UTC, 16.07 and 20.00 UTC or 22.07 and 2.00 UTC. The forecast has a limited validity, therefore only data ± 2 hours from the forecast time have been used. Applying a forecast validity of ± 1 hour would diminish the number of observations considerably. Also Dutton (1980), who used a pilot survey, assumed a period of validity of ± 2 hours. Ellrod and Knapp (1992), who used PIREPs, assumed a period of validity of 3 hours.
7. The flight phase of the present AMDAR has to be "level flight". If the flight phase is unknown the AMDAR is not selected. Other flight phases have not been selected since the number of turbulence AMDARs is very low and these phases can sometimes give errors.

The flight level can change while the flight phase is "level flight". The change is normally gradual and has little or no impact on stability of the aircraft (Stickland, pers. com.).
8. Present AMDAR has to contain a DEVG measurement.
9. Only AMDARs from 9200 m (300 hPa) to 13600 m (150 hPa), according to the ICAO standard atmosphere, are selected. Below 9200 m just 8 turbulence AMDARs, were received under the same conditions. Above 13600 m no AMDARs were received under the same conditions.
10. 10% of the observations which report no turbulence is encountered are selected. This is done random. The selection is made to limit the calculation time. After this selection the number of nonturbulence observations is still almost 4 times as large as the number of turbulence observations.

Since the clear-air turbulence indices are calculated for different layers in the atmosphere the AMDARs have to be divided in three layers:
1. 300 hPa - 250 hPa: larger than 9160 m up to 10360 m.
2. 250 hPa - 200 hPa: larger than 10360 m up to 11780 m.
3. 200 hPa - 150 hPa: larger than 11780 m up to 13600 m.
The present AMDAR is divided in a layer by comparing its pressure height (tenths of meters) with the geopotential altitude according to the ICAO standard atmosphere belonging to a layer. In Chapter 6 a clear-air turbulence index has also been calculated over the layer 400-300 hPa. Because of the small number of AMDARs in this layer this is not done here. Because of the large number of AMDARs in the layer 200-150 hPa, clear-air turbulence indices are also calculated for this layer.

7.3 Calculation of the clear-air turbulence indices

Depending on the clear-air turbulence indices, different input is used for the calculation of an index. We use input from the 12 UTC run of the ECMWF model with a horizontal resolution of 1.5º. The following fields at 150, 200, 250 and 300 hPa and for the +18, +24, +30 and +36 hour forecast are used:
- Geopotential height (m)
- *u*-component of the wind (m s^{-1})
- *v*-component of the wind (m s^{-1})
- Temperature (K)
Chapter 4 gives information about the derivations, theory, equations and calculations on grid-points of the tested clear-air turbulence indices. With FORTRAN programs (UNIX) the input fields, which are in ASIMOV-GRIB format after being converted from GRIB format, are read and the clear-air turbulence index is calculated. The output is in ASIMOV-GRIB files.

7.4 Calculation of the value of a clear-air turbulence index at a certain position

Program Extravert (UNIX) reads the ASIMOV-GRIB files which contain the clear-air turbulence index and determines the value of the index for a certain geographical position belonging to an AMDAR. The DEVG is a peak value. It is unknown whether this peak is reached at the beginning, at the end or somewhere in between in the 7 minute period. Therefore with program Extravert the value of the index is calculated for the position of the previous AMDAR and the position of the present AMDAR.
Figure 7.1 gives an overview of the connection between the programs and the data streams. Program DEVGSelect selects the AMDARs according to section 7.2, program Extravert interpolates, program CAT index calculates the CAT index according to section 7.3 and program Validate verifies the clear-air turbulence forecast.

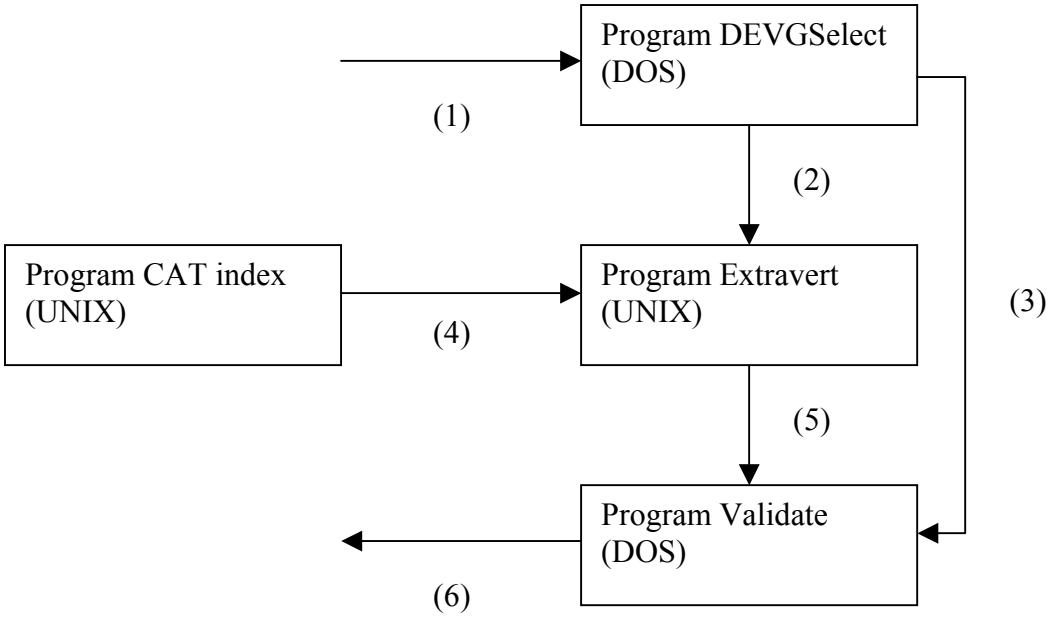

Figure 7.1: Verification of CAT forecasts with AMDARs occurs according to this scheme. Arrows indicate data streams. (1): AMDARs. (2): script files which call the interpolation program Extravert and which contain the geographical position of the AMDARs. (3): Files containing the number of received AMDARs per day, the latitude, longitude and DEVG of the AMDARs. (4): ASIMOV files of the clear-air turbulence index. (5): Files with the value of the clear-air turbulence index and the high cloud cover for the position of the AMDARs. (6): Results of the verification.

7.5 Verification method

7.5.1 Program Validate

From the magnitude of the CAT index at the position of the previous and present AMDAR the average index is calculated. Because of the horizontal resolution of the ECMWF data (1.5º) and the distance an aircraft travelles in 7 minutes (100 km ± 50 km), calculating the average index with more positions is not necessary.

Program Validate determines the best threshold value of a CAT index. If the average CAT index is above or is equal to the threshold this means CAT is forecasted and the forecast is assigned "Yes". If the average CAT index is below the threshold the forecast is assigned "No". If the DEVG is equal to or larger than 20 tenths of m s^{-1} the observation is assigned "Yes" because such a DEVG value is defined as light or greater turbulence (see section 5.6). If the DEVG is smaller than 20 tenths of m s^{-1} it is assigned "No". When the forecast is "Yes" and the observation is "Yes", or the forecast is "No" and the observation is "No", the forecast is correct. The threshold value is varied in the range of the value of the index and the best threshold value is determined when a certain percentage of the turbulence observations is correctly forecasted. As soon as the percentage of forecasted turbulence observations reaches 50% and 80%, a threshold value and the percentage of forecasted nonturbulence observations is given. The latter is important to obtain an impression of the overestimation of the CAT index.

7.5.2 Exclusion of convection

Clear-air turbulence above 9200 m can also be caused by convection. Convection is a serious problem in our research area since the measurements have been taken for a large part in the tropics. Satellite images could indicate whether the turbulence was convective, but have not been used because of a lack of time. Instead we have chosen to use the +18, +24, +30, and +36 hour ECMWF model forecasts (based on ECMWF 12 UTC run) of the high level cloud cover. The high level cloud cover consists of convective and non-convective clouds. Clear-air turbulence in non-convective clouds will also be left out if a certain percentage of cloud cover is not accepted. Since only the large-scale motions will be forecasted by the ECMWF model, it is still possible that individual cumulonimbi or cirrus clouds have

not been left out and will cause turbulence. The high cloud cover corresponding to an AMDAR has been calculated in the same manner as the average CAT index.
The high cloud cover is the cloud cover between 450 hPa and the top of the model. Convection is not the only source for cirrus, also large-scale vertical wind speed and radiation cooling can produce cirrus (Beljaars, pers. com.).
To investigate the effect of the exclusion of convection, and because many good observations in non-convective clouds will probably also be left out, different criteria of cloud cover have been used:
1. Select turbulence AMDARs if average forecasted high cloud cover is smaller than 50%.
2. Select turbulence AMDARs if average forecasted high cloud cover is smaller than 10%.
This means the number of nonturbulence AMDARs is the same for each selection, but the number of turbulence AMDARs changes for different high cloud cover selections. We also investigate when no forecasted high cloud cover is used to exclude convection, so when all turbulence AMDARs are selected.
Appendix B gives the distribution of received AMDARs in time which comply with the 10 selections for turbulence and nonturbulence observations (section 7.2.2) if no convection is excluded.

7.5.3 Geographical distribution of AMDARs

Figures 7.2 to 7.5 give the geographical distribution of the AMDARs we selected. Figure 7.2 displays the 3755 nonturbulence AMDARs. Figures 7.3 to 7.5 give the distribution in space of turbulence AMDARs. Figure 7.3 gives the distribution if no convection is excluded (1087 AMDARs), Figure 7.4 gives the distribution for AMDARs with a forecasted high cloud cover smaller than 50% (356 AMDARs), and Figure 7.5 gives the distribution for AMDARs with a forecasted high cloud cover smaller than 10% (190 AMDARs).

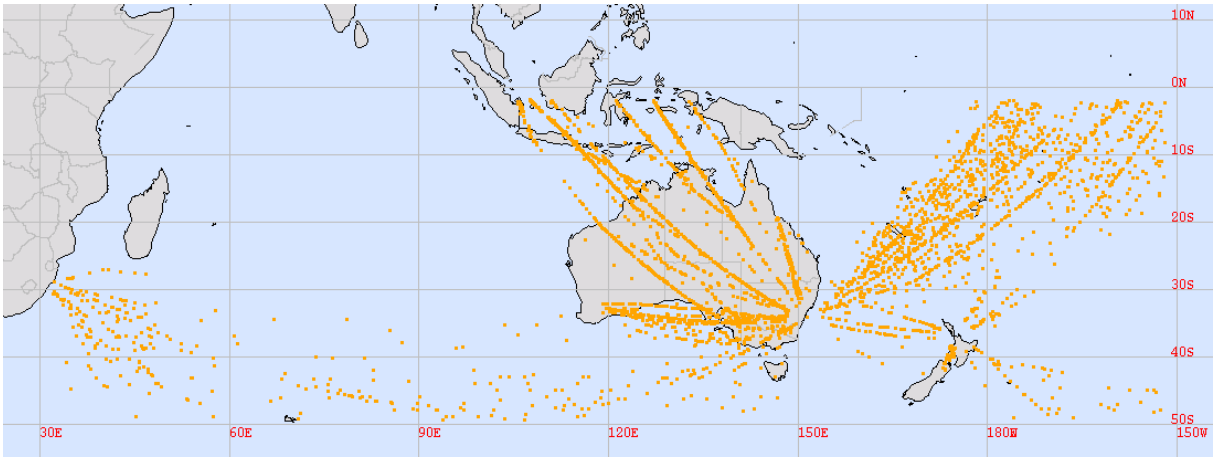

Figure 7.2: Distribution of nonturbulence AMDARs.

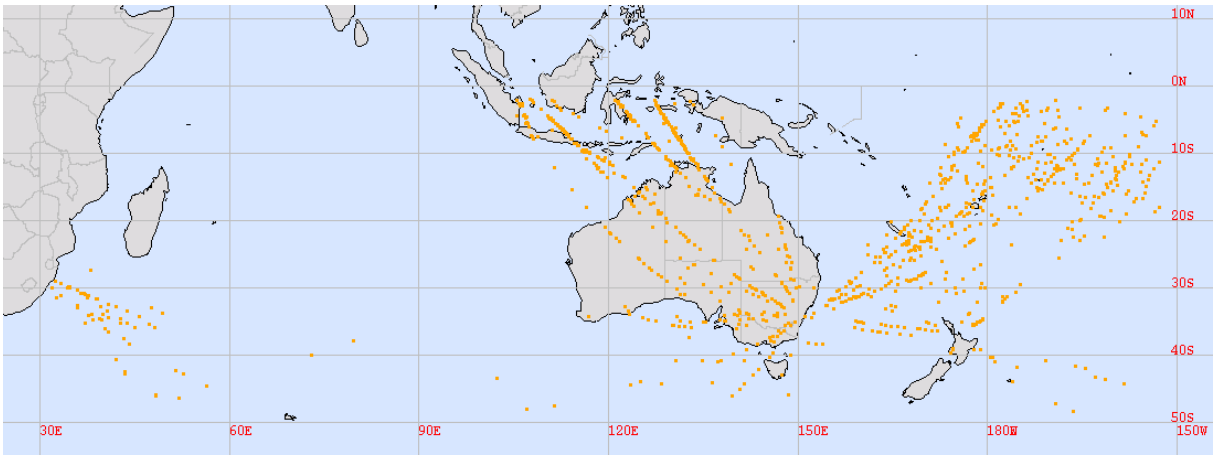

Figure 7.3: Distribution of turbulence AMDARs if no selection is made with the forecasted high cloud fraction (no convection excluded).

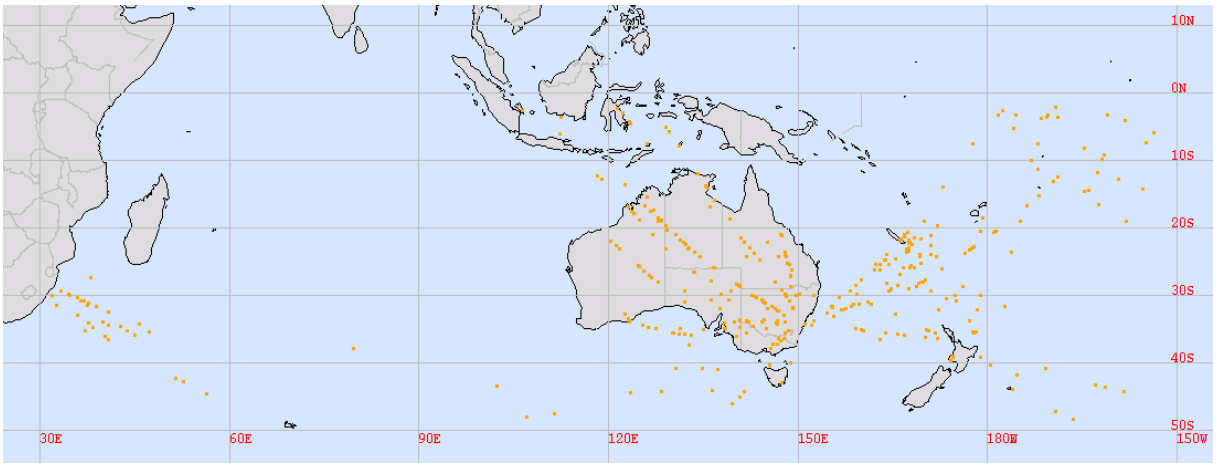

Figure 7.4: Distribution of turbulence AMDARs. Only AMDARs with a forecasted high cloud fraction smaller than 50% have been included.

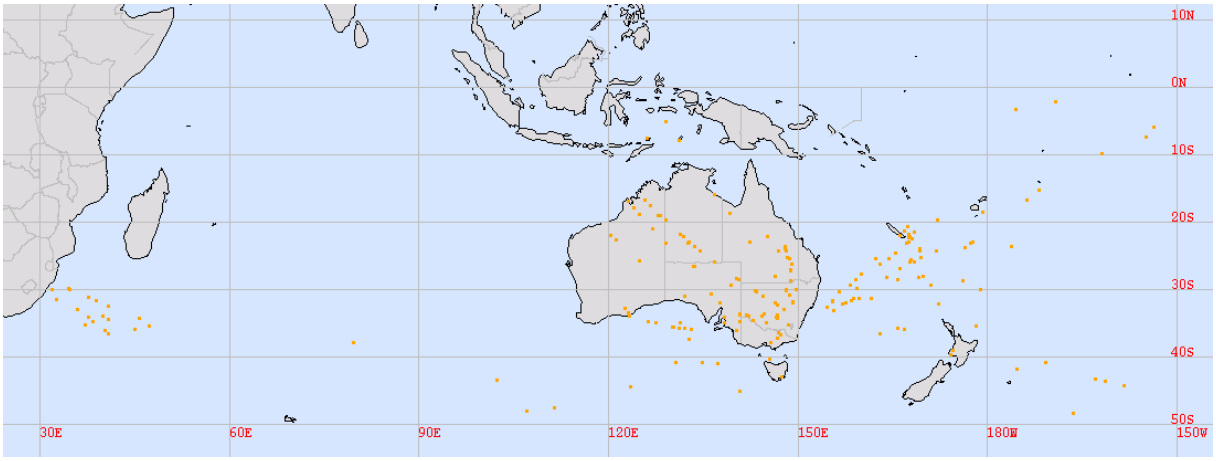

Figure 7.5: Distribution of turbulence AMDARs. Only AMDARs with a forecasted high cloud fraction smaller than 10% have been included.

7.5.4 Division in geographical areas

Since the weather is quite different between the tropics and higher latitudes, and also the causes of clear-air turbulence can be different, apart from the area 0ºS-50ºS, we also investigate the performance of the CAT indices in:

1. The tropics, defined here as 0ºS-20ºS
2. The midlatitudes, defined here as 20ºS-50ºS

7.6 Results

7.6.1 Introduction

In section 7.6.2 the results for the total research area (0ºS-50ºS) are given. Section 7.6.3 gives the results for 0ºS-20ºS, and section 7.6.4 the results for 20ºS-50ºS. Per Table two threshold values are given, determined when the number of correctly forecasted turbulence observations (forecast is "Yes" and observation is "Yes") becomes equal or larger than 50% and 80%.

For the area from 0ºS-50ºS more than 95% of the turbulence observations we select fall into the light turbulence intensity category when no selection is made to exclude convection, so moderate or greater turbulence is very rare.

Appendix C gives a visualization of the seven tested clear-air turbulence indices for one forecast. The start value is the first value which is presented with isolines of the clear-air turbulence index. The interval value is the value between two succeeding isolines of the clear-air turbulence index.

7.6.2 Results in the area from 0ºS-50ºS

1. Results if no AMDARs are excluded with the high cloud fraction

Most turbulence and nonturbulence observations are in the 250-200 hPa layer. Distribution of turbulence observations is about the same for the +18, +24, and +30 forecast, only the +36 forecast has few turbulence observations. Distribution of nonturbulence observations is also largely in the +18, +24, and +30 forecast, but the +30 forecast has the most observations. The +36 forecast has the least nonturbulence observations. See Table 7.1.

Based on 1087 turbulence and 3755 nonturbulence observations the VWS is the best index: 81% of the turbulence observations are forecasted in combination with 26% of the nonturbulence observations, and 51% of the turbulence observations are forecasted in combination with 59% of nonturbulence observations. The Dutton index and the TI1 perform almost as good as the VWS. See Table 7.2.

Table 7.1: Distribution of AMDARs (0ºS-50ºS) given for each forecast and each layer if no convection is excluded.

	300-250 hPa	250-200 hPa	200-150 hPa	Total
+18, turbulence	127	174	25	326
+24, turbulence	26	240	82	348
+30, turbulence	4	232	109	345
+36, turbulence	28	19	21	68
Total turbulence	185	665	237	1087
+18, no turbulence	323	532	154	1009
+24, no turbulence	85	654	199	938
+30, no turbulence	8	912	520	1440
+36, no turbulence	57	172	139	368
Total no turbulence	473	2270	1012	3755
Total	658	2935	1249	4842

Table 7.2: Performance of CAT indices (0ºS-50ºS) for two thresholds if no convection is excluded.

Forecast	**Observation Yes**	**No**	**Threshold**	**Observation Yes**	**No**	**Threshold**
Frontogenesis			$-0.4 \cdot 10^{-9}$ K m^{-1} s^{-1}			$-3.8 \cdot 10^{-9}$ K m^{-1} s^{-1}
YES (%)	50.0	58.8		80.3	87.9	
NO (%)	50.0	41.2		19.7	12.1	
TI1			$0.7 \cdot 10^{-7}$ s^{-2}			$0.2 \cdot 10^{-7}$ s^{-2}
YES (%)	51.1	42.1		87.4	85.2	
NO (%)	48.9	57.9		12.6	14.8	
TI2			$0.5 \cdot 10^{-7}$ s^{-2}			$0.1 \cdot 10^{-7}$ s^{-2}
YES (%)	54.1	55.3		87.1	91.9	
NO (%)	45.9	44.7		12.9	8.1	
Brown index			$3.4 \cdot 10^{-5}$ s^{-2}			$2.0 \cdot 10^{-5}$ s^{-2}
YES (%)	50.4	53.3		80.7	82.8	
NO (%)	49.6	46.7		19.3	17.2	
VWS			$2.8 \cdot 10^{-3}$ s^{-1}			$1.6 \cdot 10^{-3}$ s^{-1}
YES (%)	51.2	41.2		80.7	74.2	
NO (%)	48.8	58.8		19.3	25.8	
Wind speed			15.3 m s^{-1}			7.0 m s^{-1}
YES (%)	50.2	56.8		80.2	81.9	
NO (%)	49.8	43.2		19.8	18.1	
Dutton index			14.2			11.5
YES (%)	50.6	41.8		80.6	74.9	
NO (%)	49.4	58.2		19.4	25.1	

2. Results for AMDARs with a forecasted high cloud fraction smaller than 50%

Based on 356 turbulence and 3755 nonturbulence observations the TI1 is the best index: 81% of the turbulence observations are forecasted in combination with 44% of the nonturbulence observations. 50% of the turbulence observations are forecasted in combination with 77% of nonturbulence observations.

3. Results for AMDARs with a forecasted high cloud fraction smaller than 10%

Based on 190 turbulence and 3755 nonturbulence observations the TI2 is the best index: 81% of the turbulence observations are forecasted in combination with 58% of the nonturbulence observations. 52% of the turbulence observations are forecasted in combination with 83% of nonturbulence observations. See Table 7.3.

Table 7.3: Performance of CAT indices (0ºS-50ºS) for two thresholds. Only AMDARs with a corresponding forecasted high cloud cover smaller than 10% have been included.

Forecast	**Observation Yes**	**No**	**Threshold**	**Observation Yes**	**No**	**Threshold**
Frontogenesis			$2.7 \cdot 10^{-9}$ K m^{-1} s^{-1}			$-2.9 \cdot 10^{-9}$ K m^{-1} s^{-1}
YES (%)	50.0	25.4		81.1	84.3	
NO (%)	50.0	74.6		18.9	15.7	
TI1			$1.5 \cdot 10^{-7}$ s^{-2}			$0.6 \cdot 10^{-7}$ s^{-2}
YES (%)	50.0	16.9		80.5	48.2	
NO (%)	50.0	83.1		19.5	51.8	
TI2			$1.7 \cdot 10^{-7}$ s^{-2}			$0.7 \cdot 10^{-7}$ s^{-2}
YES (%)	51.6	16.6		81.1	42.5	
NO (%)	48.4	83.4		18.9	57.5	
Brown index			$5.8 \cdot 10^{-5}$ s^{-2}			$3.6 \cdot 10^{-5}$ s^{-2}
YES (%)	50.5	24.9		80.0	50.0	
NO (%)	49.5	75.1		20.0	50.0	
VWS			$3.6 \cdot 10^{-3}$ s^{-1}			$2.2 \cdot 10^{-3}$ s^{-1}
YES (%)	50.5	27.6		80.5	56.5	
NO (%)	49.5	72.4		19.5	43.5	
Wind speed			28.6 m s^{-1}			19.1 m s^{-1}
YES (%)	50.0	30.0		80.0	47.9	
NO (%)	50.0	70.0		20.0	52.1	
Dutton index			16.3			12.5
YES (%)	50.0	23.0		80.0	61.4	
NO (%)	50.0	77.0		20.0	38.6	

7.6.3 Results in the area from 0ºS-20ºS

If only AMDARs with a corresponding forecasted high cloud fraction smaller than 10% are included 22 turbulence observations remain. This are too few observations to draw conclusions from. Therefore results are only given for all AMDARs, so if no convection is excluded, and for AMDARs with a corresponding forecasted high cloud fraction smaller than 50%.

1. Results if no AMDARs are excluded with the high cloud fraction

Based on 592 turbulence and 1581 nonturbulence observations the VWS is the best index: 81% of the turbulence observations are forecasted in combination with 28% of the nonturbulence observations. 52% of the turbulence observations are forecasted in combination with 61% of nonturbulence observations.

2. Results for AMDARs with a forecasted high cloud fraction smaller than 50%

Based on 72 turbulence and 1581 nonturbulence observations the Brown index is the best index: 83% of the turbulence observations are forecasted in combination with 38% of the nonturbulence

observations. 50% of the turbulence observations are forecasted in combination with 73% of nonturbulence observations. See Table 7.4.

Table 7.4: Performance of CAT indices (0ºS-20ºS) for two thresholds. Only AMDARs with a corresponding forecasted high cloud cover smaller than 50% have been included.

Forecast	Observation Yes	No	Threshold	Observation Yes	No	Threshold
Frontogenesis			$0.1 \cdot 10^{-9}$ K m^{-1} s^{-1}			$-1.7 \cdot 10^{-9}$ K m^{-1} s^{-1}
YES (%)	50.0	40.5		80.6	81.7	
NO (%)	50.0	59.5		19.4	18.3	
TI1			$0.5 \cdot 10^{-7}$ s^{-2}			$0.2 \cdot 10^{-7}$ s^{-2}
YES (%)	52.8	28.8		84.7	71.2	
NO (%)	47.2	71.2		15.3	28.8	
TI2			$0.5 \cdot 10^{-7}$ s^{-2}			$0.1 \cdot 10^{-7}$ s^{-2}
YES (%)	50.0	25.9		94.4	83.3	
NO (%)	50.0	74.1		5.6	16.7	
Brown index			$2.8 \cdot 10^{-5}$ s^{-2}			$2.0 \cdot 10^{-5}$ s^{-2}
YES (%)	50.0	27.0		83.3	62.3	
NO (%)	50.0	73.0		16.7	37.7	
VWS			$2.5 \cdot 10^{-3}$ s^{-1}			$1.3 \cdot 10^{-3}$ s^{-1}
YES (%)	50.0	30.0		80.6	72.4	
NO (%)	50.0	70.0		19.4	27.6	
Wind speed			10.6 m s^{-1}			6.1 m s^{-1}
YES (%)	50.0	34.9		80.6	67.6	
NO (%)	50.0	65.1		19.4	32.4	
Dutton index			12.9			11.0
YES (%)	50.0	39.5		80.6	81.5	
NO (%)	50.0	60.5		19.4	18.5	

7.6.4 Results in the area from 20ºS-50ºS

1. Results if no AMDARs are excluded with the high cloud fraction

Based on 495 turbulence and 2174 nonturbulence observations the TI1, VWS, and the Dutton index are the best indices: respectively about 82%, 81%, and 81% of the turbulence observations are forecasted in combination with about 32%, 34%, and 33% of the nonturbulence observations. 51% of the turbulence observations are forecasted in combination with about 73%, 68%, and 72% of nonturbulence observations.

2. Results for AMDARs with a forecasted high cloud fraction smaller than 10%.

Based on 168 turbulence and 2174 nonturbulence observations the TI2 is the best index: 82% of the turbulence observations are forecasted in combination with 43% of the nonturbulence observations. 52% of the turbulence observations are forecasted in combination with 75% of nonturbulence observations. For the TI1 53% of the turbulence observations are forecasted in combination with 75% of the nonturbulence observations. See Table 7.5.

7.6.5 Correlation between magnitude of CAT indices and intensity of observed turbulence

The correlation between magnitude of the seven CAT indices and intensity of observed turbulence by AMDARs has been investigated for each area and each different criterion (when used) to exclude convection.

No correlation exists between observations with a DEVG ≥ 20 and the magnitude of clear-air turbulence indices, since the R^2 (square of the sample correlation coefficient) is less than 0.05. Appendix D displays this correlation for the area 20ºS-50ºS based on AMDARs with a corresponding forecasted high cloud cover smaller than 10%.

Table 7.5: Performance of CAT indices (20ºS-50ºS) for two thresholds. Only AMDARs with a corresponding forecasted high cloud cover smaller than 10% have been included.

Forecast	Observation Yes	No	Threshold	Observation Yes	No	Threshold
Frontogenesis			$3.1 \cdot 10^{-9}$ K m^{-1} s^{-1}			$-3.5 \cdot 10^{-9}$ K m^{-1} s^{-1}
YES (%)	50.0	37.8		80.4	80.6	
NO (%)	50.0	62.2		19.6	19.4	
TI1			$1.6 \cdot 10^{-7}$ s^{-2}			$0.6 \cdot 10^{-7}$ s^{-2}
YES (%)	53.0	24.8		84.5	67.7	
NO (%)	47.0	75.2		15.5	32.3	
TI2			$1.8 \cdot 10^{-7}$ s^{-2}			$0.8 \cdot 10^{-7}$ s^{-2}
YES (%)	51.8	24.9		81.5	57.0	
NO (%)	48.2	75.1		18.5	43.0	
Brown index			$6.2 \cdot 10^{-5}$ s^{-2}			$4.0 \cdot 10^{-5}$ s^{-2}
YES (%)	50.0	36.5		80.4	72.1	
NO (%)	50.0	63.5		19.6	27.9	
VWS			$3.9 \cdot 10^{-3}$ s^{-1}			$2.3 \cdot 10^{-3}$ s^{-1}
YES (%)	50.6	35.2		80.4	66.4	
NO (%)	49.4	64.8		19.6	33.6	
Wind speed			29.9 m s^{-1}			21.2 m s^{-1}
YES (%)	50.0	46.5		80.4	71.6	
NO (%)	50.0	53.5		19.6	28.4	
Dutton index			16.5			12.5
YES (%)	50.6	33.1		81.0	70.6	
NO (%)	49.4	66.9		19.0	29.4	

7.7 Discussion

7.7.1 Faults in the clear-air turbulence indices

The clear-air turbulence indices are based on macro-meteorological parameters while CAT is a micro-scale phenomenon. This seems the major limitation of these indices.
The threshold values of frontogenesis are often below 0 (frontolysis), and this is physically not correct. The frontogenesis, the only index which is not empirical, is obviously the index with the least performance of all seven tested indices. This may be attributed to the assumptions made during the derivation of frontogenesis: the air parcel is adiabatic, vertical motion is neglected and the field of motion is linear.
The Brown index is not valid for strongly anticyclonic flows. Frontogenesis is also not correct in and near centers of strong anticyclonic flow. The TI1 and TI2 may underpredict CAT in case of sharply sheared and curved ridges (Knox, 1997).

7.7.2 Faults in the AMDAR data

The peak value of DEVG is encountered in a time span of 7 minutes, so it is unknown where exactly the turbulence is encountered. Only the value of height of the present AMDAR is used to divide an observation into a certain layer. Only level flights are selected, but sometimes the height of the aircraft changes between previous and present AMDAR. So for some observations the peak value may have occurred in another layer than the observation was assigned to. About 9% of the turbulence observations and 3% of the nonturbulence observations have a height change larger than 100 m during the 7 minute period.

7.7.3 Faults due to convection and mountain-waves

The exclusion of turbulence by using a model forecast of high cloud cover will not exclude all convective turbulence since a large-scale model cannot predict an individual cumulonimbus or other convective cloud, and convection is also possible in clear-air. The exclusion of convection by using forecasted high cloud cover seems to work a bit, because the performance of the indices on average increases by excluding convection by means of high cloud cover forecasts.
Another possible fault is mountain-waves, but the number and height of the mountains in our research area is quite low, so this seems to be of limited importance. In Australia the heighest mountains are approximately 2 km. Only some parts of South-Africa, New-Zealand, and Indonesia have larger mountains.

7.7.4 Other faults

The period of validity of the forecast is assumed to be ± 2 hours and this may also give an error. Further, the observations are only obtained from three months. Maybe the relatively coarse horizontal resolution of the ECMWF data (1.5º) will give a larger overestimation of CAT areas than a higher horizontal resolution. Finally, different model forecast have been used, although in general the +36 hour forecast has relatively few observations.

7.7.5 Advantages of this study

Although in the past larger data sets have been used to verify numerical clear-air turbulence forecasts, these data were often subjective pilot reports and often did not divide into different aircraft types. The DEVG we use is aircraft independent and also takes into account the air speed and the aircraft mass during the flight. As far as the author knows, DEVG has not been used until now to verify numerical clear-air turbulence forecasts.

7.7.6 Comparison with some other studies

McCann (1993) used rawinsonde data to compute clear-air turbulence indices and compared these with 567 pilot reports of CAT. The turbulence intensity could not be predicted well. The latter is in agreement with our findings. The indices do not describe what really causes turbulence. New indices are needed to recognize severity. More recent studies have shown that wind shear alone is just as good as the TI1 and TI2. A reason for a bad VWS performance is that stability may be so high that the flow remains smooth (McCann, 1993; McCann, pers.com.).
Turner and Bysouth (1999), who used ASDAR reports, show that the false alarm ratio of predicting turbulence observations is over 90% for the TI1, TI2, Brown index, and Dutton index.
There does not seem to be a good correlation between TI and turbulence intensity, based on various studies (Ellrod, pers. com.). According to Dutton (1980) the relation between wind speed and pilot reports is weak.

7.8 Conclusions

We only give the best result, thus give the best forecast of CAT possible with a clear-air turbulence index based on our research.
The index with the best result is the TI2 in the area 0ºS-50ºS if only AMDARs with a forecasted high cloud cover smaller than 10% are included. The TI2 predicts 81% of the turbulence observations and 58% of the nonturbulence observations for a threshold of $0.7 \cdot 10^{-7}$ s^{-2}, and predicts 52% of turbulence observations and 83% of nonturbulence observations for a threshold of $1.7 \cdot 10^{-7}$ s^{-2}. These results are based on 190 turbulence and 3755 nonturbulence observations.

In the research area 0ºS-50ºS, 2.8% of the total observations (selected according to section 7.2.2) are turbulence observations if no AMDARs are excluded due to convection. This means nonturbulence conditions are far more frequent than turbulence conditions. Because of this we assume that the chance of a random encounter of CAT along a 100 km flight segment (which corresponds to a 7 minute period) is 3%. Part of these 3% will be caused by convective turbulence, so this is a conservative estimate.
Then we convert the best result above to chances: assume we have 100 observations, so 100 flight segments. Then 3 are turbulence observations and 97 are nonturbulence observations. 81% of the

turbulence observations is correctly forecasted, that is about 2 turbulence observations. 42% of the nonturbulence observations are not correctly forecasted, that is about 41 nonturbulence observations. This yields a total of about 43 observations in forecasted CAT areas, implying CAT is forecasted along 44% of a flight route and the chance of encountering CAT along a 100 km flight segment in a forecasted CAT area is about 6%.
The same reasoning for 52% correctly forecasted turbulence observations and 83% correctly forecasted nonturbulence observations yields that CAT is forecasted along 18% of a flight route and the chance of encountering CAT along a 100 km flight segment in a forecasted CAT area is about 9% (based on the exact percentages from Table 7.3).
The same reasoning for 10% correctly forecasted turbulence observations (threshold is $6.0 \cdot 10^{-7}$ s^{-2}) yields that CAT is forecasted along 1% of a flight route and the chance of encountering CAT along a 100 km flight segment in a forecasted CAT area is about 20%.

The chance of encountering CAT along a 100 km flight segment in a forecasted CAT area is very low and especially for the 80% criterion very often a CAT forecast is given. These are the results for the best index, for the other results the overestimation is even larger. With the 50% criterion the forecasted CAT areas can be reasonably confined, and the chance of encountering CAT in a forecasted CAT area is about 2 times as high as random, but is still very low (about 6%). With the 10% criterion the chance of encountering CAT in a forecasted CAT area is about 20%, which is still low and just 10% of the turbulence observations is forecasted correctly.
So CAT indices are not a reliable predictor of CAT. The CAT indices are only an aid for the aviation meteorologist and such an index should be used with precaution. This is probably due to the fact that CAT is a micro-scale phenomenon and therefore hard to predict. Chances increase only gradually for a higher threshold of the CAT index.
No correlation exists between the magnitude of clear-air turbulence indices and observations with a DEVG $\geq$ 20. So for example the turbulence intensities belonging to the threshold values in the report of Bakker (1993) are not valid for the ECMWF data we used.
If a threshold value is used in forecasting CAT, this means that if the average CAT value over a distance of about 100 km is above or equal to the threshold value, CAT has to be forecasted.

8 IMPLICATIONS FOR CLEAR-AIR TURBULENCE FORECASTS AT KNMI AND FUTURE DEVELOPMENTS IN DETECTING CLEAR-AIR TURBULENCE

8.1 Introduction

Based on the results of the verification of the clear-air turbulence indices with the pilot survey and AMDARs we conclude if a clear-air turbulence index can be used in operational weather forecasting at KNMI. Further, information is given about future developments in detecting clear-air turbulence. Will a clear-air turbulence forecast still be necessary in future, or will CAT be detected by measuring instruments on-board of an aircraft?
The aviation weather forecaster at KNMI is primarily responsible for the short weather forecast in his FIR (Flight Information Region, see Figure 8.1), which is the airspace over the land area of the Netherlands and part of the North Sea. The ECMWF 12 UTC run, and so the TI1, becomes available every day at 0 UTC. The +24 hour forecast is then valid for 12 UTC that day.

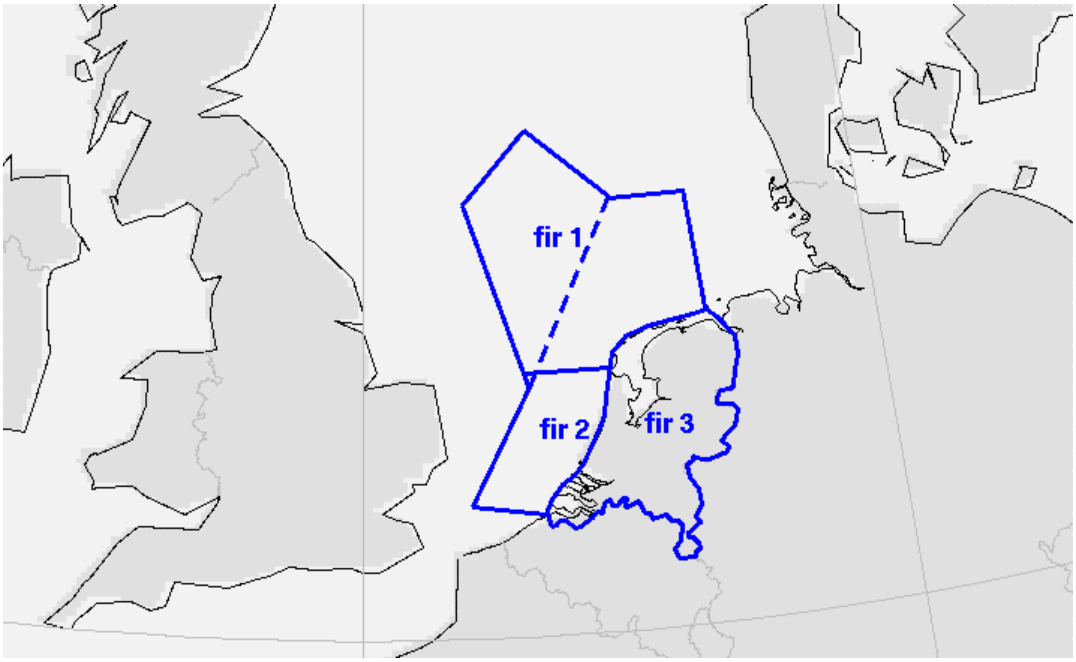

Figure 8.1: Flight information regions over the Netherlands.

8.2 Is a clear-air turbulence index reliable in forecasting clear-air turbulence over Europe?

8.2.1 Pilot survey

Based on the results of the pilot survey, the TI1 is not a reliable predictor of clear-air turbulence. 56.5% of the CAT events is correctly forecasted for a threshold of $2 \cdot 10^{-7}$ s^{-2}. Most serious limitation is the large overestimation of CAT areas, because 38.0% of the nonturbulence observations occurs for a CAT index of $2 \cdot 10^{-7}$ s^{-2} or higher. Because nonturbulence observations are far more common than turbulence observations, only a small percentage of flights moving through a forecasted CAT area will indeed encounter CAT.

8.2.2 AMDARs

It is doubtful if results obtained from the Southern Hemisphere may be applied to Europe.
For the research area of 20ºS-50ºS, which is best comparable with Europe, best results are obtained if only AMDARs with a forecasted high cloud cover smaller than 10% are included. The TI1 and the TI2 give the best results of the seven tested CAT indices.

The TI2 predicts 82% of the turbulence observations for a threshold of $0.8 \cdot 10^{-7}$ s^{-2}. This implies CAT is forecasted along 58% of a flight route and the chance of encountering CAT along a 100 km flight segment in a forecasted CAT area is about 4%.
The TI2 predicts 52% of turbulence observations for a threshold of $1.8 \cdot 10^{-7}$ s^{-2}. This implies CAT is forecasted along 26% of a flight route and the chance of encountering CAT along a 100 km flight segment in a forecasted CAT area is about 6%.
The TI1 predicts 85% of turbulence observations for a threshold of $0.6 \cdot 10^{-7}$ s^{-2}. This implies CAT is forecasted along 68% of a flight route and the chance of encountering CAT along a 100 km flight segment in a forecasted CAT area is about 4%.
The TI1 predicts 53% of turbulence observations for a threshold of $1.6 \cdot 10^{-7}$ s^{-2}. This implies CAT is forecasted along 26% of a flight route and the chance of encountering CAT along a 100 km flight segment in a forecasted CAT area is about 6%.

As a supplement we have also calculated the chances in case 10% of turbulence observations is correctly forecasted:
The TI2 predicts 10% of turbulence observations for a threshold of $6.3 \cdot 10^{-7}$ s^{-2}. This implies CAT is forecasted along 2% of a flight route and the chance of encountering CAT along a 100 km flight segment in a forecasted CAT area is about 14%.
The TI1 predicts 10% of turbulence observations for a threshold of $5.2 \cdot 10^{-7}$ s^{-2}. This implies CAT is forecasted along 3% of a flight route and the chance of encountering CAT along a 100 km flight segment in a forecasted CAT area is about 10%.
Chances of encountering CAT in a forecasted CAT area are still quite low and only 10% of the turbulence observations is forecasted.

Chances of encountering CAT in a forecasted CAT area are very low, so easily an overestimation of CAT is given. Since chances are higher than the random chance of encountering CAT, these CAT indices may be of some aid to the aviation meteorologist, but have to be used with precaution. The thresholds belonging to 50% and 10% forecasted turbulence observations seem to be most useful. Only for the latter the TI2 performs a bit better than the TI1. Therefore we recommend to use the TI1, which is already available at KNMI, and only visualize the areas with a value $\geq 1.6 \cdot 10^{-7}$ s^{-2} and a value $\geq 5.2 \cdot 10^{-7}$ s^{-2}. The first is in reasonable correspondence with the threshold of $2 \cdot 10^{-7}$ s^{-2} found for the pilot survey. The TI2 has the advantage that the threshold belonging to 10% forecasted turbulence observations performs better than for TI1, so the TI2 can be of some value to the aviation meteorologist at KNMI. These indices can be of some aid to pilots who plan their flight. Note that these recommended thresholds are based on observations from the Southern Hemisphere, so they will probably be somewhat different for CAT forecasts in Europe.

8.3 Future developments in clear-air turbulence detection

8.3.1 Introduction

CAT is not visible and not detectable by contemporary technology. A turbulence-avoidance system has to give a warning in an aircraft two or three minutes before the onset of CAT and false warnings should be limited to a maximum of 5 percent. In this way occupants have time to get seated and secured. To avoid turbulence, the detection time has to be larger than 3 minutes, but the problem with detection devices is their limited range. The primary limiting factor to implement on-board measurement devices in clear-air turbulence detection is the competition for funding and other resources with other aviation hazards. The costs and risks of turbulence are low when compared to less common but more severe other aviation hazards (Matthews, 2001). According to Lindsey (1998) the state of the science and technology for predicting or detecting turbulence is not yet mature. Even if in future an on-board CAT detection device is operational, forecasting CAT is still necessary for flight-planning purposes (Hopkins, 1977).

8.3.2 LIDAR

Light Detection and Ranging (LIDAR) is based on laser technology and gives an accurate prediction within maximal 8 kilometers. To give a 2- to 3-minute warning this distance should be increased to 32

or 40 kilometers. If such a LIDAR system is developed with current technology this could considerably increase the weight of the aircraft. Another problem is that false warnings cannot be limited to 5 percent. This will be achievable in a decade or more.
Large costs are involved to develop LIDAR systems and a relatively small number of serious injuries could be prevented by using this technology. This suggests LIDAR will never meet cost-benefit requirements (Matthews, 2001).

8.3.3 X-band radar

Another option is improvement of existing on-board weather radar systems, the X-band radar. An X-band radar returns signals from water droplets and thus recognizes most large weather systems, active weather cells and significant convection. Liquid water can be detected, but snow and hail cannot be detected well by X-band radar. CAT cannot be identified by X-band radar, because no liquid water particles are present. Enhanced X-band has a chance it gives enough benefits compared to the costs, provided implementation in aircraft focuses on incremental change to software and existing cockpit displays (Matthews, 2001).

9 CONCLUSIONS AND RECOMMENDATIONS

9.1 Conclusions

1. Can the TI1 be used as a predictor of clear-air turbulence over Europe based on the comparison with a pilot survey?
   Based on the pilot survey the TI1 is not a reliable predictor of clear-air turbulence over Europe, particularly because of the large overestimation of forecasted CAT areas. Chances of encountering CAT in such an area will be low. The TI1 may be of some use in some cases.
2. Which correlation exists between the magnitude of the tested clear-air turbulence indices and the intensity of observed turbulence by AMDARs?
   There is absolutely no correlation between the magnitude of the tested clear-air turbulence indices and the intensity of observed turbulence as reported by DEVG.
3. Which of the seven clear-air turbulence indices gives the best prediction of clear-air turbulence over the Southern Hemisphere when compared to AMDAR observations? And for which threshold values?
   The TI2 when calculated with AMDARs with a forecasted high cloud cover smaller than 10% obtained from 0ºS-50ºS. 81% of turbulence observations and 58% of nonturbulence observations are predicted for a threshold value of $0.7 \cdot 10^{-7}$ s^{-2}, 52% of turbulence observations and 83% of nonturbulence observations are predicted for a threshold value of $1.7 \cdot 10^{-7}$ s^{-2}.
4. Can a clear-air turbulence index be used in forecasting clear-air turbulence?
   The random chance of encountering CAT is about 3%. For the best result (see 3.) the chance of encountering CAT along a 100 km flight segment in a forecasted CAT area is 6%, 9%, and 20% for respectively 81%, 52%, and 10% correctly forecasted turbulence observations. CAT will be forecasted along 44%, 18%, and 1% of a flight route for respectively 81%, 52%, and 10% correctly forecasted turbulence observations. Note that for a large part of the other results (other indices, other areas, other criteria to exclude convection) the performance will be much lower.
   Conclusion is CAT indices cannot give a reliable forecast of CAT. The chance of encountering turbulence in a forecasted CAT area is very low and CAT is forecasted during a large part of a flight route or only few turbulence is forecasted. Though, chances of encountering CAT in a CAT area are higher than a random encounter, so CAT indices can be of some use in forecasting CAT, but have to be used with precaution. Problem is other methods of predicting CAT are also not reliable. The main problem is that CAT is a micro-scale phenomenon, and therefore hard to predict with a macro-scale numerical model forecast, which only predicts the circumstances which are needed for the production of Kelvin-Helmholtz waves.

9.2 Recommendations

Test clear-air turbulence indices based on ECMWF data with a horizontal resolution of 0.5º, or with output from the HIRLAM model version 5.06 (0.2·0.2º horizontal resolution), which has a high resolution and a high frequency of available model runs (four a day) and forecasts when compared to the ECMWF model. Use DEVG data from several years and all seasons of the year.

The HIRLAM model gives the turbulent kinetic energy (TKE) as output. Maybe TKE gives better results than the tested clear-air turbulence indices, which are based on large-scale models.

To validate numerical model forecasts in the Northern Hemisphere the DEVG has to be implemented correctly in aircraft. Further, turbulence observations due to convection should be excluded with measurements, like satellite images. Particularly test forecasts with moderate or larger turbulence, which are most important for flight safety.

Maybe the most promising option is to investigate for which weather situation CAT indices give a good prediction of CAT. Maybe the chance of encountering CAT in a forecasted CAT area is considerably higher for certain weather situations.

Make AMDARs with nonturbulence and turbulence measurements reported according to DEVG available to aviation meteorologists. In this way turbulence areas can be identified, and other aircraft can be warned. Disadvantage is that this does not give a forecast of CAT. To achieve this DEVG has to be implemented correctly in aircraft over Europe and the Atlantic, because this seems not to be the case.

REFERENCES

Badgley, F.I., 1969. Large-scale processes contributing energy to clear air turbulence, *Clear air turbulence and its detection,* Proceedings of a Symposium on Clear Air Turbulence and Its Detection, August 14-16 1968, Flight Sciences Laboratory, Boeing Scientific Research Laboratories, The Boeing Company, Plenum Press, New York, 109-123.

Bakker, H., 1993: *Drie objectieve indices voor clear-air turbulence nader bekeken*, Technische rapporten; TR-160, KNMI, de Bilt.

Barry, R.G., 1992: *Mountain weather and climate*, 2nd edition, Routledge, London.

Bass, E. J., 1999a. Turbulence assessment and decision making on the flight deck and in the cabin, *18th Digital Avionics Systems Conference Proceedings*, St. Louis, MO, 4.A.4-1 - 4.A.4-8.

Bass, E. J., 1999b. Towards a pilot-centered turbulence assessment and monitoring system, *18th Digital Avionics Systems Conference Proceedings*, St. Louis, MO, 6.D.3-1 - 6.D.3-8.

Beckwith, W.B., 1971. The effect of weather on the operations and economics of air transportation today, *Bulletin of the American Meteorological Society*, 52, 863-868.

Brown, R., 1973. New indices to locate clear-air turbulence, *Meteorological Magazine*, 102, 347-361.

Bysouth, C., 2000. Short range CAT forecasting, *The aeronautical forecasting training seminar: the application of numerical weather prediction products in aviation and dissemination through satellite and terrestrial means*, The Met. Office, Bracknell.

Dutton, M.J.O., 1980. Probability forecasts of clear-air turbulence based on numerical model output. *Meteorological Magazine*, 109, 293-310.

Ellrod, G.P., 1989: *A decision tree approach to clear air turbulence analysis using satellite and upper air data*, NOAA Technical Memorandum NESDIS 23, Satellite Applications Laboratory, Washington.

Ellrod, G.P. and D.I. Knapp, 1992. An objective clear-air turbulence forecasting technique: verification and operational use, *Weather and forecasting*, 7, 150-165.

Ellrod, G.P., 2000. Satellite images provide valuable information supplement to the aviation meteorologist, *ICAO Journal*, 55, no.2, 6-10.

Glickman, T.S., 2000: *Glossary of Meteorology*, 2nd ed., American Meteorological Society, Boston.

Hemink, H.J. and K. Verbeek, 1997. LMD Reisverslag: Northwest Airlines/Minneapolis en NWS/Chicago, 16-19 december 1996, personal memorandum, april 1997, KNMI, de Bilt. [internal publication]

Hopkins, R.H., 1977: *Forecasting techniques of clear-air turbulence including that associated with mountain waves*, WMO – No. 482, technical note no. 155, WMO, Secretariat of the World Meteorological Organization, Geneva, Switzerland.

Houghton, D.D., 1985: *Handbook of applied meteorology*, Wiley, New York.

Joint Action Group for Aviation Weather, 1999: *National aviation weather initiatives*, FCM-P34-1999, National Aviation Weather Program Council Office of the Federal Coordinator for Meteorology, Washington.

Keller, J.L., 1986: *The physical and empirical basis for a specific clear-air turbulence risk index, National Aeronautics and Space Administration*, Prepared for George C. Marshall Space Flight Center under contract NAS8-34687 (NASA contractor report ; 3971), NASA, Washington D.C.

Keller, J.L., 1990. Clear air turbulence as a response to meso- and synoptic-scale dynamic processes, *Monthly weather review*, 118, 2228-2242.

Knox, J.A., 1997. Possible mechanisms of clear-air turbulence in strongly anticyclonic flows, *Monthly weather review*, 125, 1251-1258.

Knox, J.A., 2001. The breakdown of balance in low potential vorticity regions: evidence from a clear air turbulence outbreak, *Preprint Atmospheric and Oceanic Fluid Dynamics Meeting*, June 2001, American Meteorological Society, Breckenridge, Colorado, P2.4-P.2.7.

Lester, P.F., 1994: *Turbulence: a new perspective for pilots*, Jeppesen Sanderson, Englewood.

Lindsey, C.G., 1998: *Aviation Weather Study Final Report*, NWRA-CR-98-R185, NorthWest Research Associates, Inc., Bellevue.

Long, R.R., 1969: A Theory Of Clear-air Turbulence, *Clear air turbulence and its detection,* Proceedings of a Symposium on Clear Air Turbulence and Its Detection, August 14-16 1968, Flight Sciences Laboratory, Boeing Scientific Research Laboratories, The Boeing Company, Plenum Press, New York, 51-62

Luchtmacht meteorologische groep (LMG), 1995: *Luchtvaartmeteorologie*, dictaat LVM, voortgezette opleiding meteorologie, Koninklijke Luchtmacht.

Mancuso, R.L. and R.M. Endlich, 1966. Clear air turbulence frequency as a function of wind shear and deformation, *Monthly weather review*, 94, 581-585.

Marroquin, A., 1999. Turbulence forecasting algorithms: calibration, comparison, and verification, *Eight conference on aviation, range, and aerospace meteorology*, 10-15 January 1999, American Meteorological Society, Dallas, Texas, 72–76.

Matthews, R., 2001: *Turbulence accidents among U.S. air carriers: their scale and possible solutions*, Annual symposium international society of air safety investigators, Office of Accident Investigation. Federal Aviation Administration, USA, Victoria B.C.

McCann, D.M., 1993. An evaluation of clear-air turbulence indices. *Preprints, Fifth Int. Conf. on Aviation Weather Systems*, Amer. Meteor. Soc., Vienna, V.A., 449-453.

Meteorological Office, 1971: *Handbook of aviation meteorology*, Her Majesty's Stationery Office, London.

Meteorological Office College, 1997: *Forecaster's reference book*, MET.O.1023, The Met. Office, Bracknell.

Painting, D.J., 1997: *Study on automated meteorological reporting from aircraft* (The Amdar study), s.n., s.l.

Painting, D., 2001: *Amdar Reference Manual*, WMO Amdar Panel, draft for discussion.

Panofsky, H.A. and J.A. Dutton, 1984: *Atmospheric turbulence: models and methods for engineering applications*, Wiley, New York.

Pao, Y. and A. Goldburg, 1969a. Foreword, *Clear air turbulence and its detection,* Proceedings of a Symposium on Clear Air Turbulence and Its Detection, August 14-16 1968, Flight Sciences Laboratory, Boeing Scientific Research Laboratories, The Boeing Company, Plenum Press, New York, VI – IX.

Pao, Y. and A. Goldburg, 1969b. Conclusion, *Clear air turbulence and its detection,* Proceedings of a Symposium on Clear Air Turbulence and Its Detection, August 14-16 1968, Flight Sciences Laboratory, Boeing Scientific Research Laboratories, The Boeing Company, Plenum Press, New York, 523-525.

Petterssen, S., 1935. Contribution to the theory of frontogenesis, *Geofysiske publikasjoner*, XI, Det Norske Videnskaps-akademi, Oslo, 5-27. No. 6

Petterssen, S., 1956: *Weather analysis and forecasting*, Vol. 1, second edition, McGraw-Hill Book Co.

Reap, R.M., 1996. Probability forecasts of clear-air-turbulence for the contiguous U.S., *Preprints, 13th conference on probability and statistics*, Amer. Meteor. Soc., San Francisco, C.A , 66-71.

Reiter, E.R., 1969. The nature of clear air turbulence: a review, *Clear air turbulence and its detection,* Proceedings of a Symposium on Clear Air Turbulence and Its Detection, August 14-16 1968, Flight Sciences Laboratory, Boeing Scientific Research Laboratories, The Boeing Company, Plenum Press, New York, 19-34.

Roach, W.T. and C.E. Bysouth, 2002. How often does severe clear air turbulence occur over tropical oceans?, *Weather*, 57, 8-19.

Saraber, M.J.M., 1999: *Dynamische meteorologie, practicum handleiding*, Wageningen Universiteit, Leerstoelgroep meteorologie en luchtkwaliteit.

Schairer, G.S. and G.L. Hollingsworth, 1969. Preface, *Clear air turbulence and its detection,* Proceedings of a Symposium on Clear Air Turbulence and Its Detection, August 14-16 1968, Flight Sciences Laboratory, Boeing Scientific Research Laboratories, The Boeing Company, Plenum Press, New York, V.

Schwartz, B., 1996. The quantitative use of PIREPs in developing aviation weather guidance products, *Weather and Forecasting*, 11, 372-384.

Sherman, D.J., 1985: *The Australian implementation of AMDAR/ACARS and the use of derived equivalent gust velocity as a turbulence indicator*, Structures report 418, Department of defence, defence science and technology organisation, aeronautical research laboratories, Melbourne.

Stull, R.B., 1988: *An introduction to boundary layer meteorology*, Kluwer Academic Publishers, Dordrecht.

Truscott, B., 2002: *EUMETNET AMDAR, AAA AMDAR Software Developments – AMDAR II Technical Specification*, version 4, The UK Meteorological Office, Berkshire.

Turner, J.A. and C.E. Bysouth, 1999. Automated systems for predicting clear air turbulence in global aviation forecasts, *Eight conference on aviation, range, and aerospace meteorology*, 368-372.

Villiers, M.P. de and J. van Heerden, 2001. Clear air turbulence over South Africa, *Meteorol. Appl.*, 8, 119-126.

Vinnichenko, N.K., N.Z. Pinus, S.M. Shmeter and G.N. Shur, 1980: *Turbulence in the free atmosphere*, 2nd ed., Consultants Bureau, New York.

Woods, J.D., 1969. On Richardson's number as a criterion for laminar-turbulent-laminar transition in the ocean and atmosphere, *Radio Science*, 4, 1289 - 1298.

Internet sources:

ADDS - PIREPs, Aviation Digital Data Service (ADDS), 18-12-2001,
http://adds.aviationweather.noaa.gov/projects/adds/pireps/

Aviation Weather Center (AWC) - Ellrod Index (RUC2), AWC, 22-05-2002,
http://aviationweather.noaa.gov/awc/ellrod_ruc2.html

Boeing 737-300, KLM, 27-11-2001,
http://nl.corporate.klm.com/Fleet/frame/Boeing737-300.asp

Boeing 737-400, KLM, 27-11-2001,
http://nl.corporate.klm.com/Fleet/frame/Boeing737-400.asp

Boeing 737-800, KLM, 27-11-2001,
http://nl.corporate.klm.com/Fleet/frame/Boeing737-800.asp

Clear Air Turbulence, NOAA/NESDIS, 17-09-2001,
http://orbit-net.nesdis.noaa.gov/arad/fpdt/CAT.html

http://weather.ou.edu/~som/computing/docs/gempak/apxB2.pdf, School of Meteorology/University of Oklahoma, 24-05-2002,
http://weather.ou.edu/~som/computing/docs/gempak/apxB2.pdf

Appendix A : Example of the pilot survey

KNMI enquête naar clear-air turbulence

De CAT-index, afkomstig uit een weermodel, geeft aan waar clear-air turbulence verwacht kan worden. Het doel van deze enquête is het bepalen van de betrouwbaarheid van deze index voor de weersverwachting, zodat onder andere duidelijker wordt in hoeverre deze index gebruikt kan worden voor het maken van een SIGMET.
Het verzoek is om, om het half uur een waarneming uit te voeren. Echter, belangrijker is nog dat tussentijdse turbulentie wordt opgeschreven.
Alleen waarnemingen tussen 9 en 15 UTC en tussen FL200 en FL380 zijn bruikbaar!
De enquête kan worden geretourneerd in de groene envelop.
Wij willen u van te voren bedanken voor uw medewerking,

Jan Hemink, luchtvaartmeteoroloog (KNMI)
Aart Overeem, student meteorologie (Wageningen Universiteit)

KNMI

Formulier enquête:
Datum waarop vlucht wordt uitgevoerd : ..16-01-02..... (dag-maand-jaar)
Vluchtnummer : ...KL.a903.....

Grootheid:	**Waarneming 1:**	**Waarneming 2:**	**Waarneming 3:**	**Waarneming 4:**	**Waarneming 5:**
Positie[1]	N053.04.7 E006.18.0	N055.09.4 E.014.17.3	N055.36.1 E021.45.7	N055.20.8 E029.33.1	N56 32.3 E029325
Tijd (UTC)	09.11	09.53	1027	1105	1350
Flight level	260	330	330	364	390
Windsnelheid	275/19	180/32	165/27	110/6	257/19
Temperatuur	-41	-58	-58	-65	-65
Bewolking (ja/nee)	N	N	N	N	N
Turbulentie[2]	2	0	0	0	0
Opmerkingen[3]	RIEMEN-VAST SERVICE-STOP	—	—	—	—

[1] Breedtegraad en lengtegraad in graden en minuten.
[2] 0: Geen turbulentie
1: Lichte turbulentie
2: Matige turbulentie
3: Zware turbulentie
[3] Ruimte voor opmerkingen die te maken hebben met de invloed van clear-air turbulence op de vluchtuitvoering, bijvoorbeeld het stoppen van de bediening of het vastmaken van de riemen i.v.m. clear-air turbulence.

Appendix B: Distribution of received and selected AMDARs in time

The Figure gives the distribution in time of received nonturbulence and turbulence observations after they have been selected according to the 10 selection criteria in section 7.2.2. Observations are from 0ºS-50ºS. No AMDARs are excluded with the forecasted high cloud fraction (no convection excluded).
White bars denote nonturbulence observations, black bars denote turbulence observations. Day 1 = 13 November 2001 and day 97 = 17 February 2002.

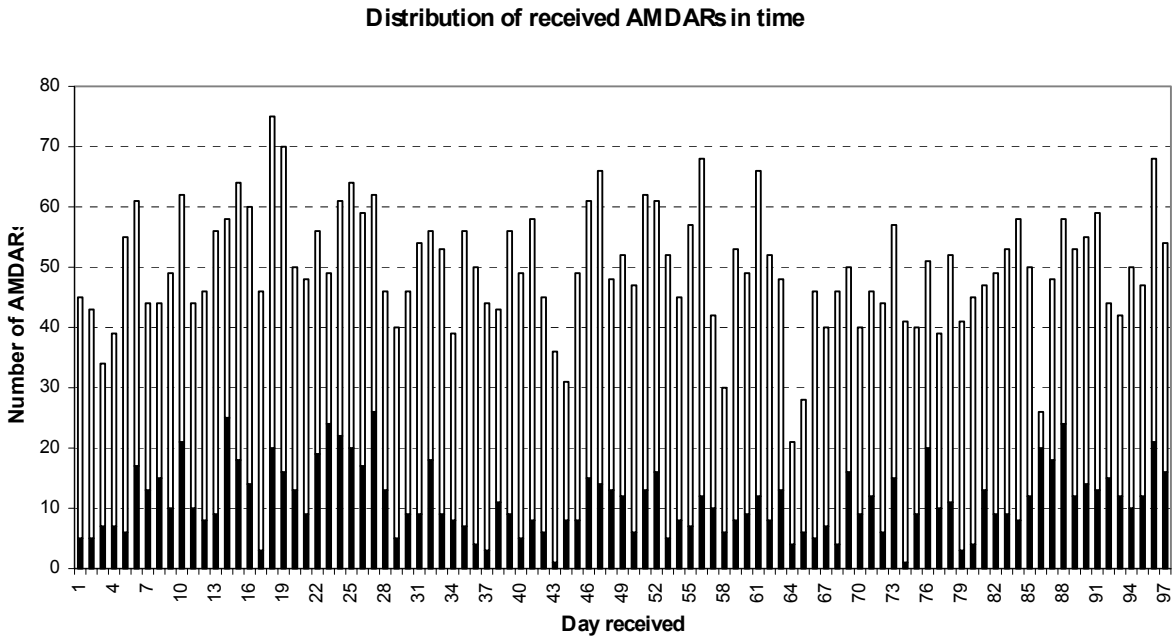

Appendix C: Visualization of clear-air turbulence indices

This Appendix gives the model fields of the seven tested clear-air turbulence indices from 30ºE-150ºW and 0ºS-50ºS. Model fields are given for 18 November 18 UTC (+30 hour forecast) for respectively TI1, TI2, Brown index, VWS (vertical wind shear), horizontal wind speed, and Dutton index. The last Figure gives the model field of frontogenesis. Because the data contained an error for frontogenesis, the model field for 18 November 12 UTC (+24 hour forecast) is given.
The start value is the first value which is presented with isolines (the blue lines) of the clear-air turbulence index. The interval value is the value between two succeeding isolines of the clear-air turbulence index.
The large blue H indicates a DEVG observation of 101 tenths of m s^{-1} (severe turbulence), which is the largest value of DEVG encountered in our research period. Further, turbulence observations are given (in red). These have to be interpreted according to Figure 6.1 in section 6.6.1.

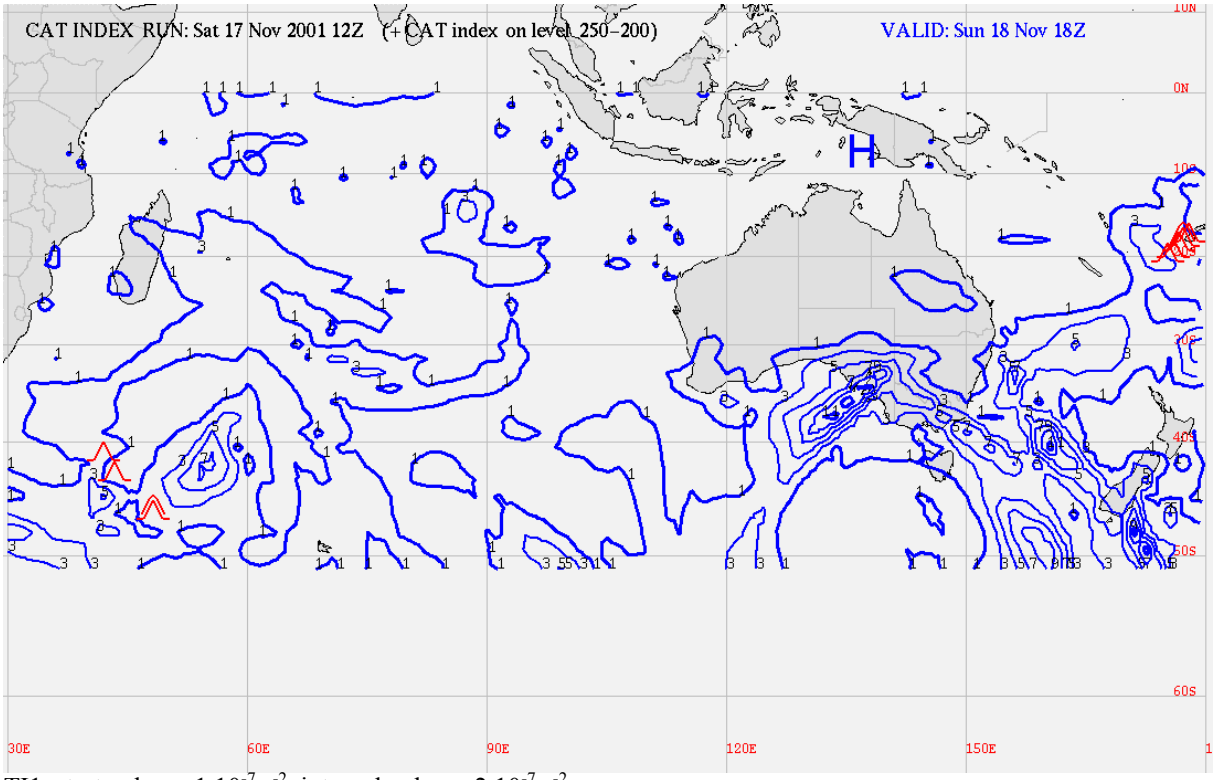

TI1, start value = $1 \cdot 10^{-7}$ s^{-2}, interval value = $2 \cdot 10^{-7}$ s^{-2}.

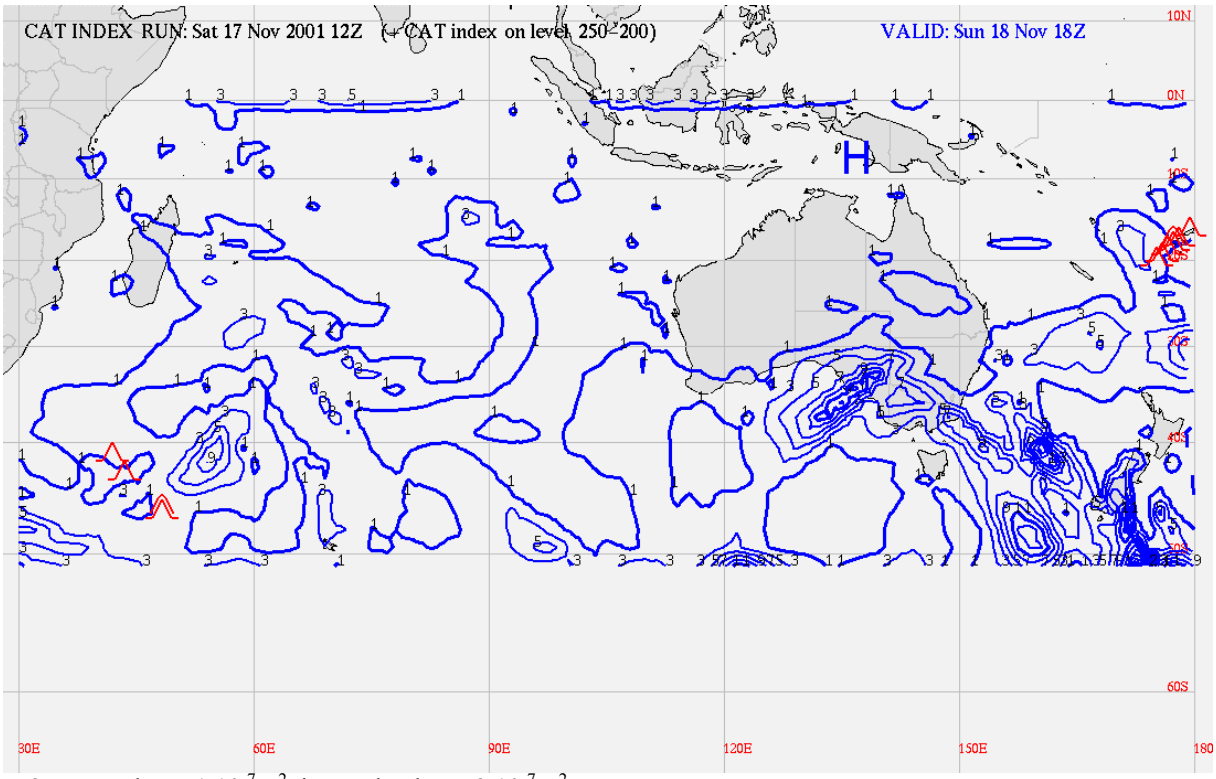

TI2, start value = $1 \cdot 10^{-7}$ s^{-2}, interval value = $2 \cdot 10^{-7}$ s^{-2}.

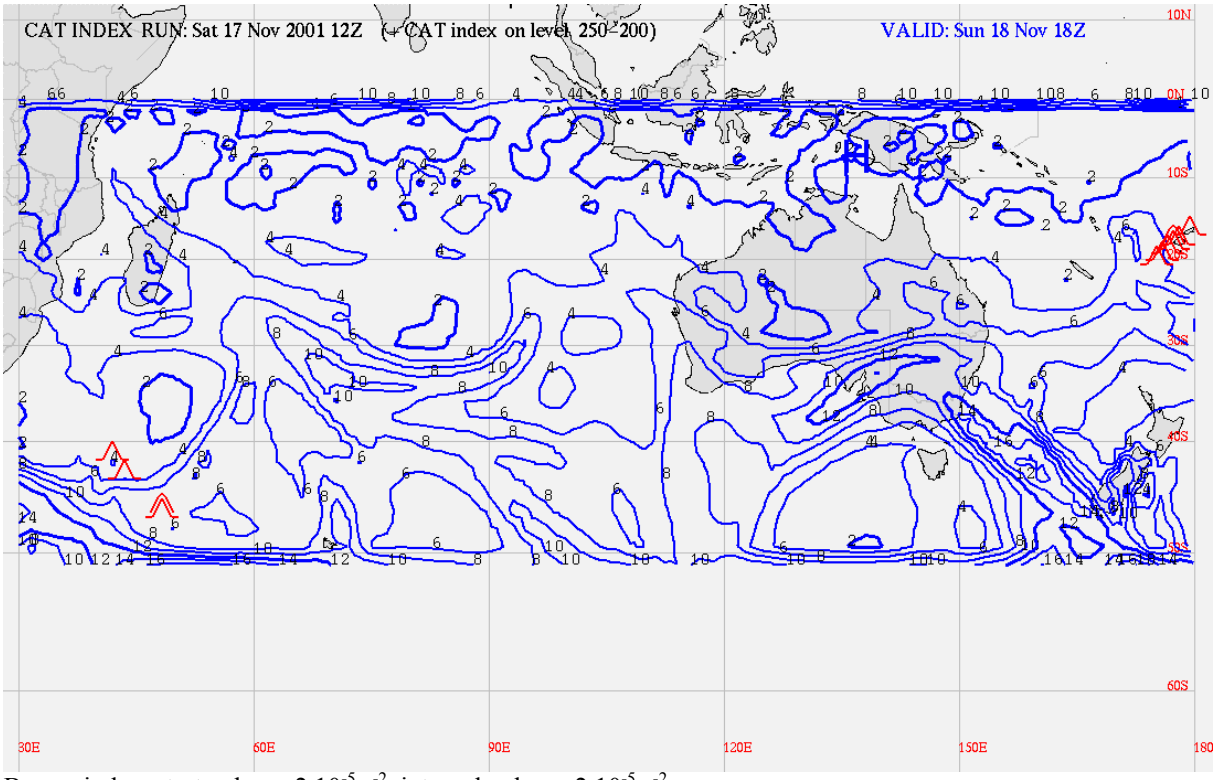

Brown index, start value = $2 \cdot 10^{-5}$ s^{-2}, interval value = $2 \cdot 10^{-5}$ s^{-2}.

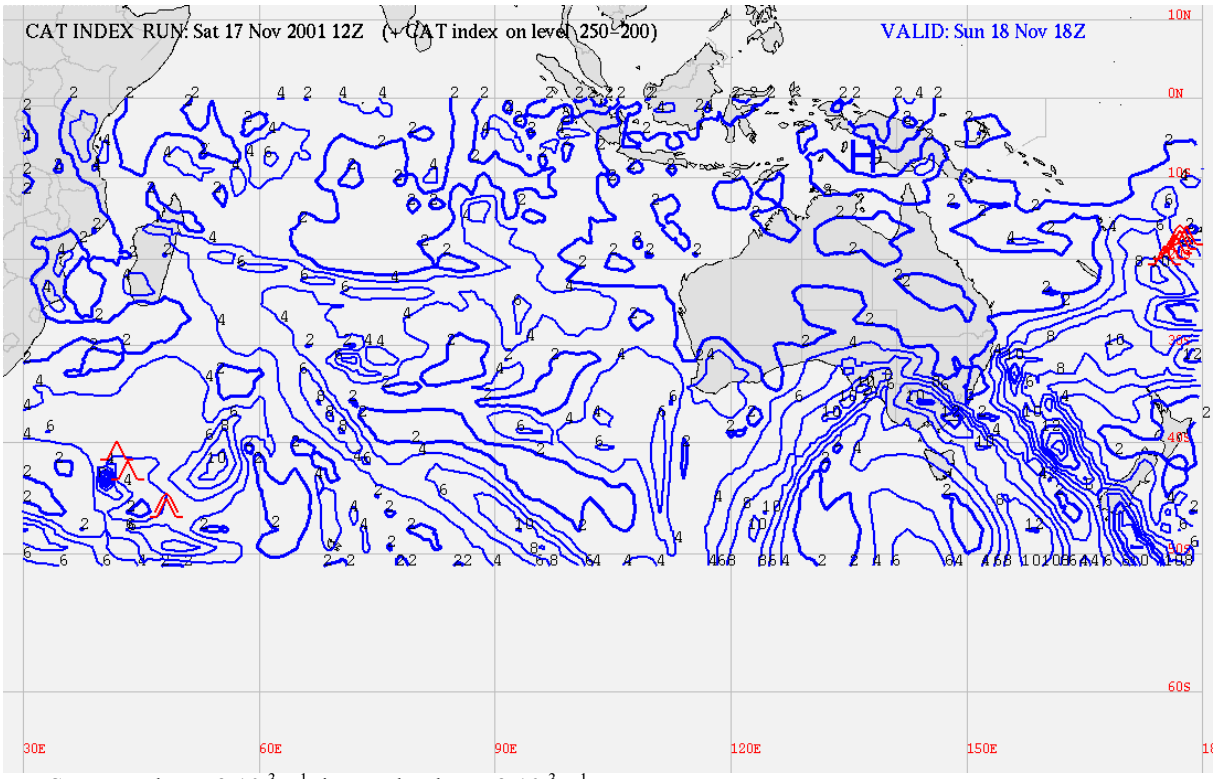

VWS, start value = $2 \cdot 10^{-3}$ s^{-1}, interval value = $2 \cdot 10^{-3}$ s^{-1}.

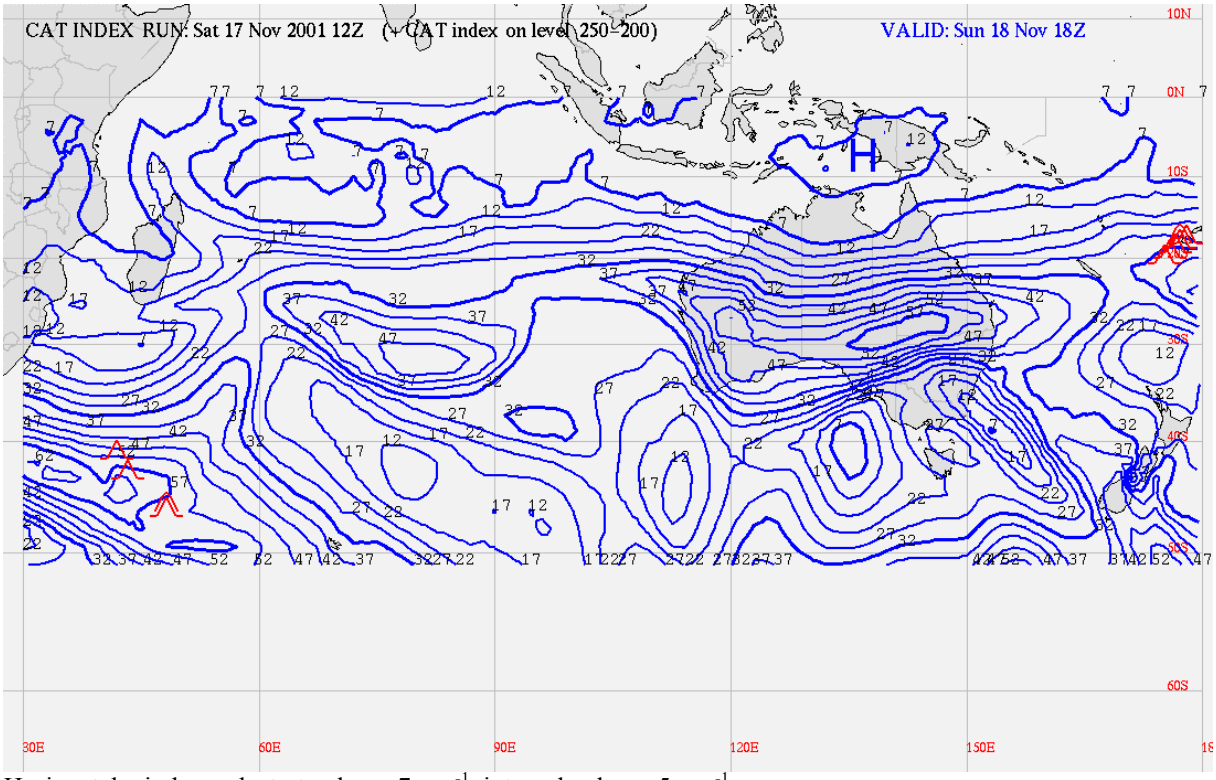

Horizontal wind speed, start value = 7 m s^{-1}, interval value = 5 m s^{-1}.

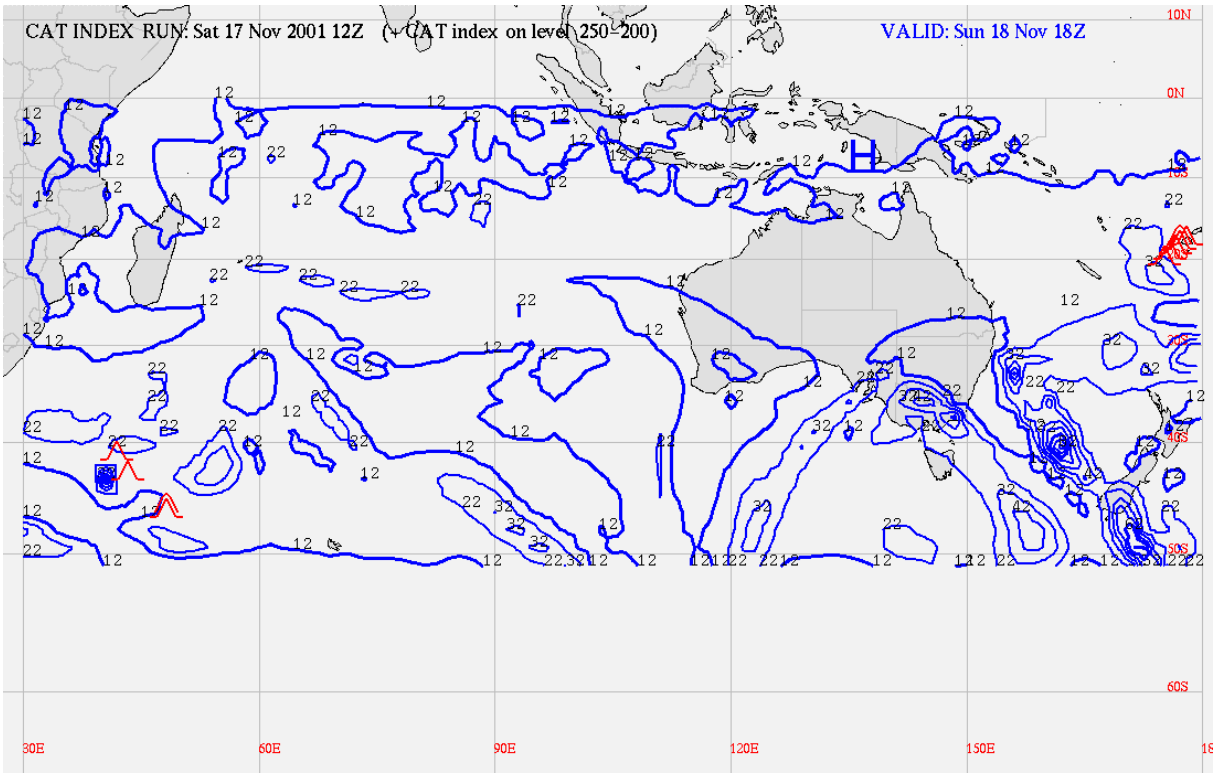

Dutton index, start value = 12, interval value = 10.

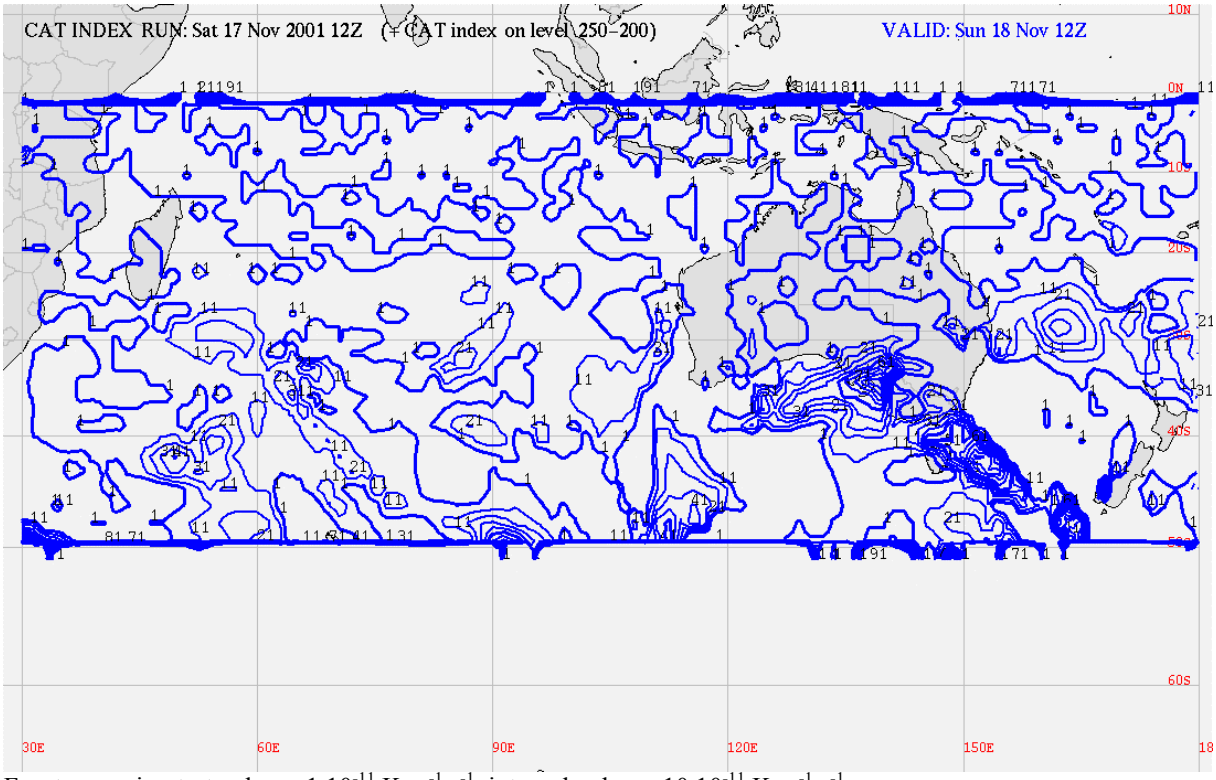

Frontogenesis, start value = $1 \cdot 10^{-11}$ K m^{-1} s^{-1}, interval value = $10 \cdot 10^{-11}$ K m^{-1} s^{-1}.

Appendix D: Magnitude of clear-air turbulence indices compared to observed turbulence intensities

In this Appendix for each turbulence observation (DEVG ≥ 20 tenths of m s^{-1}) the magnitude of the clear-air turbulence index and the intensity of the turbulence measurement are given. The R^2 (square of the sample correlation coefficient) between the magnitude of the CAT index and the intensity of the turbulence measurement is given in each Figure. Only turbulence observations (AMDARs) from 20º-50ºS and with a corresponding forecasted high cloud cover smaller than 10% have been used, yielding 168 observations. The DEVG is in tenths of meters s^{-1}.

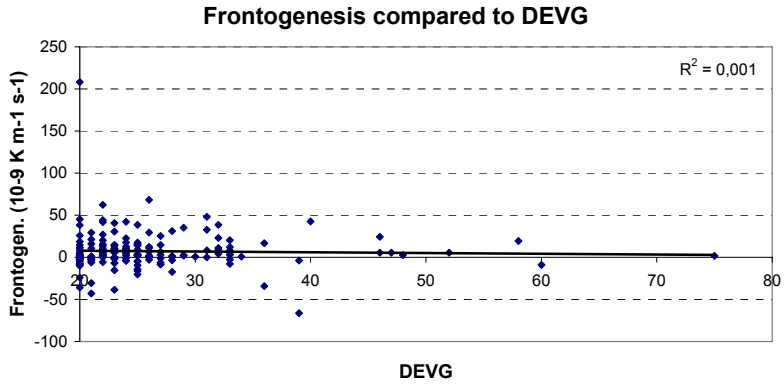

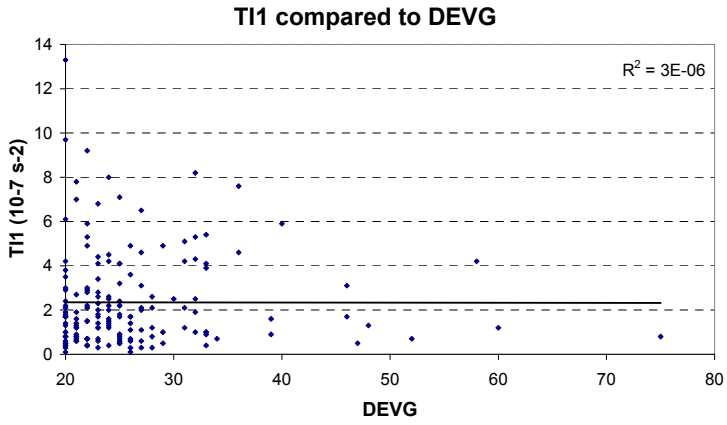

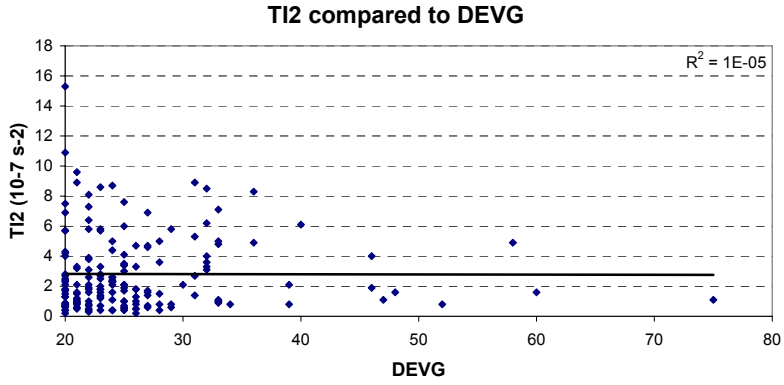

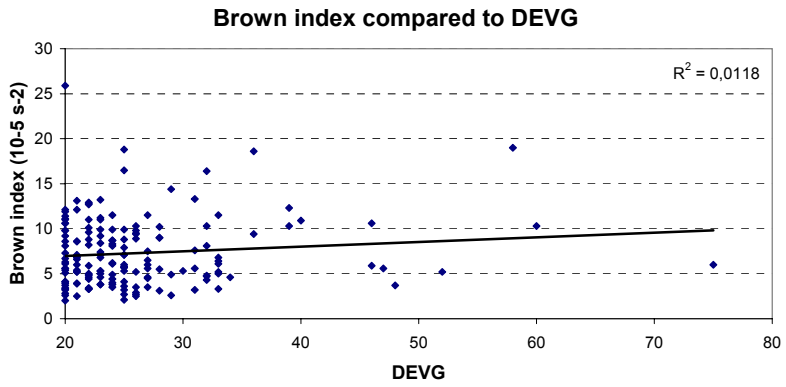
Brown index compared to DEVG
R^2 = 0,0118
Brown index (10-5 s-2)
DEVG
0
5
10
15
20
25
30
20
30
40
50
60
70
80

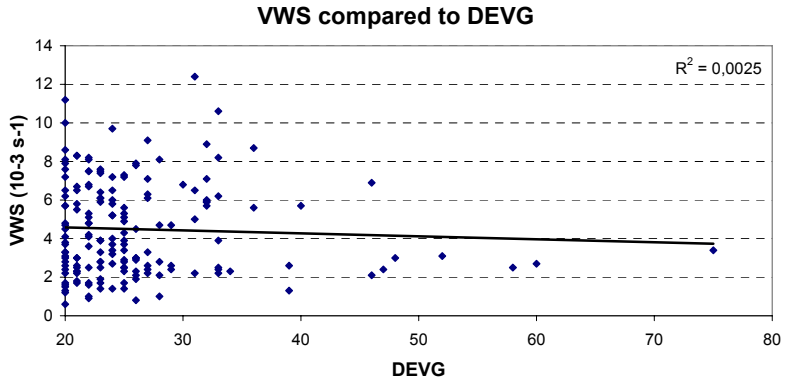
VWS compared to DEVG
R^2 = 0,0025
VWS (10-3 s-1)
DEVG
0
2
4
6
8
10
12
14
20
30
40
50
60
70
80

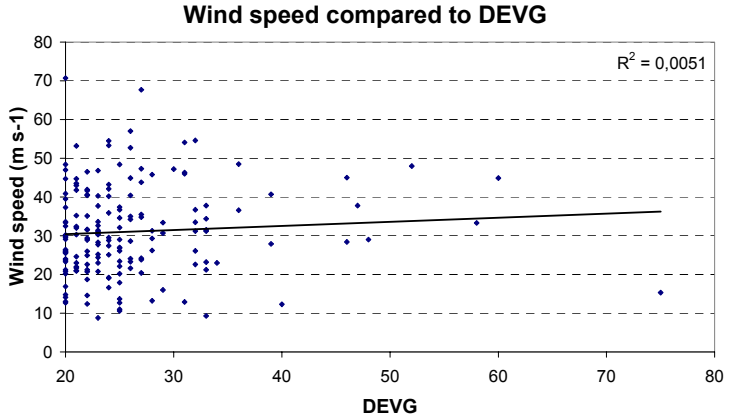
Wind speed compared to DEVG
R^2 = 0,0051
Wind speed (m s-1)
DEVG
0
10
20
30
40
50
60
70
80
20
30
40
50
60
70
80

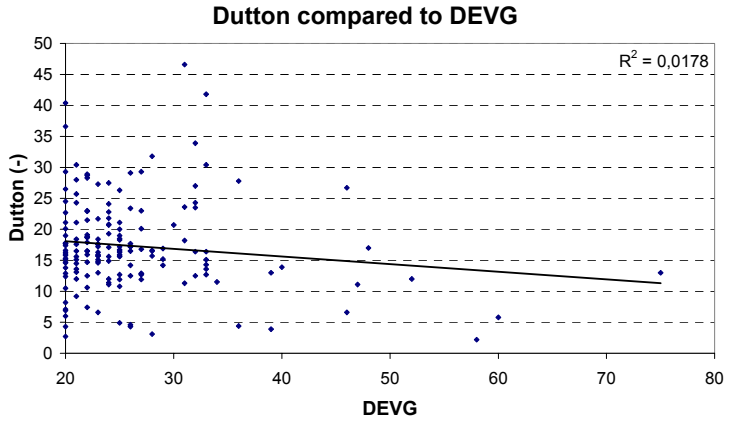
Dutton compared to DEVG
R^2 = 0,0178
Dutton (-)
DEVG
0
5
10
15
20
25
30
35
40
45
50
20
30
40
50
60
70
80